The Biophysical Properties of Rat Hindlimb Motoneurones Before and After the Removal of Descending, Ascending, And Afferent Inputs

by

Duane C. Button

A Thesis submitted to the Faculty of Graduate Studies of
The University of Manitoba in partial fulfilment
of the requirements of the degree of

DOCTOR OF PHILOSOPHY

Department of Physiology
University of Manitoba
Winnipeg, Manitoba

THE UNIVERSITY OF MANITOBA

FACULTY OF GRADUATE STUDIES

*****

COPYRIGHT PERMISSION

The Biophysical Properties of Rat Hindlimb Motoneurones Before and After the Removal of Descending, Ascending, And Afferent Inputs

BY

Duane C. Button

A Thesis/Practicum submitted to the Faculty of Graduate Studies of The University of Manitoba in partial fulfillment of the requirement of the degree

DOCTOR OF PHILOSOPHY

ABSTRACT

Motoneurones (MN) provide the link between the central nervous system and muscle fibers for relaying input required for movement. The study of the mechanisms by which motoneurones translate inputs has revealed a complex system. MNs combine its morphological features with various ion channels to govern membrane excitability, rhythmic and basic properties. This thesis was developed to describe these properties in the rat hindlimb MN before and after spinal cord injury.

Chapter 2 describes frequency-current (f-I) relationships of hindlimb MNs in anaesthetized and decerebrated rats in-situ. Rat hindlimb motoneurones injected with ramp currents are categorized into four different f-I relationship types. Two of these demonstrate persistent inward current (PIC). Although the anesthetic mixture of ketamine/xylazine renders the MN as less excitable to initiate spike threshold or rhythmic threshold compared to decerebration MNs, it does not affect the PIC amplitude.

Chapter 3 describes MN spike frequency adaptation (SFA). Rat hindlimb MNs show similar SFA patterns when injected with prolonged intracellular square-wave current injections of various intensities. Our results show SFA is only stimulus current-dependent within the first two seconds of current injection. We also developed an index of SFA that produced a wide range of SFA amongst MNs and significant correlations between SFA and PIC amplitude, rheobase current, input resistance, and f-I slope. These correlations are consistent with the notion that larger MNs exhibit greater SFA.

Chapter 4 assesses and compares the effects of chronic spinal cord transection (ST) *vs.* chronic spinal cord isolation (SI) on the biophysical properties of rat hindlimb MNs. We hypothesized that the ablation of ascending and afferent inputs in addition to the spinal transections induced by SI would have a more pronounced effect on MNs than the lack of descending inputs induced by ST. Although there were significant differences between ST and SI *vs.* Control MN properties, no differences existed between ST and SI MN properties. These findings suggest that descending input has a dominating effect compared to afferent and ascending inputs on MN biophysical properties.

The findings of this thesis are discussed and summarized in the Chapter 5.

ACKNOWLEDGEMENTS

The journey to my Ph.D. would never have taken place without Dr. Phillip Gardiner. He has been my guidance and mentor throughout my tenure at the Spinal Cord Research Centre and I will be forever grateful that he gave me the opportunity to study under his auspices. He is an "ultimate" academic mentor.

I would like to thank Kalan Gardiner for providing her technical support, friendship and advice. I would have never completed this research without her.

Dr. Jayne Kalmar came into the Gardiner Lab approximately half-way throughout my Ph.D. studies. She has given me additional insight into how to better perform research in various ways. Her advice and contributions towards this research was instrumental.

I was very fortunate to have a world class Ph.D. Committee. Drs. David McCrea, Brent Fedirchuk, and Jiming Kong provided me continuous feedback on my research and academic progress throughout my Ph.D. program. I will always remember their open door policy, conversations on scientific and non-scientific topics, and unconditional support.

I would like to thank Gail and Judy for all of their administrative help and friendship. Drs. Kris Cowley, Janice Dodd, Yue Dai, Larry Jordan and Brian Schimdt also deserve acknowledgement for the many helpful conversations we have had. Thank you to Matt Ellis, Gilles Detillieux, Sharon McCartney and Maria Setterbom for technical support. Thank you to Farrell Cahill for his much appreciated assistance with data analysis.

Finally, I would like to thank my lab mates and fellow graduate students; Tanguy, Dan, Jun, Carl, Myriam, Katinka, Jane and especially Kevin (it has been a long journey my friend, 10 years of post-secondary education together, I hope our paths cross again in the near future) for their support and friendship.

I would like to acknowledge the financial supporters for this research; Natural Science and Engineering Research Council, Manitoba Health Reseach Council, Canadian Institute for Health Research and National Institutes of Health.

DEDICATION

I would like to dedicate this work to my family.

To my wife Danielle and daughter Olivia; "Danielle you have been there for me from day one, through the good times and bad and have unconditionally supported me." You have helped me in so many ways and I would not be in this current situation without you." "Olivia, you have inspired me to continue forward and do the best I can." "I love you both."

To my father and mother, Calvin and Elizabeth; "I would have never made it here without you." "Thank you for constructing an environment which provided me with all of the preceding ingredients to reach this academic achievement."

To my second set of parents, William and Nadine; "Following departure from my parents, you continued to provide the environment that was initiated by them." "I have never considered you in-laws, but instead my second set of parents."

To the rest of my family; "I hope that seeing an average person like me, who has reached the highest academic achievement, enables you to strive for such achievements in future years to come no matter the task at hand."

> The difference between a successful person and others is not a lack of strength, not a lack of knowledge, but rather in a lack of will.
> --Vince Lombardi

LIST OF ABBREVIATIONS

4-AP	4-aminopyridine
5-HT	Serotonin
AHP	Afterhyperpolarization
BDNF	Brain-derived neurotrophic factor
cAMP	Cyclic adenosine monophosphate
CGRP	Calcitonin gene-related peptide
EMG	Muscle electromyography
ePIC	Estimated persistent inward current
EPSP	Excitatory post synaptic potential
fAHP	Fast afterhyperpolarization
f-I	Frequency-current
FF	Fast fatiguable
FR	Fast resistant
GABA	Gamma-aminobutyric acid
H-reflex	Hoffman reflex
IA	Transient outward K+ channel
IKCa (BK)	Ca++ -activated K+ current (big conductance)
IKCa (SK)	Ca++ -activated K+ current (small conductance)
IKdr	Delayed rectifier K+ channel
Ih	Hyperpolarization-activated channel
IKir	Inward rectifier K+ channel
IL	K+ leak channel
IKNa	Na+ activated K+ channels
I Nap	Persistent non-inactivating Na+ channel
I Nat	Fast transient Na+ channel
IR	Input resistance
LG	Lateral gastrocnemieus
mAHP	Medium afterhyperpolarization
MG	Medial gastrocnemieus
MN	Motoneurone
NA	Noradrenaline
NMDA	N-Methyl-D-Aspartate
NT-3	Neurotrophin 3
PIC	Persistent inward current
PKA	Phosphokinase A
PKC	Phosphokinase C
RAMP	Triangular current pulse
RMP	Resting membrane potential
Rth	Rhythmic threshold of firing
sAHP	Slow afterhyperpolarization
S	Slow
SFA	Spike frequency adaptation
SI	Spinal cord isolated
SOL	Soleus

SSFF	Steady-state firing frequency
ST	Spinal cord transected
TASK-1	TWIK-related acid sensitive K+
trkB	Tyrosine kinase B
TTX	Tetrodotoxin
Vth	Voltage threshold

TABLE OF CONTENTS

CHAPTER 1: GENERAL INTRODUCTION

The mammalian spinal cord can be thought of as a very elaborate and complex relay centre that carries information to and from the brain and peripheral organs via cells located in its grey matter. One very interesting spinal cord cell, the motoneurone (MN), is located in dorsal-lateral and ventral-medial motor nuclei of lamina 9. Essentially, its sole function is to induce skeletal muscle contraction and receive ongoing motor and sensory information from higher order centers and sensory information from the periphery to control the contracting muscle. Simply put, the MN receives and integrates various inputs, convert these inputs into a frequency code and send an output to the muscle for force production. Thus, the MN is crucial for mammalian survival. Fortunately, the MN is very accessible for research. A great deal of information is known about the cell type which it innervates and its size is relatively large making it easy for impalement with a microelectrode.

Much advancement has been made to further our understanding of MN electrophysiology since the development of intracellular MN recordings by Sir John Eccles in the late 1940s and 50s. Since then, the question "how do MNs receive and integrate input and turn it into a subsequent output?" has generated a large amount of research interest and subsequent experimentation using different: 1) mammalian models (cats, rats, mice and etc.), 2) preparations (*in vivo*, *in vitro,* in culture), and physiological conditions (spinal cord injury, exercise, locomotion, aging, disease, axotomy, etc.).

This thesis is an examination of MN electrophysiological properties and how these properties change when their activity have been decreased. In particular, the

introduction will describe: 1) the morphological features of the MN with some emphasis on its environmental surroundings, 2) MN electrophysiological properties including a description of the ion channels underlying these properties, 3) types of MNs and 4) models used to decrease MN activity with a focus on how and why MN electrophysiological properties change after their activity has been altered.

Section 1: Motoneurone morphology. The MN is a multipolar neurone composed of a soma, dendrites that extend from the soma into both spinal cord grey and white matter (Ulfhake & Kellerth 1981), and an axon which innervates muscle. The soma represents a small portion of the total MN size but contains the nucleus and machinery essential for protein synthesis and survival. Furthermore, it integrates incoming information from the dendrites and its own self to determine an output through the axon. Typically rat and cat MN soma sizes average 40 (Swett et al. 1986; Ichiyama et al. 2006) and 60 μm (Kernell 1966; Burke et al. 1977), respectively. The dendrites constitute about 97% of the surface area of the entire MN (Ulfhake & Kellerth 1981; Gazula et al. 2004b) and forms thousands of synapses with other neurones. The cat and rat MN typically has a total of 10 or more dendrites that are composed of primary, secondary and tertiary branches and altogether forms a dendritic tree that can extend beyond 1 mm from the soma (Ulfhake & Kellerth 1981; Kitzman 2005; Cullheim et al. 1987). The axon projects away from the MN towards the muscle and contains the site for action potential initiation and the machinery to carry that action potential to the muscle to elicit contraction. In the cat, axons can reach up to 24 cm with diameters reaching 9 μm (Cullheim & Kellerth 1978a) while

in the rat the longest axons are only several cm with diameters of approximately 6 μm (Delaney et al. 1981).

Other very important anatomical features of MNs are ion channels, membrane receptors, and different types of synapses (excitatory and inhibitory). There are several types of ion channels which allow current to flow in or out of the MN. Ion channels are formed by calcium (Ca^{++}), potassium (K^{+}) sodium (Na^{+}) and chloride (Cl^{-}) subunits, giving each ion channel a specific function which underlies specific portions of developing and maintaining the MN action potential and/or train of action potentials (for an in depth review see Toledo-Rodriguez et al. 2005; Hille 2001; Rekling et al. 2000; McLarnon 1995; Sah 1996 and see Section 2 – *Ion Channels of Motoneurones*). MNs also have many cell surface receptors that are modulated by neurotransmitters and act to excite or inhibit MNs by direct or indirect contact with the ion channels. The main receptors include: excitatory iono- and metabotropic glutamate receptors, inhibitory iono- and metabotropic gamma-aminobutyric acid (GABA) receptors, inhibitory glycine receptors, and excitatory monoaminergic receptors (serotonin, 5-HT and noradenaline, NA) (for an in depth review see Rekling et al. 2000). There are also several other key MN membrane receptors (i.e. g- protein coupled receptors, receptor tyrosine kinase) that once activated play a role in regulating both ion channels and membrane receptors through a cascade of intracellular events in the cytoplasm and nucleus. Finally, MNs are surrounded by many of several types of synapses from thousands of neurones originating in the brain, spinal cord and periphery. These synapses are either excitatory or inhibitory depending on the neurotransmitter released from its terminal. Types of synapses

include F-type which are inhibitory since they release GABA and glycine, S-type which are excitatory since they release glutamate, C-type which are of cholinergic phenotype and M-type which contain glutamate and are of group Ia primary afferent origin and in the rat all range in size from 1-2 μm (Ichiyama et al. 2006).

The MN is not a simple input-output processing cell as was once thought. Its behavior is very dependent on morphology, ion channels, receptors, synapses and type of muscle innervated. All of these factors play a role in determinig MN electrophysiological properties. Furthermore, there are MNs of various sizes throughout the motor pool and heavily contributes to differences amongst MN passive and active properties.

Section 2: Motoneurone Electrophysiological Properties. Typically MN electrophysiological properties are placed into two groups; 1) passive properties, which comprise those elements in physiological situations that remain unchanged during changed membrane potentials and ion currents (Kandel et al. 2000) or the measurement of voltage responses elicited by weak current pulses while the cell is at rest (Kernell 2006). 2) Active properties result from opening and closing of ion channels as a function of changed membrane potentials (voltage gated ion channels) and time which alters the MNs excitability and firing properties (Kernell 2006; Kandel et al. 2000). MN passive and active properties will now be discussed.

Motoneurone Passive Properties. Voltage transients are seen when a MN is subjected to small current steps. These voltage transients can be used to measure cell size by application of Rall's Equivalent Cylinder Model (Rall 1959; Rall et al. 1992). In the model the MN is represented as a soma with resistance and capacitance in

parallel attached to a uniform diameter cylinder of finite length. Several assumptions have to be made 1) soma isopotentiality, 2) uniform membrane properties throughout the somatodendritic surface and 3) dendrtic trees have similar dendritic branching and termination. The dendrites can be treated as an unbranched cylinder such that the sum of the branch points ($\sum^{3/2}$ d) is equal to the diameter of the parent branch ($D^{3/2}$) and subsequently collapsed into one equivalent cylinder. The Rall model is composed of four major parameters 1) the ratio of the input conductance of the dendritic cylinder to that of the soma, 2) space constant, 3) the membrane time constant, and 4) the Rin which can be measure by injecting current into the MN soma. From these and a series of simplified equations one can determine MN electrotonic length or the length at which a voltage transient will decay to 37% of its value, by measuring the time constant of the voltage transient. The measured values for electrotonic length, time constant and Rin allows for the calculation of total cell capacitance (i.e. estimate of cell size) (Hochman & McCrea 1994; Burke & ten Bruggencate 1971; Rall 1969; Beaumont & Gardiner 2003; Gustafsson & Pinter 1984b). On average the electrotonic length is ~1.5 for both cat and rat MNs, and time constants range from 2-12 ms and 1-5 ms and total cell capacitance (assuming specific membrane capacitance of 1 $\mu F/cm^2$ ranges from 2-9 nF and 1-6 nF for cat and rat MNs, respectively (Gustafsson & Pinter 1984b; Ulfhake & Kellerth 1982; Hochman & McCrea 1994; Beaumont & Gardiner 2003; Burke & ten Bruggencate 1971; Zengel et al. 1985; Cormery et al. 2005). While the assumed specific membrane capacitance is useful in determining MN area, the combination of electrical and geometrical measurements of rat and cat MNs have indicated that

specific membrane capacitance are much higher (Thurbon et al. 1998; Barrett & Crill 1974). Thus, the assumption made in Rall's Equivalent Cylinder Model may not always apply. Nonetheless, Rall's model and morphological measurements have given us much insight as how the MN functions.

Another very important MN passive property is Rin. By intracellularly injecting a known current into the soma and measuring the change in the subsequent voltage transient, the Rin can be calculated. Rins of cat and rat MNs range from 0.4-5.5 MΩ (Hochman & McCrea 1994; Gustafsson & Pinter 1984b; Zengel et al. 1985; Gardiner 1993; Kernell & Zwaagstra 1981) with a specific membrane resistance of 1-5 KΩ cm^2 (Barrett & Crill 1974), which differ between the soma and dendrites (i.e. higher in the dendrites) (Clements & Redman 1989; Thurbon et al. 1998). Typically Rin and membrane time constant increase together, indicating that smaller area MNs have larger Rin s (Hochman & McCrea 1994; Gustafsson & Pinter 1984b). Thus, total Rin depends on the size and shape of the MN and the resistance of a unit of given membrane (i.e. specific resistivity). However, there are two other important mechanisms that underlie MN Rin; leak and sag conductances. Dispersed throughout the membrane are voltage insensitive leak channels that are mainly selective for K^+ ions and their density per given unit of membrane helps determine specific resistivity and overall Rin. The amount of leak conductance is regulated by changes in second messenger systems (Gonzalez-Forero et al. 2007), neurotrophins (Gonzalez & Collins 1997), pH, neurotransmitters, and pharmacological agents. For example, in turtle MNs, the drug anandamide, decreased pH, and 5-HT_{1A} agonists can all block TWIK-related acid sensitive K^+ (TASK-1) leak channels, thereby increasing Rin,

subsequently increasing MN excitability (Perrier et al. 2003). Similar findings have been found in neonatal rat facial (Larkman & Perkins 2005; Larkman & Kelly 1992) and adult rat sacrocaudal (Harvey et al. 2006a) MNs.

The phenomenon of 'sag' was first illustrated in work by Ito & Oshima (1965). During low intensities of continuous and steady current injections the voltage response can be seen as slow 'sag' following the peak voltage (~15 ms) depolarization or hyperpolarization which declines gradually to a steady level at about 100 ms. It has been found that a hyperpolarization-activated current (I_h) which carries both Na^+ and K^+ ions, is voltage dependent, activated by potentials negative to ~-60 mV, has a reversal potential at ~-40 mV, and slowly inactivates underlie the 'sag' conductance (for review see Pape 1996; Robinson & Siegelbaum 2003; Rekling et al. 2000). The activation of sag conductance can lead to an underestimation of true MN Rin (Zengel et al. 1985; Gustafsson & Pinter 1984b; Burke & ten Bruggencate 1971) and should be taken into consideration during Rin measurements (Hochman & McCrea 1994). Similar to the leak conductance, 5-HT can also modulate I_h conductance, and subsequently MN excitability (Wang & Dun 1990; Kjaerulff & Kiehn 2001). Interestingly, MNs with low Rins tend to have a greater sag conductance than those with higher Rins (Gustafsson & Pinter 1985; Zengel et al. 1985).

The current intensity used to depolarize the MN's resting membrane potential to its voltage threshold (i.e. voltage at which an action potential is elicited) depends strongly on the MN's Rin. Thus, Rin is a very important measurement of excitability. Essentially higher Rin MNs require less current to drive the membrane potential to

the voltage threshold for an action potential. MN Rin has been shown to correlate to other MN properties and size. However, the multiplication of MN values for rheobase and Rin do not give actual voltage threshold values, indicating that factors other than rheobase and Rin are involved in determining the voltage threshold (Gustafsson & Pinter 1984c).

The Action Potential. When a MN is impaled with a microelectrode, action potentials can be elicited either orthodromically or antidromically. In general, the resting membrane potential for a MN is ~-70 mV (Coombs et al. 1955) for cats and rats. Upon receiving a depolarizing current or excitatory post synaptic current, the resting potential usually depolarizes by ~18 mV before an action potential (also referred to as a spike) is initiated. The action potential reaches peak amplitudes of 70 to 90 mV (positive overshoot reaching >0 mV) and lasts 1-2 ms. The spike portion of the action potential can be broken into two parts 1) the initial segment spike (IS) which is initiated near the IS or beginning of the axon and 2) somato-dendritic (SD) spike which represents the activation of the SD membrane. Both spikes occur during antidromically and orthodromically activated action potentials (Coombs et al. 1955) and are seen due to the regional differences in Na^+ ion channels (Safronov et al. 2000). When the membrane potential is hyperpolarized, only the IS spike can be initiated.

Once the action potential reaches its peak, a repolarization begins followed by an afterhyperpolarization (AHP). In spinal MNs the AHP has two components 1) fast (fAHP) which starts during the repolarization phase and lasts up to 10s of ms and 2) medium (mAHP) which activates rapidly following the action potential but decays

over several 100 ms. However, the presence of a third AHP (slow, sAHP) has been found in other neuron types (Sah 1996; Sah & Faber 2002). In cat MNs, the AHP reaches its peak amplitude and duration at ~10-20 ms and 200 ms, respectively (Kernell 1965c). The AHP is important for several reasons 1) it plays a key role in regulating MN firing frequency (Kernell 1965c; Brownstone et al. 1992; Baldissera et al. 1978; Brownstone 2006), 2) it is correlated to many other MN properties (Gardiner 1993; Zengel et al. 1985) and 3) its half-decay time has been instrumental to identifying MN type. For example, rat MNs are designated as fast or slow based on the half-decay time of the AHP (fast < 20 ms, slow > 20 ms) (Gardiner 1993).

Ion Channels of the Motoneurone. The seminal work on the giant axon of the squid by Hodgkin and Huxley (Hodgkin et al. 1952; Hodgkin & Huxley 1952b; Hodgkin & Huxley 1952a) along with the development of the patch clamp (Neher & Sakmann 1976; Neher 1992; Sakmann 1992) and with use of pharmacological agents has given major insight as to the mechanisms (see Hille 2001 for details), underlying the MN action potential. Work by Barrett & Crill (1980) illustrated that similar to the axon, cat MNs had similar time and voltage-dependent inward Na^+ conductances and outward K^+ conductances. A brief description on ion channels (excluding sub-types) located in the MN soma and dendtrites follows (for more information see reviews by Rekling et al. 2000; Russo & Hounsgaard 1996; Hille 2001; Sah & Faber 2002; Catterall 1995; Kernell 2006; McLarnon 1995).

There are two main types of sodium channels 1) fast transient Na^+ channels (I_{Nat}), which is responsible the up phase of the spike. When these channels are blocked by tetrodotoxin (TTX) the MN will no longer be able to elicit a spike. 2) persistent

non-inactivating Na^+ channels (I_{Nap}) activate below spike threshold and are very important for repetitive firing. When these channels are blocked by riluzole rhythmic firing ceases (Lee & Heckman 2001; Harvey et al. 2006c). The activation of both types of Na^+ channels are voltage dependent.

There are several types of K^+ channels whose role is to determine sub-threshold membrane behaviour, the shape of the action potential, and MN firing properties. 1) The K^+ leak channels (I_L) carry current out of the MN are the most important channels in determining the resting membrane potential and can be modulated in several ways (see above). 2) Inward rectifier K^+ channels (I_{Kir}) carry outward current that is reduced and increased by membrane depolarization and hyperpolarization, respectively. These channels help to stabilize the resting membrane potential and are voltage-dependent. If they are blocked in hypoglossal MNs by extracellular barium the membrane will depolarize and firing will occur (Rekling et al. 2000). 3) Delayed rectifier K^+ channels (I_{Kdr}) carry sustained outward current during depolarization. These channels are important during the repolarization phase of the spike and the fAHP. When blocked by external tetraethylammonium (TEA) there will be a lengthening of the spike duration and a blocking of the fAHP (Hounsgaard et al. 1988; Barrett et al. 1980). 4). Transient outward K^+ channels (I_A) are active during depolarization. When they are blocked by 4-aminopyridine (4-AP) there is a lengthening of the spike duration and a reduction in the fAHP (Hounsgaard et al. 1988). 5) Ca^{++} -activated K^+ currents flow through two channels, BK and SK. The BK channel ($I_{KCa\,(BK)}$) is both calcium- and voltage-dependent. This channel is selective for K^+ ions and is activated by an influx of Ca^{++} ions during the action

potential. When BK channels are blocked by external TEA the repolarization phase of the MN spike is prolonged and the fAHP is reduced (Umemiya & Berger 1994). The SK channel ($I_{KCa\,(SK)}$) is calcium-activated and voltage independent that carries $K^+$and underly the mAHP. When they are blocked by the bee venom apamin there is no mAHP (Hounsgaard et al. 1988) and firing frequency increases. (Miles et al. 2005). 6) Na^+ activated K^+ channels (I_{KNa}) play a role in MN repetitive firing by providing a net outward current and thus a hyperpolarizing affect on the MN (Powers et al. 1999). 7) A hyperpolarization-activated channel (I_h) is permeable to both Na^+ and K^+ but carries a net inward current both at rest and hyperpolarization. It opposes membrane hyperpolarization, gives rise to post-inhibitory rebound, sag (see above), and maintenance of resting membrane potential (McLarnon 1995; Pape 1996; Robinson & Siegelbaum 2003).

Finally, there are six types of calcium channels (L, N, P/Q, R, and T). The L, N, and P/Q types are high voltage activated and the T-type is low voltage activated. Although some L-type channels are low voltage activated. These channels carry Ca^{++} ions and affect the falling phase of the spike, afterdepolarization, and AHP (Hounsgaard et al. 1988; Harada & Takahashi 1983; Hounsgaard & Mintz 1988). One Ca^{++} channel that has received a lot of attention in recent years is the L-type (Hounsgaard & Kiehn 1989; Hounsgaard & Kiehn 1993). This channel which is blocked by nifedipine (Hounsgaard & Kiehn 1989; Li & Bennett 2003) slowly inactivates and along with the I_{NaP} acts as another source of persistent inward current (PIC) (Li & Bennett 2003). Together, these channels elicit MN plateau potentials which give them bistable behaviour and enable the MN to fire rhythmically for long

periods of time (Hounsgaard et al. 1988). The fact that these persistent ion channels are located on the dendrites and soma would suggest that they act as amplifiers for synaptic current and increase the gain of the MN (Grande et al. 2007; Hounsgaard & Kiehn 1993; Powers & Binder 2003; Heckman et al. 2004).

The idea of PICs in MNs was found in the late 70s and early 80s (Schwindt & Crill 1981; Schwindt & Crill 1977) when Schwint and Crill noticed that the MN demonstrated an inward deflection of current during a voltage ramp. PICs in MNs are depolarizing currents generated by non- or slow-inactivating voltage-gated Na^{+} and Ca^{++} (Li & Bennett 2003; Lee & Heckman 1999) ion channels (see above for details) and ligand-gated currents from NMDA receptors (Guertin & Hounsgaard 1998; Hochman et al. 1994). PICs are only manifested as plateaus when they are either directly facilitated or uncovered by reducing opposing outward currents (e.g., Ca^{++}-dependent K^{+} current). Thus, the PIC is considered to be the net persistent current from the combined inward and outward current sources. When the membrane potential is depolarized above the activation threshold (about –45 to –55 mV) PIC can mediate a plateau potential. A plateau potential can be initiated by a short depolarizing current and remain for a long period of time and act to amplify and sustain their motor output (Hounsgaard et al. 1988; Lee & Heckman 1998b; Bennett et al. 1998a; Bennett et al. 1998b; Hultborn 1999) until inhibited by a brief hyperpolarizing current (Hounsgaard et al. 1988; Kiehn & Eken 1998). Thus, a MN can behave in a 'bistable' manner; it can be toggled between an active and quiescent state. PICs are found in many types of cells in many different species (both

invertebrates and vertebrates), thus its biological significance must be of the utmost importance.

MN PICs are amplified by a host of neurotransmitters, neuromodulators and drugs (Heckman et al. 2004). Neuromodulatory input to a MN from the brainstem's ralphe nucleus and locus coeruleus release the monoamines 5-HT (Hounsgaard et al. 1988; Skydsgaard & Hounsgaard 1996)and NA (Lee & Heckman 2000), respectively in the dendrites can enhance the PIC and render the motoneurone as more excitable (Gilmore & Fedirchuk 2004). However, it was suggested that barbiturates inhibit PICs and plateau potentials (Hultborn & Kiehn 1992; Gandevia 2001) which is the case in turtle MNs (Guertin & Hounsgaard 1999) . Thus, experimental anesthetic plays a roll in the amount of PIC. To combat this problem, several investigators make use of the in-vivo cat decerebrate (Hounsgaard et al. 1988),(Lee & Heckman 1998b) (removal of the cortex and thalamus which alleviates the use of anesthetics) and in-vitro rat (Bennett et al. 2001) preparations. Both preparations also allow the addition of neurotransmitters and drugs to maximize PIC.

There is debate on the location and density of the known ion channels in the MN and whether or not some of these channels serve similar functions. It was once believed that persistent Ca^{++} channels were only located on MN dendrites (Hounsgaard & Kiehn 1993) but recent evidence suggest they are located on both soma and dendrites (Moritz et al. 2007; Zhang et al. 2006; Brownstone 2007). There is work indicating that the persistent and transient Na^{+} channels are actually the same channel but have different activation mechanisms (Taddese & Bean 2002; Brown et al. 1994; Crill 1996). The highest density of transient Na^{+} channels is located in the

initial segment but it remains unknown how many exist along the soma and into the dendrites. These channels must be in the soma and dendrite, since the action potential can be back propagated along initial portions of the dendrites with little or no decay (Larkum et al. 1996). Finally, differences in preparation type (species, developmental state, MN type, anesthetic etc.) give us different answers on ion channel types involved in MN output. PICs are mediated by L-type Ca^{++} channels in turtle and mouse MNs (Carlin et al. 2000a; Carlin et al. 2000b; Hounsgaard & Mintz 1988), where as the same channels only carry ~ 6% of the PIC current in neonatal rat facial and hypoglossal MNs (Umemiya & Berger 1994; Plant et al. 1998).

Motoneurone Active Properties. Injecting current and/or voltage into a MN are two ways to measure MN active properties. Active properties involve a combination of factors working together to produce a train of action potentials. The appearance (i.e. firing frequency) of the train of action potentials depend on MN type, the types of ion channels activated and the amount of current required for rhythmic threshold of firing (I_{th}). The 'supra-threshold current pulse' required for a MN to continuously fire is typically 1.5x and 1.4x the rheobase current for cats and rats, respectively (Granit et al. 1963; Kernell 1965a).

When MNs are injected with a sustained current pulse above that required for rhythmic firing, the MN can usually fire continuously for the pulse duration. As the current intensity increases the firing frequency increases until accommodation occurs (Granit et al. 1963; Kernell 1965a). The f-I relationship was first illustrated by Granit et al. (1963) in rat MNs and later more extensively studied in cat MNs (Kernell 1965a; Schwindt 1973). The f-I relationship can be described by two or sometimes

three linear relationships. There is a lower range of MN firing frequency referred to as the 'primary range of firing' and a much higher firing frequency referred to as the 'secondary range of firing'. At a certain current-intensity the f-I relationship slope suddenly and sharply increases indicating a jump from the primary to secondary range of firing. During high intensity current pulses there is sometimes a third range of firing referred to as the 'tertiary range of firing' with a slope similar to the primary range (Schwindt 1973). The primary range of steady-state firing frequencies and the mean current intensities range from 10 -90 Hz and 7.5 – 22 nA, respectively for cat MNs with a slope of 1.4 Hz/nA (Kernell 1979; Kernell 1992). In the secondary range of firing, steady-state frequencies can reach up to 200 Hz with a slope 5-6 times greater than the primary range (Kernell 1965b). Rat MNs can fire up to 70 Hz with a slope of 4 Hz/nA (Cormery et al. 2005) in the primary range. However, there is little information on secondary range of firing in rat MNs injected with square-wave current pulses.

The mechanisms underlying the sudden change in the f-I slope remain unknown. A model developed by Kernell (1968), predicted that the f-I slope could be increased by 1) decreased AHP amplitude, 2) decreased AHP duration, 3) decreased voltage threshold for spike initiation, and 4) less negative equilibrium potential for K^+. When AHP amplitude or duration is decreased in experimental conditions the f-I slope does increase (Hounsgaard et al. 1988; Gazzoni et al. 2005) and vice versa (Beaumont et al. 2004). It could be hypothesized that the activation of PICs may also be involved in increasing the f-I slope (see below for details).

MNs subjected to a supra-threshold long lasting square-wave pulse lasting longer than several 10s of ms to > 30 s undergo spike frequency adaptation (SFA). SFA is a time dependent decrease in the rate of MN action potential discharge and is commonly seen across many species (cat, rat, mouse, turtle) (Gorman et al. 2005; Miles et al. 2005; Zeng et al. 2005; Spielmann et al. 1993) and other types of neurones (reviewed in Sawczuk et al. 1997). Typically MN SFA is measured by injecting several different supra-threshold current pulses either intracellularly (Granit et al. 1963; Sawczuk et al. 1995; Kernell & Monster 1982b; Magarinos-Ascone et al. 1999; Botterman & Cope 1986) or extracellularly (Spielmann et al. 1993) for a few hundred ms up to several minutes. However, 30 s is sufficient to determine the full time course of SFA (Sawczuk et al. 1995). Increased current to the MN results in higher initial spike discharge (as high as 500 Hz) (Granit et al. 1963; Botterman & Cope 1986) and subsequently a greater extent of adaptation (Kernell & Monster 1982b). MN SFA has been mathematically defined by two separate methods 1) the time constant of the exponential decay during the early and later phases of SFA (Kernell & Monster 1982b; Spielmann et al. 1993; Granit et al. 1963; Gorman et al. 2005) and 2) the decrease in the frequency or number of spikes produced over a given amount of time by either the drop in instantaneous firing frequency or as the drop in area under the frequency-time curve over 30 s (Hornby et al. 2004; Botterman & Cope 1986; Spielmann et al. 1993; Kernell & Monster 1982b; Gorman et al. 2005).

MN SFA can be described by three phases: 1) initial adaptation or a linear decrease in spike discharge over the first two or three spikes, 2) early adaptation or an exponential decrease in spike discharge over the first couple of seconds, and 3) late

adaptation or an exponential decrease in spike discharge over several seconds to minutes (Sawczuk et al. 1997; Powers et al. 1999; Zeng et al. 2005; Sawczuk et al. 1995; Kernell & Monster 1982b; Kernell 1965a; Spielmann et al. 1993; Granit et al. 1963). Each phase have several possible mechanisms that contribute to the decrease in spike discharge rate which (see Table 1 of Sawczuk et al. 1997). However, in spinal MNs, the most likely mechanisms underlying initial SFA include: 1) summation of the medium afterhyperpolarization (AHP) amplitude (Baldissera & Gustafsson 1974; Powers et al. 1999; Kernell 1972) which is mediated by the Ca^{++} - activated K^+ channel and 2) a fast inactivation of the transient Na^+ channel (Schwindt & Crill 1982; Powers et al. 1999). Early and late adaptation is probably due to slow inactivation of the transient Na^+ channel (Miles et al. 2005; Powers et al. 1999). Other possible mechanisms underlying initial SFA in other types of MNs and neurones include inward rectifier channel deactivation and for early and late SFA; Na^+ PIC inactivation, sAHP, delayed rectifier inactivation, N^+-K^+ ATPase activity, and saturation of Ca^{++} sequestering systems (reviewed in Sawczuk et al. 1997; Powers et al. 1999). PICs probably do not have a major role in determining the pattern of SFA (Zeng et al. 2005; Miles et al. 2005). It is surprising that the blockage of the PIC Na^+ channels does not affect SFA since they are required rhythmic firing initiation and maintenance (Lee & Heckman 2001; Harvey et al. 2006c). There must be other mechanisms working together to compensate for this none change in SFA after blocking Na^+ PIC.

Another way to measure a MNs f-I relationship is by current-clamp technique in a form of a triangular current pulse (ramp) (Hounsgaard et al. 1988; Lee &

Heckman 1998b; Bennett et al. 2001). This technique is used extensively with voltage ramps (Bennett et al. 2001; Schwindt & Crill 1982; Schwindt & Crill 1977; Wu et al. 2005) (holding the MN membrane at steady linear voltages to measure current changes) to induce the activation of PIC channels and quantify the amount of PIC. Square-wave current pulses along with concomitant bias current have also been used to activate PIC channels (Heckman et al. 2004; Conway et al. 1988; Bennett et al. 2001).

The firing pattern of MN plotted from a ramp current illustrates the plateau current as a counter-clockwise f-I hysteresis (Hultborn 1999; Hounsgaard et al. 1988). The post-rise in firing frequency remains higher compared to pre-rise in firing frequency even during a reduction in injected current. The PIC amplitude is estimated by subtracting the current at which spike 'derecruitment' occurs from the current at which spike 'recruitment' occurs and gives similar amplitudes as voltage clamp (Li & Bennett 2003).

MNs injected with RAMP currents can be categorized into four f-I relationship types 1) linear, 2) adapting, 3) linear + self sustained firing, and 4) acceleration (Bennett et al. 2001). Type 1 MN f-I relationship demonstrates a firing frequency slope that overlaps on the ascending and descending portions of the ramp current, Type 2 MN f-I relationship demonstrates a clockwise hysteresis (i.e. MN firing rate adaptation) where the firing frequencies are greater during the ascending versus the descending portion of the ramp at any given current, Type 3 MN f-I relationship demonstrates a linear regression line with some self-sustained firing corresponding to tertiary range of firing (Li et al., 2004) (i.e. activation of a PIC) and

Type 4 MN f-I relationship demonstrates a counter-clockwise hysteresis. Firing frequencies are greater during the descending versus the ascending portion of the ramp at any given current. Furthermore, when an excitatory synaptic current is added upon the ramp current there is perhaps a greater activation of the PIC, and a further facilitation of the MNs firing frequency (Bennett et al. 1998b).

Differences in f-I relationship types 3 and 4 may be due to differences in PIC type and channel saturation. The PIC in Type 3 may be mediated through sodium and calcium channels activated prior to the start of rhythmic firing while the PIC in type 4 may be mediated through an L-type calcium channel activated at a voltage threshold higher than that required for rhythmic firing (Li & Bennett 2003). The Type 3 f-I relationship may activate the calcium PIC in a graded manner (i.e. it is saturated) upon which additional increases in input result in minimal changes in firing. During a type 4 f-I relationship the calcium PIC is perhaps activated upon MN recruitment, leading to a steep increase in the firing frequency coinciding with the secondary range of the f-I relationship. Once the Ca^{++} PIC is saturated the slope of the f-I relationship is then reduced, corresponding to the tertiary range of firing (Elbasiouny et al. 2005). Therefore, PIC may help to determine the slopes in the f-I relationship and increase the MNs excitability.

In general, ramp currents are not used to identify maximum firing frequencies. The current must be injected into the MN slowly in order to activate the PIC channels. A time delay of more than 6 seconds between current injections is required to avoid the phenomenon known as 'warm-up' (i.e. the drop in plateau threshold with each successive RAMP) (Bennett et al. 1998a).

Section 3 – Motoneurone Types and Correlations amongst Properties. MNs can be categorized based on the muscle fiber type they innervate. Table 1 is a summary of both cat and rat MN properties and their values based on innervated fiber type. The nomenclature for MNs include 1) fast fatigable (FF) which innervate fast glycolytic muscle fibers, 2) fast resistant (FR) which innervate fast oxidative glycolytic muscle fibers, and 3) slow (S) which innervate slow muscle fibers.

The size of the soma amongst different MN types is very similar for cat. However, when the total membrane area is calculated distinct differences are seen, which is probably due to the differences in dendrite numbers and their diameters. The average diameter of the stem dendrites were ranked as FF > FR > S (Burke et al. 1982). Fast MN axons are also bigger and have more collateral swellings (only for FF) than slow MN axons which are probably why fast MN axon conduction velocities are also higher (Cullheim & Kellerth 1978b; Burke et al. 1982).

MN type can also be divided on the basis of different passive and action potential properties. An extensive study by Zengel et al. (1985) predicted motor unit type of cat gastrocnemius MNs based on their properties. They found that membrane time constant and Rin increased in the order of FF < FR < S, which was opposite for rheobase. The AHP magnitude, duration and half decay time and axon conduction velocity were all significantly greater for fast MNs compared to slow MNs, with no differences amongst fast MN types. Based on a discriminant analysis program used to classify motor unit type, the values they had measured of the MN properties could predict motor unit type to a very high degree. The combination of rheobase and Rin

could classify 36/37 cells properly. Thus, MN rheobase and Rin are significantly correlated (negatively) and indicative of MN type. Work by Gustafsson & Pinter (1984b) also provided information relating MN size to MN passive properties. They found that a positive correlation existed between Rin and membrane time constant. However, there was considerable overlap of Rin and time constant amongst MNs of different sizes. More importantly, the relationship between Rin and AHP duration (i.e. cells with lower Rin have shorter AHP durations) was due to increased membrane resistivity. Thus, the membrane resistivity may be a better predictor of MN type. Gustafsson & Pinter (1984c) also showed that rheobase correlated well with input conductance and AHP duration and MNs with smaller rheobases generally have lower voltage thresholds. Furthermore, MNs are most often recruited based on their size in the order from smallest to largest (Henneman et al. 1965)

Literature identifying differences among rat MN types is sparse and not as clear cut as in the cat. To date there are no studies which discuss differences in MN type (i.e. FF vs. FR. vs S) based on geometrically measured sizes. Gardiner (1993) found no differences in the AHP properties, Rin, rheobase and axon conduction velocity among the fast MNs. However, each of these properties is significantly different between fast and slow MNs. The AHP half decay time is probably the best indicator of whether or not a MN is fast (< 20 ms) or slow (> 20 ms) which is significantly correlated with Rin and there was a significant correlation between Rin and rheobase. Thus, like cat MNs Rin and rheobase are good indicators of MN type.

MN passive properties also correlate to active properties. MNs with lower minimum and maximum firing frequencies have lower rheobases and higher Rin s

and AHP properties (Cormery et al. 2005). However, the slope of the f-I relationship does not seem to differ between MN types (Cormery et al. 2005). An increased rate of SFA has been shown to correlate with motor unit properties that are seen in motoneurones with higher rheobase currents and lower Rins. As motor units are recruited from type slow to type fast the conduction velocity increases, fatigue index decreases, twitch contraction times decrease and peak tetanic forces increase (Burke et al. 1973; Burke 1967) all of which have been found to correlate with the rate of MN SFA (Kernell & Monster 1981; Spielmann et al. 1993; Kernell & Monster 1982a). Kernell & Monster (1982a) showed that fast motor units demonstrate much greater rates of SFA, perhaps relating to greater muscle fatigue, compared to slow motor units. The rate of MN firing is inversely related to AHP duration. MNs with shorter AHP durations tend to fire faster (Kernell 1965b; Kernell 1965a; Kernell 1965c; Cormery et al. 2005) and have higher rates of SFA (Kernell 1965b; Kernell & Monster 1982a). However, AHP is probably not the sole determinant of MN rhythmic firing rate (see review by Stauffer et al. 2007).

Finally, fast and slow MNs demonstrate similar PIC amplitudes but slow MNs are more bistable. PIC channels probably inactivate quicker in fast MNs. However, bistable MNs tend to have lower rheobase current than low-bistable MNs (Lee & Heckman 1998b). Furthermore, MNs innervating the postural muscles (triceps surae) are more likely to demonstrate bistability (Hounsgaard et al. 1988; Conway et al. 1988). Self sustained firing via PIC would be advantageous for maintaining force output during postural tasks without voluntary activation from supra-spinal sources

(i.e. the soleus muscle is innervated by mainly slow MNs = bistability) (Alaburda et al. 2002).

Generally it can be said that MNs with low reobases, high Rins, and longer AHP half decay times are typically smaller, more bistable, have decreased SFA and are more excitable. Although there is considerable overlap amongst MN types and their property values a distinction is easily seen, not necessarily amongst fast MN types but rather between fast and slow MNs.

Section 4 –Motoneurone Properties Following Spinal Cord Injury. How do MN electrophysiological properties change when their activity has been altered? There are many animal models developed to explore this question but the focus here will mainly be on decreased MN activity via spinal cord transection. Table 2 lists a comparison for each of cat and rat MN electrophysiological properties from before to after spinal cord transection (ST).

ST is a complete spinal cord transection usually around the mid-thoracic level which removes descending input to MNs below its level. ST is probably the most utilized model to determine how elimination of descending input to MNs affects their properties. After four weeks of ST, the biophysical properties of MNs below the site of the insult undergo significant changes. Cat MNs generally have depolarized voltage thresholds, increased rheobase currents, and decreased afterhyperpolarization (AHP) time course, membrane time constants and cell capacitiance (Czeh et al. 1978; Hochman & McCrea 1994; Cope et al. 1986). Rat MNs have depolarized RMPs and voltage thresholds and a shift to the right in the f-I relationship indicating a decrease in MN output (Beaumont et al. 2004). Furthermore, since ST eliminates supraspinal

control of neurons below the transection site, there is an increase in spastic contractions that may reflect the activation of voltage-dependent persistent inward currents (PIC) (Bennett et al. 2001), which enhances MN excitability or polysynaptic reflexes. Increased spasticity after ST allows MNs to endure significant amounts of activity. This is probably due to the reflex circuit from muscle to MN being left intact and is evidenced by muscle electromyography (EMG) activity after ST only being reduced by ~50-75% (Ishihara et al. 2002).

Spinal cord isolation (SI) on the other hand, is a procedure involving complete spinal cord transections at lower thoracic and higher sacral levels and complete bilateral dorsal rhizotomy between transections. The SI model abolishes segmental reflexes (Pierotti et al. 1991) and the hindlimb muscles are almost completely quiescent such that the integrated EMG of the soleus muscle of SI rats is < than 1% of normal control values (Roy et al. 2007b; Gomez-Pinilla et al. 2004). Therefore SI removes descending, ascending and afferent synaptic activity onto the MNs of interest. The main difference between ST and SI is that following SI MNs are no longer reflexively activated. However, literature on the electrophysiological properties of SI MNs is very sparse. After two to three weeks of ST along with a bilateral deafferentation, which is very similar to the SI model, MN electrotonic lengths in cat MNs decreased and Rins and excitatory post synaptic potentials (EPSPs) increased, suggesting an overall atrophy of MNs (Gustafsson et al. 1982).

Mechanisms Underlying Motoneurone Electrophysiological Property Change after Disuse. How do changes in neurotrophins or monoamines lead to chronic alterations in MN electrophysiological properties? Two models have been proposed

to describe the intracellular pathways underlying such changes. Gardiner (2006) has proposed that altered activity results in changes in Ca^{++} entry into the MN as well as neurotrophins which results in a series of phosporylation events, changes in gene expression and protein synthesis of ion channel subunits and subsequently ion channel profile, location and distribution. It has been reported that different neurotrophins promote similar activation of initial signal transduction events but induce a unique pattern of expression of ionic currents thereby giving different excitable phenotypes (Lesser et al. 1997) and perhaps MN electrophysiological properties. For example, after exercise the action potential has a faster rise time (Beaumont & Gardiner 2003). The prime mechanism underlying this newly developed action potential would be the phosphorylation of the Na^{+} channel which could lead to changes in the RMP, voltage threshold, and firing frequency (Cantrell & Catterall 2001).

The other model comes from work on Aplysia neurones. MNs can become sensitized to a stimulus leading to hyperpolarized RMPs and voltage thresholds with a tendency to have decreased Rin and increased firing frequencies per unit of current (Cleary et al. 1998). Sensitization is a form of non-associative learning in which an animal's response to a weak stimulus is enhanced after another strong stimulus. The mechanisms underlying short- and long-term synaptic plasticity to sensitization have been proposed by Byrne & Kandel (1996). Facilitation produced by different lengths of exposure of 5-HT lead to the phosphorylation of different sets of substrate proteins. Protein kinase A (PKA) pathway appears to be involved in the early effects of 5-HT on protein phosphorylation whereas protein kinase C (PKC) is involved at later times.

PKC can down regulate the 5-HT-induced increase in cyclic adenosine monophosphate (cAMP), perhaps via action on the receptor coupled to adenylyl cyclase. PKA and PKC plays a primary role in 5-HT-induced synaptic facilitation through the modulation of membrane ion channels and spike duration-independent processes. The addition of 5-HT to neonate rat MNs induce a voltage threshold hyperpolarization (up to 14 mV) (Gilmore & Fedirchuk 2004) which can also be influenced by PKC via modulation of Na^+ currents (transient and persistent, Dai et al., submitted). Both models give insight to how MN properties change after chronic injury.

Although MN size and electrophysiological properties change after injury heterogeneity is still maintained amongst the MN pool. Furthermore, the change in electrophysiology is significant for the properties that do change while many properties are unaffected. One reason for this is substances (neurotrophins, proteins, etc.) are transferred between muscle and MN and vice-versa. Cross talk amongst muscle and MN can be illustrated by several models of altered activity. First is cross-reinnervation of nerve onto muscle. When the medial gastrocnemieus (MG) nerve is cut and replaced to innervate the lateral gastrocnemieus (LG) and soleus (SOL) muscles, MG MN properties become like those innervating the LG and SOL muscles. Furthermore, the LG and SOL muscle fiber types can change (Foehring et al. 1987a; Foehring et al. 1987b). Second is axotomy, which severs the MN axon leading to a broken connection between MN and muscle. After axotomy some properties of MNs become more uniform (Kuno et al. 1974) and fast MNs become slower (Gustafsson & Pinter 1984a). Third is hindlimb unweighting (HU) which reduces weight bearing by

suspending the hindlimbs using a body harness or tail cast. After 2 weeks of HU, MNs have decreased AHP amplitudes and cell capacitances and increased rheobase currents and minimum and maximum firing frequencies. Thus, electrophysiological properties that are typical of slow MNs are converted to that seen in fast MNs (Cormery et al. 2005), which match the slow-to-fast muscle phenotype conversion after unweighting (Talmadge et al. 1996). Finally, nerve conduction blockage of the action potential by TTX that does not block cross-talk between MN and muscle only minimally affects rat MN properties (Cormery et al. 2000; Gardiner & Seburn 1997).

Following ST the muscle and MN still remain intact allowing for cross-talk to continue. Neurotrophins are important for MN survival and maintenance and may modulate the expression of ion channel sub-units that render the MN more or less excitable (Lesser et al. 1997; Rose et al. 2004). Neurotrophins are transported from the muscle to the MN (retrograde) and from the MN to the muscle (anterograde) (Mitsumoto & Tsuzaka 1999). After spinal cord injury, the ventral horn has lower levels of brain-derived neurotrophic factor (BDNF), and neurotrophin 3 (NT-3) proteins and mRNA (Gomez-Pinilla et al. 2004). Recent evidence suggests that BDNF promotes the development of neuronal lipid rafts (Suzuki et al. 2007) which compose the MN membrane and its constituents. Interestingly, there is no difference in the expression of neurotrophins between fast and slow MNs (Copray & Kernell 2000). Finally, MN properties in ST rats are maintained near control values when fetal tissue, which contains neurotrophins, is transplanted into the spinal cord immediately after the transection (Beaumont et al. 2004). A decrease in neurotrophin activity in the spinal cord after ST may affect the number, density, composition,

activation, and/or location of the MN ion channels thereby altering their conductance and subsequently eliciting changes in MN electrophysiological properties. Because MN properties change, neurotrophins are therefore not suffiecient to maintain all of the MN properties.

An increase in the presence of PIC is another indication that MN ion channel profiles and other receptors may have changed after ST. ST MNs may be more sensitive to 5-HT and NA. After acute ST, descending input from the brainstem is terminated and facilitation of the PIC by 5-HT and NA is compromised. Four weeks later, ST MNs become supersensitive to 5-HT and NA and small amounts of exogenous application of each are sufficient to activate their receptors (Harvey et al. 2006a; Rank et al. 2007) or there is an increase in MN sensitivity to residual endogenous 5-HT in the spinal cord (Harvey et al. 2006b) both of which enhance PIC and increase MN bistability. On the other hand these receptors may become constituatively active, thus increasing the PIC (Li et al., 2007). Thus, weeks after spinal cord injury, MNs develop large PICs that cause sustained reflexes and associated muscle spasms. The increased spasticity does not appear to involve changes in glutamatergic or glycinergic inputs to sacrocaudal motoneurons (Kitzman 2007).

A reduction in f-I slopes following ST of rats indicates a decreased input-output gain of the MN and a change to the ion channel profile. Because, a decrease in AHP amplitude increases the f-I slope (Hounsgaard et al. 1988; Hounsgaard & Kiehn 1989; Hultborn et al. 2004), the most logical explanation for the smaller MN f-I slope following ST is due to changes in AHP properties, which have been reported

for MNs of ST rats previously (Petruska et al. 2007; Beaumont et al. 2004), but not in rat sacral cord MNs (Li et al., 2007). However, MNs of cats subjected to ST with a bilateral deafferentation have no changes seen in the f-I slope (Gustafsson et al. 1982). It remains unknown if ST affects MN SFA. But, considering the above changes to MN properties following ST, one would expect that SFA will be altered after ST.

There are several other reasons why MN properties may change after injury. After spinal cord injury several inputs onto MNs are inhibited. Vestibulospinal, rubrospinal, and pyramidal tract inputs which provide effective synaptic hyperpolarizing and depolarizing currents (Grillner et al. 1970; Powers et al. 1993; Binder et al. 1998) are all cut off from the MN, inerneurones, and renshaw cells. Rubrospinal and pyramidal tract inputs tend to provide greater effective depolarizing current to high threshold MNs (i.e. fast) and inhibit low threshold MNs. Thus, a loss of these inputs may lead to changes in MN morphology and electrophysiological properties.

MNs become smaller after ST. Morphologically, MN soma sizes show either no change (Chalmers et al. 1992) or become reduced (Kitzman 2005) after ST. There is a loss, however, in the number of primary, secondary, and tertiary dendrites (Kitzman 2005; Bose et al. 2005; Gazula et al. 2004a). Due to a trimming of the dendritic tree after spinal cord injury, the overall MN size will become smaller whether or not the soma size is affected. The reported reductions in rat MN cell capacitance following ST (Beaumont et al. 2004) and decrease in electrophysiologically calculated MN diameter of cat MNs following ST with a

partial dorsal rhizotomy (Gustafsson et al. 1982) further suggest that chronic inactivity may diminish overall MN size.

Interestingly, increased activity to MNs changes some properties in the opposite direction compared to that of decreased activity. MNs of rats trained on voluntary wheel cages or a treadmill demonstrate a significant hyperpolarization of the RMP and spike threshold, increased AHP amplitude, and a faster antidromic action potential rise time (Beaumont & Gardiner 2003; Beaumont & Gardiner 2002). Training also increases; 1) base-line fast axon transport (Gharakhanlou et al. 1999), 2) calcitonin gene-related peptide (CGRP), a myotrophic factor that influences the expression of acetylcholine receptors at the neuromuscular junction when it is co-released with acetylcholine (Gharakhanlou et al. 1999), 3) quantal contents and sustained quantal release at their neuromuscular junctions (Desaulniers et al. 2001) all of which indicate an altered metabolism and 4) dendritic arbors (Clark et al. 2006). In addition, MNs increase expression of the neurotrophin brain –derived neurotrophic factor (BDNF) and of its receptor tyrosine kinase B (trkB) after acute electrical stimulation of it's severed axon (Al-Majed et al. 2000). After ST, MN property values are reverted towards control values after fetal tissue transplants and/or passive cycling exercise (Beaumont et al. 2004), or step training (Petruska et al. 2007; Gazula et al. 2004a), probably because of increased neurotrophin levels (Beaumont et al. 2004; Gomez-Pinilla et al. 2001; Li et al. 2007; Qin et al. 2006) and other factors mentioned above (for example, regrowth of dendritic arbors, (Gazula et al. 2004a).

Section 5 – Motoneurone Properties in Humans. Currently there is no way of recording intracellularly from MNs in humans. Motor unit recordings have provided

the most information in relation to how human MNs work. Evidence has illustrated that human MNs may be recruited (Stephens & Usherwood 1977), fire at similar frequencies (Monster & Chan 1977; de Luca et al. 1996), have similar speed match between AHP duration and muscle unit (Gossen et al. 2003), adapt (Macefield et al. 2000), and undergo plateau potentials (Gorassini et al. 1998; Gorassini et al. 2002a) and warm-up (Gorassini et al. 2002b) in a similar manner as rat and cat MNs. Human MN excitability can be tested via the Hoffman Reflex (H-reflex) and is used to determined changes in MN excitability after altered activity (Duchateau & Hainaut 1990). Typical responses are similar to those (Sale et al. 1982) seen in animals (Wolpaw & Tennissen 2001). Human MN active properties probably behave similar to that of rats following spinal cord injury or reduced activity. After 6-8 weeks of immobilization of the adductor pollicis and first dorsal interosseus muscles in humans, maximum motor unit firing frequencies decline ~ 50%. Furthermore, after spinal cord injury human motor units spontaneously fire with increases in frequency in response to afferent activity (i.e. bistable behaviour) (Cope et al. 1986) and remain active for long periods of time, presumably due to plateau potentials (i.e. activation of PICs) (Gorassini et al. 2004), both of which may contribute to spasticity.

Section 6 – Conclusion. A lot of work has been done over the years to quantify MN properties in many different species and following many types of interventions. At the present time much work is being completed on the underlying mechanisms for these properties and how and why they change after injury. MNs are formed by a flexible but complex interaction system composed of morphological, electrophysiological and molecular properties (ion channels, receptors,

neurotransmitters, intracellular signaling pathways and etc.) that work together to interpret and transduce incoming and outgoing activity, respectively. These properties dictate; 1) how a MN reacts to small voltage transients, 2) how a MN forms an action potential or train of action potentials, and 3) MN sensitivity to various extracellular and intracellular signals. Not all MNs innervating any given muscle are the same in these properties. MN functional properties covary with the properties of muscle fibers. If muscle fiber types change in their properties, their innervating MNs may follow suit. This may be the case after a spinal cord injury where it is known that both the MN and muscle fibers undergo significant changes. However, our understanding of the mechanisms governing MN change after spinal cord injury is just at its inception. Hopefully, the reduced animal model will continue to give insight on how human MNs may function before and after injury.

Finally, the literature reporting MN properties and the effects of decreased activity on these properties is inconsistent. For example, it has been reported that MN AHP durations tend to become faster, rheobase increases and there is no change in the f-I slope after periods of decreased activity in cat (Cope et al. 1986; Hochman & McCrea 1994; Czeh et al. 1978), however, this is not the case in the rat (Beaumont et al. 2004; Petruska et al. 2007; Cormery et al. 2005). One must consider: differences in the decreased activity models, duration of decreased activity, differences in electrophysiological techniques, species, MN type and muscle type.

Section 7- Hypotheses and Rationale for Rat Motoneurone Projects

Overall this dissertation presents a body of work pertaining to rat hindlimb MN properties. Although, many of the passive properties have been well quantified

in the literature, the active properties have not. The first two projects focus on implementing two separate techniques to describe and measure active properties that have not been quantified in adult rat hindlimb MNs. The third project utilizes the findings from the first two projects to determine the effects of 4 weeks of SI on these properties and others. To my knowledge the SI model has never been used for the purpose of measuring the electrophysiological properties of MNs. The following includes the title, hypothesis and rationale for each body of work presented in chapters 2, 3, and 4 of this dissertation.

TITLE 1 – Frequency-current relationships of rat hindlimb α-motoneurones

Hypothesis 1: PICs will be activated by the injection of RAMP current pulses into lumbar MNs of anaesthetized rats.

Rationale 1: One way to measure the activation and amplitude of PICs in vivo is by current-clamp in a form of a triangular current pulse and plot the subsequent f-I relationship patterns (Bennett et al. 2001; Hounsgaard et al. 1988; Lee & Heckman 1998b). The PIC amplitude is estimated by subtracting the current at which MN rhythmic firing spike-derecruitment occurs from the current at which MN rhythmic firing spike-recruitment occurs. It has been suggested (Hultborn & Kiehn 1992; Hultborn 1999) and found (Guertin & Hounsgaard 1999) that PICs are substantially decreased when animals are anaesthetized with barbiturates. Since we anesthetize rats with a ketamine/xylazine (ketamine is an N-methyl-D-aspartate receptor antagonist (Liu et al. 2001) and Xylazine is an alpha 2-adrenoceptor agonist) mixture, PICs will be activated during ramps. Finally, the presence of PIC in adult rat hindlimb MNs has not been repoted in the literature.

TITLE 2 – Spike frequency adaptation of rat hindlimb motoneurons

Hypothesis 2: Rat hindlimb MNs will demonstrate a variety of SFA patterns that are not current-dependent and will correlate to MN excitability.

Rational 2: MN SFA has been mathematically defined by 1) the time constant of the exponential decay in spike discharge rate during the early and later phases of SFA (Kernell & Monster 1982b; Spielmann et al. 1993) and 2) the decrease in the instantaneous discharge frequency or number of spikes over a given time period (Hornby et al. 2004; Botterman & Cope 1986). However, both measures can be problematic. Thus, we wanted to develop a simple method of quantifying SFA and determine if SFA is current-dependent. Furthermore, we wanted to develop an SFA index and determine if these correlate well with MN properties and are sensitive to a variety of SFA patterns. We also sought to develop a way to compare SFA across different physiological interventions used to alter MN activity. Since we have demonstrated (Button et al. 2006) that hindlimb MNs of rats anesthetized by a ketamine/xylazine mixture demonstrate the presence of PICs, we will use our *in vivo* rat preparation determine whether or not MN PIC correlates with MN SFA. Previously, this was not possible in *in vivo* experiments because animals (Spielmann et al. 1993) were anesthetized with pentobarbital (Kernell & Monster 1982b), which abolished PICs. Finally, SFA of adult rat hindlimb MNs has not been demonstrated in the literature.

TITLE 3 - Does elimination of afferent information via dorsal roots modify the changes in rat motoneurone properties that occur following chronic spinal cord transection?

Hypothesis 3: In SI, the ablation of ascending and afferent inputs in addition to the spinal transection will have a more pronounced effect on MNs than the lack of descending inputs induced by ST alone.

Rationale 3: After ST the electrophysiological properties of MNs below the site of the lesion undergo significant changes. Although ST eliminates supraspinal input to neurons below the transection site, the afferent connections are intact and significant activity levels remains in the muscle (Alaimo et al. 1984; Ishihara et al. 2002), probably due to the activation of intact segmental reflexes (Li & Bennett 2003). The relatively high amount of residual neuromuscular activity after ST may help maintain the biophysical properties of the affected MNs. To address this issue, we used the SI model which combines ST with surgical ablation of afferent and ascending inputs (Grossman et al. 1998). The SI model abolishes segmental reflexes (Pierotti et al. 1991) and the hindlimb muscles are almost completely quiescent such that the integrated EMG of the soleus muscle of SI rats is < than 1% of normal control values (Roy et al. 2007b; Gomez-Pinilla et al. 2004). Unlike chronic ST, spasticity does not develop following chronic SI, myofibers undergo severe atrophy and remain atrophied, and myofiber types are transformed to predominantly fast type with no reverting back to those seen in controls (Harris et al. 2007). Furthermore, SI has a more pronounced affect on muscular force properties and different myosin heavy chain proportions than ST (Roy et al. 2002; Talmadge et al. 2002; Grossman et al. 1998). Despite the known effects of SI on muscle, the effect of SI on MN biophysical properties remains unknown.

TABLES

MOTONEURONE PROPERTY	CAT: Motoneurones types innervating the Gastronemieus					RAT: Motoneurones types of Tibial Nerve		
	S	**FR**	**Fint**	**FF**	**Ref.**	**S**	**F**	**Ref**
Morphology								
1. Soma Diameter (μm)	49	53	?	53	3	35.2	SeeT	6
2. Total Membrane Area (x 10^3 μm^2)	249	323	?	369	3	151	SeeT	6
3. Stem Dendrite Number	10	12.6	?	12	3	8.0	SeeT	6
4. Axon Diameter (μm)	6.4	7.4	?	7.4	4	5.0	7.0	5
5. Axon Collateral Swelling number	44.4	54	?	98	4	?	?	
Passive Properties								
1. Electrotonic Length (λ)	1.4	?	?	1.6	2	1.6	1.4	4
2. Cell Capacitance (nF)	4.0	6.0	?	6.4	12	2.6	3.6	4
3. Tau (ms)	10.4	8	5.3	5.9	1	3.6	3.1	4
4. Input Resistance (MΩ)	1.6	0.9	0.7	0.6	1	3.3	1.4	1
5. Specific Resistivity (Ω/cm^2)	>2000	<2000	<2000	<2000	3	5300	SeeT	7
6. Sag	-	+	?	++	1	?	?	
Action Potential								
1. Spike height (mV)	91.9	93.1	?	89.5	5	79	74	3
2. RMP (mV)	-72	-75	?	-75	5	-61	-60	3
3. Threshold Depolarization (mV)	14.4	18.5	?	20.1	5	21	18.5	3
4. Rheobase Current (nA)	5.0	12	16.8	21.3	1	2.3	3.8	1
5. AHP amplitude(mV)	4.9	4.3	2.8	3	1	4.5	2.5	1
6. AHPduration (ms)	161	78	63	65	1	75	54	2
7. AHP ½ decay time (ms)	44	22	17	18	1	30	14	1
8. ACV(m/s)	86	100	104	99	1	50	60	1
Active Properties								
1. Bistability	+++	?	?	+	11	?	?	
2. I_{th} for rhythmic firing	7.5	11	?	22	6	8	11	8
3. FF (Min) (Hz)	10	?	?	22	7,8	18	28	8
4. FF (Max) (Hz)	20	?	?	90	7,8	48	70	8
5. FF f-I slope (Hz/nA)	1.4	1.4	?	1.4	7,8	4	4	8
6. Spike Frequency adaptation	+	++		+++	9,10	?	?	

Table 1: A summary of cat and rat MN types and their properties. Throughout the table, values are presented as means. ? denotes information remains unknown. +, ++, +++ denotes least, medium, most, respectively. – denotes none. Membrane time constant (Tau), resting membrane potential (RMP), threshold depolarization (voltage threshold), afterhyperpolarization (AHP), axonal conduction velocity (ACV), persistent inward current (PIC), firing frequency (FF), threshold current for rhythmic firing (I_{th}).

Cat Motoneurone Data References. All data reported are from anaesthetized cats. Firing frequencies are taken from primary range of firing. 1. Zengel et al. (1985), 2. Burke & ten Bruggencate (1971), 3. Burke et al. (1982), 4. Cullheim & Kellerth (1978b), 5. Gustafsson & Pinter (1984c), 6. Kernell & Monster (1981), 7. Kernell (1979), 8. Kernell (1992), 9. Kernell & Monster (1982a), 10. Spielmann et al. (1993), 11. Lee & Heckman (1998a); Lee & Heckman (1998b), 12. Gustafsson & Pinter (1984b)

Rat Motoneurone Data References. All data reported from anaesthetized rats. Firing frequencies are taken from steady state firing. See text (SeeT) refers to average taken from mean values of both MN types. 1. Gardiner (1993), 2. Bakels & Kernell (1993), 3. Beaumont & Gardiner (2002), 4. Beaumont & Gardiner (2003), 5. Delaney et al. (1981), 6. Chen & Wolpaw (1994), 7. Thurbon et al. (1998), 8. Cormery et al. (2005).

MOTONEURONE PROPERTIES	CAT			RAT		
Before and After Spinal Cord Transection	**CON**	**ST**	**Ref.**	**CON**	**ST**	**Ref.**
Morphology						
1. Soma Diameter (μm)	?	?		~30	~30	4
2. Stem Dendrite Number	?	?		10.4	6.9*	3
Passive Properties						
1. Electrotonic Length (λ)	1.4	1.4	1	~1.6	~1.6	1
2. Cell Capacitance (nF)	9.4	8.4*	1	3.1	2.2	1
3. Tau (ms)	5.5	4.6*	1	3.8	3.2	1
4. Input Resistance (MΩ)	1.1	0.96	1	2.2	2.0	1
Action Potential						
1. Spike height (mV)	88	88	1	83	77	1
2. RMP (mV)	-70	-70	1	-61	-54*	1
3. Threshold Depolarization (mV)	11.6	13.3*	1	20	17	1
4. Voltage threshold (mV)	-68.4	-66.7	1	-41	-37*	1
5. Rheobase Current (nA)	13.4	15.3	1	7.5	6.4	1
6. AHP amplitude(mV)	3.27	3.67	1	1.7	2.1	1
7. AHPduration (ms)	86.3	76.6*	1	?	?	
8. AHP ½ decay time (ms)	22.1	20.3	1	21.4	19.7	1
9. ACV(m/s)	70	74	2	?	?	
Active Properties						
1. Bistability	?	?		+	+++	2
2. I_{th} for rhythmic firing	?	?		12	14	1
3. FF (Min) (Hz)	?	?		23	23	1
4. FF (Max) (Hz)	?	?		55	41*	1
5. FF f-I slope (Hz/nA)	?	?		6	3.4*	1
6. Spike Frequency adaptation	?	?		?	?	

Table 2: A summary of the effects of ST on cat and rat MN properties. MN properties were recorded from animals following 30-60 days of ST. Table is presented the same as Table 1. There is no distinction of MN type. * denotes significant difference. Control (CON) and spinal cord transected (ST).

Cat Motoneurone Data References. 1. Hochman & McCrea (1994), 2. Cope et al. (1986)

Rat Motoneurone Data References. Length constant is based on assuming a T_1 that is 33% of T_m. 1. Beaumont et al. (2004), 2. Bennett et al. (2001), 3. Kitzman (2005), 4. Roy et al. (2007a).

REFERENCE LIST

Al-Majed AA, Brushart TM & Gordon T (2000). Electrical stimulation accelerates and increases expression of BDNF and trkB mRNA in regenerating rat femoral motoneurons. *Eur J Neurosci* **12**, 4381-90.

Alaburda A, Perrier JF & Hounsgaard J (2002). Mechanisms causing plateau potentials in spinal motoneurones. *Adv Exp Med Biol* **508**, 219-26.

Alaimo MA, Smith JL, Roy RR & Edgerton VR (1984). EMG activity of slow and fast ankle extensors following spinal cord transection. *J Appl Physiol* **56**, 1608-13.

Bakels R & Kernell D (1993). Matching between motoneurone and muscle unit properties in rat medial gastrocnemius. *J Physiol* **463** , 307-24.

Baldissera F & Gustafsson B (1974). Firing behaviour of a neurone model based on the afterhyperpolarization conductance time course and algebraical summation. Adaptation and steady state firing. *Acta Physiol Scand* **92**, 27-47.

Baldissera F, Gustafsson B & Parmiggiani F (1978). Saturating summation of the afterhyperpolarization conductance in spinal motoneurones: a mechanism for 'secondary range' repetitive firing. *Brain Res* **146** , 69-82.

Barrett EF, Barrett JN & Crill WE (1980). Voltage-sensitive outward currents in cat motoneurones. *J Physiol* **304**, 251-76.

Barrett JN & Crill WE (1974). Specific membrane properties of cat motoneurones. *J Physiol* **239**, 301-24.

Barrett JN & Crill WE (1980). Voltage clamp of cat motoneurone somata: properties of the fast inward current. *J Physiol* **304** , 231-49.

Beaumont E & Gardiner P (2002). Effects of daily spontaneous running on the electrophysiological properties of hindlimb motoneurones in rats. *J Physiol* **540**, 129-38.

Beaumont E & Gardiner PF (2003). Endurance training alters the biophysical properties of hindlimb motoneurons in rats. *Muscle Nerve* **27**, 228-36.

Beaumont E, Houle JD, Peterson CA & Gardiner PF (2004). Passive exercise and fetal spinal cord transplant both help to restore motoneuronal properties after spinal cord transection in rats. *Muscle Nerve* **29**, 234-42.

Bennett DJ, Hultborn H, Fedirchuk B & Gorassini M (1998a). Short-term plasticity in hindlimb motoneurons of decerebrate cats. *J Neurophysiol* **80**, 2038-45.

Bennett DJ, Hultborn H, Fedirchuk B & Gorassini M (1998b). Synaptic activation of plateaus in hindlimb motoneurons of decerebrate cats. *J Neurophysiol* **80**, 2023-37.

Bennett DJ, Li Y & Siu M (2001). Plateau potentials in sacrocaudal motoneurons of chronic spinal rats, recorded in vitro. *J Neurophysiol* **86**, 1955-71.

Binder MD, Robinson FR & Powers RK (1998). Distribution of effective synaptic currents in cat triceps surae motoneurons. VI. Contralateral pyramidal tract. *J Neurophysiol* **80**, 241-8.

Bose P, Parmer R, Reier PJ & Thompson FJ (2005). Morphological changes of the soleus motoneuron pool in chronic midthoracic contused rats. *Exp Neurol* **191**, 13-23.

Botterman BR & Cope TC (1986). Discharge properties of motoneurons supplying distal forelimb muscles in the cat. *Brain Res* **379** , 192-5.

Brown AM, Schwindt PC & Crill WE (1994). Different voltage dependence of transient and persistent Na+ currents is compatible with modal-gating hypothesis for sodium channels. *J Neurophysiol* **71**, 2562-5.

Brownstone RM (2006). Beginning at the end: repetitive firing properties in the final common pathway. *Prog Neurobiol* **78**, 156-72.

Brownstone RM (2007). Take your PIC: motoneuronal persistent inward currents may be somatic as well as dendritic. *J Neurophysiol*

Brownstone RM, Jordan LM, Kriellaars DJ, Noga BR & Shefchyk SJ (1992). On the regulation of repetitive firing in lumbar motoneurones during fictive locomotion in the cat. *Exp Brain Res* **90**, 441-55.

Burke RE (1967). Motor unit types of cat triceps surae muscle. *J Physiol* **193**, 141-160.

Burke RE, Dum RP, Fleshman JW, Glenn LL, Lev-Tov A, O'Donovan MJ & Pinter MJ (1982). A HRP study of the relation between cell size and motor unit type in cat ankle extensor motoneurons. *J Comp Neurol* **209**, 17-28.

Burke RE, Levine DN, Tsairis P & Zajac FE 3rd (1973). Physiological types and histochemical profiles in motor units of the cat gastrocnemius. *J Physiol* **234**, 723-48.

Burke RE, Strick PL, Kanda K, Kim CC & Walmsley B (1977). Anatomy of medial gastrocnemius and soleus motor nuclei in cat spinal cord. *J Neurophysiol* **40**, 667-80.

Burke RE & ten Bruggencate G (1971). Electrotonic characteristics of alpha motoneurones of varying size. *J Physiol* **212**, 120

Button DC, Gardiner K, Marqueste T & Gardiner PF (2006). Frequency-current relationships of rat hindlimb {alpha}-motoneurones. *J Physiol* **573**, 663-77.

Byrne JH & Kandel ER (1996). Presynaptic facilitation revisited: state and time dependence. *J Neurosci* **16**, 425-35.

Cantrell AR & Catterall WA (2001). Neuromodulation of Na+ channels: an unexpected form of cellular plasticity. *Nat Rev Neurosci* **2**, 397-407.

Carlin KP, Jiang Z & Brownstone RM (2000a). Characterization of calcium currents in functionally mature mouse spinal motoneurons. *Eur J Neurosci* **12**, 1624-34.

Carlin KP, Jones KE, Jiang Z, Jordan LM & Brownstone RM (2000b). Dendritic L-type calcium currents in mouse spinal motoneurons: implications for bistability. *Eur J Neurosci* **12**, 1635-46.

Catterall WA (1995). Structure and function of voltage-gated ion channels. *Annu Rev Biochem* **64**, 493-531.

Chalmers GR, Roy RR & Edgerton VR (1992). Adaptability of the oxidative capacity of motoneurons. *Brain Res* **570**, 1-10.

Chen XY & Wolpaw JR (1994). Triceps surae motoneuron morphology in the rat: a quantitative light microscopic study. *J Comp Neurol* **343**, 143-57.

Clark BC, Manini TM, Bolanowski SJ & Ploutz-Snyder LL (2006). Adaptations in human neuromuscular function following prolonged unweighting: II. Neurological properties and motor imagery efficacy. *J Appl Physiol* **101**, 264-72.

Cleary LJ, Lee WL & Byrne JH (1998). Cellular correlates of long-term sensitization in Aplysia. *J Neurosci* **18**, 5988-98.

Clements JD & Redman SJ (1989). Cable properties of cat spinal motoneurones measured by combining voltage clamp, current clamp and intracellular staining. *J Physiol* **409**, 63-87.

Conway BA, Hultborn H, Kiehn O & Mintz I (1988). Plateau potentials in alpha-motoneurones induced by intravenous injection of L-dopa and clonidine in the spinal cat. *J Physiol* **405**, 369-84.

Coombs JS, Eccles JC & Fatt P (1955). The electrical properties of the motoneurone membrane. *J Physiol* **130**, 291-325.

Cope TC, Bodine SC, Fournier M & Edgerton VR (1986). Soleus motor units in chronic spinal transected cats: physiological and morphological alterations. *J Neurophysiol* **55**, 1202-20.

Copray S & Kernell D (2000). Neurotrophins and trk-receptors in adult rat spinal motoneurons: differences related to cell size but not to 'slow/fast' specialization. *Neurosci Lett* **289**, 217-20.

Cormery B, Beaumont E, Csukly K & Gardiner P (2005). Hindlimb unweighting for 2 weeks alters physiological properties of rat hindlimb motoneurones. *J Physiol* **568**, 841-50.

Cormery B, Marini JF & Gardiner PF (2000). Changes in electrophysiological properties of tibial motoneurones in the rat following 4 weeks of tetrodotoxin-induced paralysis. *Neurosci Lett* **287**, 21-4.

Crill WE (1996). Persistent sodium current in mammalian central neurons. *Annu Rev Physiol* **58**, 349-62.

Cullheim S, Fleshman JW, Glenn LL & Burke RE (1987). Membrane area and dendritic structure in type-identified triceps surae alpha motoneurons. *J Comp Neurol* **255**, 68-81.

Cullheim S & Kellerth JO (1978a). A morphological study of the axons and recurrent axon collaterals of cat alpha-motoneurones supplying different hind-limb muscles. *J Physiol* **281**, 285-99.

Cullheim S & Kellerth JO (1978b). A morphological study of the axons and recurrent axon collaterals of cat alpha-motoneurones supplying different functional types of muscle unit. *J Physiol* **281**, 301-13.

Czeh G, Gallego R, Kudo N & Kuno M (1978). Evidence for the maintenance of motoneurone properties by msucel activity. *J Physiol* **281**, 239-52.

de Luca CJ, Foley PJ & Erim Z (1996). Motor unit control properties in constant-force isometric contractions. *J Neurophysiol* **76**, 1503-16.

Delaney AJ, Samorajski T, Fuller GN & Wiggins RC (1981). A morphometric comparison of central and peripheral hypomyelination induced by postnatal undernourishment of rats. *J Nutr* **111**, 746-54.

Desaulniers P, Lavoie PA & Gardiner PF (2001). Habitual exercise enhances neuromuscular transmission efficacy of rat soleus muscle in situ. *J Appl Physiol* **90**, 1041-8.

Duchateau J & Hainaut K (1990). Effects of immobilization on contractile properties, recruitment and firing rates of human motor units. *J Physiol* **422**, 55-65.

Elbasiouny SM, Bennett DJ & Mushahwar VK (2005). Simulation of Ca+2 Persistent Inward Currents in Spinal Motoneurons: Mode of Activation and Integration of Synaptic Inputs. *J Physiol*

Foehring RC, Sypert GW & Munson JB (1987a). Motor-unit properties following cross-reinnervation of cat lateral gastrocnemius and soleus muscles with medial gastrocnemius nerve. II. Influence of muscle on motoneurons. *J Neurophysiol* **57**, 1227-45.

Foehring RC, Sypert GW & Munson JB (1987b). Motor-unit properties following cross-reinnervation of cat lateral gastrocnemius and soleus muscles with medial gastrocnemius nerve. I. Influence of motoneurons on muscle. *J Neurophysiol* **57**, 1210-26.

Gandevia SC (2001). Spinal and supraspinal factors in human muscle fatigue. *Physiol Rev* **81**, 1725-89.

Gardiner PF (1993). Physiological properties of motoneurons innervating different muscle unit types in rat gastrocnemius. *J Neurophysiol* **69**, 1160-70.

Gardiner PF (2006). Changes in alpha-motoneuron properties with altered physical activity levels. *Exerc Sport Sci Rev* **34**, 54-8.

Gardiner PF & Seburn KL (1997). The effects of tetrodotoxin-induced muscle paralysis on the physiological properties of muscle units and their innervating motoneurons in rat. *J Physiol* **499 (Pt 1)**, 207-16.

Gazula VR, Roberts M, Luzzio C, Jawad AF & Kalb RG (2004a). Effects of limb exercise after spinal cord injury on motor neuron dendrite structure. *J Comp Neurol* **476**, 130-45.

Gazula VR, Roberts M, Luzzio C, Jawad AF & Kalb RG (2004b). Effects of limb exercise after spinal cord injury on motor neuron dendrite structure. *J Comp Neurol* **476**, 130-45.

Gazzoni M, Camelia F & Farina D (2005). Conduction velocity of quiescent muscle fibers decreases during sustained contraction. *J Neurophysiol* **94**, 387-94.

Gharakhanlou R, Chadan S & Gardiner P (1999). Increased activity in the form of endurance training increases calcitonin gene-related peptide content in lumbar motoneuron cell bodies and in sciatic nerve in the rat. *Neuroscience* **89**, 1229-39.

Gilmore J & Fedirchuk B (2004). The excitability of lumbar motoneurones in the neonatal rat is increased by a hyperpolarization of their voltage threshold for activation by descending serotonergic fibres. *J Physiol* **558**, 213-24.

Gomez-Pinilla F, Ying Z, Opazo P, Roy RR & Edgerton VR (2001). Differential regulation by exercise of BDNF and NT-3 in rat spinal cord and skeletal muscle. *Eur J Neurosci* **13**, 1078-84.

Gomez-Pinilla F, Ying Z, Roy RR, Hodgson J & Edgerton VR (2004). Afferent input modulates neurotrophins and synaptic plasticity in the spinal cord. *J Neurophysiol* **92**, 3423-32.

Gonzalez-Forero D, Portillo F, Gomez L, Montero F, Kasparov S & Moreno-Lopez B (2007). Inhibition of resting potassium conductances by long-term activation of the NO/cGMP/protein kinase G pathway: a new mechanism regulating neuronal excitability. *J Neurosci* **27**, 6302-12.

Gonzalez M & Collins WF 3rd (1997). Modulation of motoneuron excitability by brain-derived neurotrophic factor. *J Neurophysiol* **77**, 502-6.

Gorassini M, Yang JF, Siu M & Bennett DJ (2002a). Intrinsic activation of human motoneurons: possible contribution to motor unit excitation. *J Neurophysiol* **87**, 1850-8.

Gorassini M, Yang JF, Siu M & Bennett DJ (2002b). Intrinsic activation of human motoneurons: reduction of motor unit recruitment thresholds by repeated contractions. *J Neurophysiol* **87**, 1859-66.

Gorassini MA, Bennett DJ & Yang JF (1998). Self-sustained firing of human motor units. *Neurosci Lett* **247**, 13-6.

Gorassini MA, Knash ME, Harvey PJ, Bennett DJ & Yang JF (2004). Role of motoneurons in the generation of muscle spasms after spinal cord injury. *Brain* **127**, 2247-58.

Gorman RB, McDonagh JC, Hornby TG, Reinking RM & Stuart DG (2005). Measurement and nature of firing rate adaptation in turtle spinal neurons. *J Comp Physiol A Neuroethol Sens Neural Behav Physiol* **191**, 583-603.

Gossen ER, Ivanova TD & Garland SJ (2003). The time course of the motoneurone afterhyperpolarization is related to motor unit twitch speed in human skeletal muscle. *J Physiol* **552**, 657-64.

Grande G, Bui TV & Rose PK (2007). Estimates of the Location of L-type Ca2+ Channels in Motoneurons of Different Sizes: A Computational Study. *J Neurophysiol* **97**, 4023-35.

Granit R, Kernell D & Shortess GK (1963). Quantitative aspects of repetitive firing of mammalian motoneurones, caused by injected currents. *J Physiol* **168**, 911-31.

Grillner S, Hongo T & Lund S (1970). The vestibulospinal tract. Effects on alpha-motoneurones in the lumbosacral spinal cord in the cat. *Exp Brain Res* **10**, 94-120.

Grossman EJ, Roy RR, Talmadge RJ, Zhong H & Edgerton VR (1998). Effects of inactivity on myosin heavy chain composition and size of rat soleus fibers. *Muscle Nerve* **21**, 375-89.

Guertin PA & Hounsgaard J (1998). NMDA-Induced intrinsic voltage oscillations depend on L-type calcium channels in spinal motoneurons of adult turtles. *J Neurophysiol* **80**, 3380-2.

Guertin PA & Hounsgaard J (1999). Non-volatile general anaesthetics reduce spinal activity by suppressing plateau potentials . *Neuroscience* **88**, 353-8.

Gustafsson B, Katz R & Malmsten J (1982). Effects of chronic partial deafferentiation on the electrical properties of lumbar alpha-motoneurones in the cat. *Brain Res* **246**, 23-33.

Gustafsson B & Pinter MJ (1984a). Effects of axotomy on the distribution of passive electrical properties of cat motoneurones. *J Physiol* **356**, 433-42.

Gustafsson B & Pinter MJ (1984b). Relations among passive electrical properties of lumbar alpha-motoneurones of the cat. *J Physiol* **356**, 401-31.

Gustafsson B & Pinter MJ (1984c). An investigation of threshold properties among cat spinal alpha-motoneurones. *J Physiol* **357** , 453-83.

Gustafsson B & Pinter MJ (1985). Factors determining the variation of the afterhyperpolarization duration in cat lumbar alpha-motoneurones. *Brain Res* **326**, 392-5.

Harada Y & Takahashi T (1983). The calcium component of the action potential in spinal motoneurones of the rat. *J Physiol* **335** , 89-100.

Harris RL, Putman CT, Rank M, Sanelli L & Bennett DJ (2007). Spastic tail muscles recover from myofiber atrophy and myosin heavy chain transformations in chronic spinal rats. J Neurophysiol **97**, 1040-51.

Harvey PJ, Li X, Li Y & Bennett DJ (2006a). 5-ht2 receptor activation facilitates a persistent sodium current and repetitive firing in spinal motoneurons of rats with and without chronic spinal cord injury. *J Neurophysiol* **96**, 1158-70.

Harvey PJ, Li X, Li Y & Bennett DJ (2006b). Endogenous monoamine receptor activation is essential for enabling persistent sodium currents and repetitive firing in rat spinal motoneurons. *J Neurophysiol* **96**, 1171-86.

Harvey PJ, Li Y, Li X & Bennett DJ (2006c). Persistent sodium currents and repetitive firing in motoneurons of the sacrocaudal spinal cord of adult rats. *J Neurophysiol* **96**, 1141-57.

Heckman CJ, Gorassini MA & Bennett DJ (2004). Persistent inward currents in motoneuron dendrites: Implications for motor output. *Muscle Nerve*

Henneman E, Somjen G & Carpenter DO (1965). Functional significance of cell size in spinal motoneurons. *J Neurophysiol* **28**, 560-80.

Hille B (2001). *Ion Channels of Excitable Membranes*. Sunderland, MA, USA: Sinauer Associates, Inc.

Hochman S, Jordan LM & Schmidt BJ (1994). TTX-resistant NMDA receptor-mediated voltage oscillations in mammalian lumbar motoneurons. *J Neurophysiol* **72**, 2559-62.

Hochman S & McCrea DA (1994). Effects of chronic spinalization on ankle extensor motoneurons. II. Motoneuron electrical properties. *J Neurophysiol* **71**, 1468-79.

Hodgkin AL & Huxley AF (1952a). The components of membrane conductance in the giant axon of Loligo. *J Physiol* **116**, 473-96.

Hodgkin AL & Huxley AF (1952b). Currents carried by sodium and potassium ions through the membrane of the giant axon of Loligo. *J Physiol* **116**, 449-72.

Hodgkin AL, Huxley AF & Katz B (1952). Measurement of current-voltage relations in the membrane of the giant axon of Loligo. *J Physiol* **116**, 424-48.

Hornby TG, Heckman CJ, Harvey RL & Rymer WZ (2004). Changes in voluntary torque and electromyographic activity following oral baclofen. *Muscle Nerve* **30**, 784-95.

Hounsgaard J, Hultborn H, Jespersen B & Kiehn O (1988). Bistability of alpha-motoneurones in the decerebrate cat and in the acute spinal cat after intravenous 5-hydroxytryptophan. *J Physiol* **405**, 345-67.

Hounsgaard J & Kiehn O (1989). Serotonin-induced bistability of turtle motoneurones caused by a nifedipine-sensitive calcium plateau potential. *J Physiol* **414**, 265-82.

Hounsgaard J & Kiehn O (1993). Calcium spikes and calcium plateaux evoked by differential polarization in dendrites of turtle motoneurones in vitro. *J Physiol* **468**, 245-59.

Hounsgaard J, Kiehn O & Mintz I (1988). Response properties of motoneurones in a slice preparation of the turtle spinal cord . *J Physiol* **398**, 575-89.

Hounsgaard J & Mintz I (1988). Calcium conductance and firing properties of spinal motoneurones in the turtle. *J Physiol* **398** , 591-603.

Hultborn H (1999). Plateau potentials and their role in regulating motoneuronal firing. *Prog Brain Res* **123**, 39-48.

Hultborn H, Brownstone RB, Toth TI & Gossard JP (2004). Key mechanisms for setting the input-output gain across the motoneuron pool. *Prog Brain Res* **143**, 77-95.

Hultborn H & Kiehn O (1992). Neuromodulation of vertebrate motor neuron membrane properties. *Curr Opin Neurobiol* **2**, 770-5.

Ichiyama RM, Broman J, Edgerton VR & Havton LA (2006). Ultrastructural synaptic features differ between alpha- and gamma-motoneurons innervating the tibialis anterior muscle in the rat. *J Comp Neurol* **499**, 306-15.

Ishihara A, Roy RR, Ohira Y & Edgerton VR (2002). Motoneuron and sensory neuron plasticity to varying neuromuscular activity levels. *Exerc Sport Sci Rev* **30**, 152-8.

Ito M & Oshima T (1965). Electrical behaviour of the motoneurone membrane during intracellularly applied current steps. *J Physiol* **180**, 607-35.

Kandel ER, Schwartz JH & Jessell TM (2000). *Principles of Neuroscience*. United States of America - New York, New York: McGraw-Hill .

Kernell D (1965a). The adaptation and the Relation Between Discharge Frequency and Current Strength of Cat Lumbosacral Motoneurones Stimulated by Long-Lasting Injected Currents. *Acta. Physiol. Scand.* 65-73.

Kernell D (1965b). High-Frequency Repetitive Firing of Cat Lumbosacral Motoneurones Stimulated by Long-Lasting Injected Currents. *Acta. Physiol. Scand.* **65**, 74-86.

Kernell D (1965c). The Limits of Firing Frequency in Cat Lumbosacral Motoneurones Possessing Different Time Course of Afterhyperpolarization. *Acta. Physiol. Scand.* **65**, 87-100.

Kernell D (1966). Input resistance, electrical excitability, and size of ventral horn cells in cat spinal cord. *Science* **152**, 1637-40.

Kernell D (1968). The repetitive impulse discharge of a simple neurone model compared to that of spinal motoneurones. *Brain Res* **11**, 685-7.

Kernell D (1972). The early phase of adaptation in repetitive impulse discharges of cat spinal motoneurones. *Brain Res* **41**, 184-6.

Kernell D (1979). Rhythmic properties of motoneurones innervating muscle fibres of different speed in m. gastrocnemius medialis of the cat. *Brain Res* **160**, 159-62.

Kernell D (1992). Organized variability in the neuromuscular system: a survey of task-related adaptations. *Arch Ital Biol* **130**, 19-66.

Kernell D (2006). *The motoneurone and its muscle fibres*. New York: Oxford: University Press.

Kernell D & Monster AW (1981). Threshold current for repetitive impulse firing in motoneurones innervating muscle fibres of different fatigue sensitivity in the cat. *Brain Res* **229**, 193-6.

Kernell D & Monster AW (1982a). Motoneurone properties and motor fatigue. An intracellular study of gastrocnemius motoneurones of the cat. *Exp Brain Res* **46**, 197-204.

Kernell D & Monster AW (1982b). Time course and properties of late adaptation in spinal motoneurones of the cat. *Exp Brain Res* **46**, 191-6.

Kernell D & Zwaagstra B (1981). Input conductance axonal conduction velocity and cell size among hindlimb motoneurones of the cat. *Brain Res* **204**, 311-26.

Kiehn O & Eken T (1998). Functional role of plateau potentials in vertebrate motor neurons. *Curr Opin Neurobiol* **8**, 746-52.

Kitzman P (2005). Alteration in axial motoneuronal morphology in the spinal cord injured spastic rat. *Exp Neurol* **192**, 100-8.

Kitzman P (2007). VGLUT1 and GLYT2 labeling of sacrocaudal motoneurons in the spinal cord injured spastic rat. *Exp Neurol* **204**, 195-204.

Kjaerulff O & Kiehn O (2001). 5-HT modulation of multiple inward rectifiers in motoneurons in intact preparations of the neonatal rat spinal cord. *J Neurophysiol* **85**, 580-93.

Kuno M, Miyata Y & Munoz-Martinez EJ (1974). Differential reaction of fast and slow alpha-motoneurones to axotomy. *J Physiol* **240**, 725-39.

Larkman PM & Kelly JS (1992). Ionic mechanisms mediating 5-hydroxytryptamine- and noradrenaline-evoked depolarization of adult rat facial motoneurones. *J Physiol* **456**, 473-90.

Larkman PM & Perkins EM (2005). A TASK-like pH- and amine-sensitive 'leak' K+ conductance regulates neonatal rat facial motoneuron excitability in vitro. *Eur J Neurosci* **21**, 679-91.

Larkum ME, Rioult MG & Luscher HR (1996). Propagation of action potentials in the dendrites of neurons from rat spinal cord slice cultures. *J Neurophysiol* **75**, 154-70.

Lee RH & Heckman CJ (1998a). Bistability in spinal motoneurons in vivo: systematic variations in persistent inward currents. *J Neurophysiol* **80**, 583-93.

Lee RH & Heckman CJ (1998b). Bistability in spinal motoneurons in vivo: systematic variations in rhythmic firing patterns. *J Neurophysiol* **80**, 572-82.

Lee RH & Heckman CJ (1999). Paradoxical effect of QX-314 on persistent inward currents and bistable behavior in spinal motoneurons in vivo. *J Neurophysiol* **82**, 2518-27.

Lee RH & Heckman CJ (2000). Adjustable amplification of synaptic input in the dendrites of spinal motoneurons in vivo. *J Neurosci* **20**, 6734-40.

Lee RH & Heckman CJ (2001). Essential role of a fast persistent inward current in action potential initiation and control of rhythmic firing. *J Neurophysiol* **85**, 472-5.

Lesser SS, Sherwood NT & Lo DC (1997). Neurotrophins differentially regulate voltage-gated ion channels. *Mol Cell Neurosci* **10**, 173-83.

Li XL, Zhang W, Zhou X, Wang XY, Zhang HT, Qin DX, Zhang H, Li Q, Li M & Wang TH (2007). Temporal changes in the expression of some neurotrophins in spinal cord transected adult rats. *Neuropeptides* **41**, 135-43.

Li Y & Bennett DJ (2003). Persistent sodium and calcium currents cause plateau potentials in motoneurons of chronic spinal rats. *J Neurophysiol* **90**, 857-69.

Li Y, Gorassini MA & Bennett DJ (2004). Role of persistent sodium and calcium currents in motoneuron firing and spasticity in chronic spinal rats. *J Neurophysiol* **91**, 767-83.

Liu HT, Hollmann MW, Liu WH, Hoenemann CW & Durieux ME (2001). Modulation of NMDA receptor function by ketamine and magnesium: Part I. *Anesth Analg* **92**, 1173-81.

Macefield VG, Fuglevand AJ, Howell JN & Bigland-Ritchie B (2000). Discharge behaviour of single motor units during maximal voluntary contractions of a human toe extensor. *J Physiol* **528 Pt 1**, 227-34.

Magarinos-Ascone C, Nunez A & Delgado-Garcia JM (1999). Different discharge properties of rat facial nucleus motoneurons. *Neuroscience* **94**, 879-86.

McLarnon JG (1995). Potassium currents in motoneurones. *Prog Neurobiol* **47**, 513-31.

Miles GB, Dai Y & Brownstone RM (2005). Mechanisms underlying the early phase of spike frequency adaptation in mouse spinal motoneurones. *J Physiol* **15**, 519-532
.

Mitsumoto H & Tsuzaka K (1999). Neurotrophic factors and neuro-muscular disease: II. GDNF, other neurotrophic factors, and future directions. *Muscle Nerve* **22**, 1000-21.

Monster AW & Chan H (1977). Isometric force production by motor units of extensor digitorum communis muscle in man. *J Neurophysiol* **40**, 1432-43.

Moritz AT, Newkirk GS, Powers RK & Binder MD (2007). Facilitation of somatic calcium channels can evoke prolonged tail currents in rat hypoglossal motoneurons. *J Neurophysiol*

Neher E (1992). Ion channels for communication between and within cells. *Biosci Rep* **12**, 1-14.

Neher E & Sakmann B (1976). Single-channel currents recorded from membrane of denervated frog muscle fibres. *Nature* **260**, 799-802.

Pape HC (1996). Queer current and pacemaker: the hyperpolarization-activated cation current in neurons. *Annu Rev Physiol* **58**, 299-327.

Perrier JF, Alaburda A & Hounsgaard J (2003). 5-HT1A receptors increase excitability of spinal motoneurons by inhibiting a TASK-1-like K+ current in the adult turtle. *J Physiol* **548**, 485-92.

Petruska JC, Ichiyama RM, Jindrich DL, Crown ED, Tansey KE, Roy R, Edgerton VR & Mendell LM (2007). Changes in motoneuron properties and synaptic inputs related to step training after spinal cord transection in rats. *J Neurosci* **27**, 4460-71.

Pierotti DJ, Roy RR, Bodine-Fowler SC, Hodgson JA & Edgerton VR (1991). Mechanical and morphological properties of chronically inactive cat tibialis anterior motor units. *J Physiol* **444**, 175-92.

Plant TD, Schirra C, Katz E, Uchitel OD & Konnerth A (1998). Single-cell RT-PCR and functional characterization of Ca2+ channels in motoneurons of the rat facial nucleus. *J Neurosci* **18**, 9573-84.

Powers RK & Binder MD (2003). Persistent sodium and calcium currents in rat hypoglossal motoneurons. *J Neurophysiol* **89**, 615-24.

Powers RK, Robinson FR, Konodi MA & Binder MD (1993). Distribution of rubrospinal synaptic input to cat triceps surae motoneurons. *J Neurophysiol* **70**, 1460-8.

Powers RK, Sawczuk A, Musick JR & Binder MD (1999). Multiple mechanisms of spike-frequency adaptation in motoneurones. *J Physiol Paris* **93**, 101-14.

Qin DX, Zou XL, Luo W, Zhang W, Zhang HT, Li XL, Zhang H, Wang XY & Wang TH (2006). Expression of some neurotrophins in the spinal motoneurons after cord hemisection in adult rats. *Neurosci Lett* **410**, 222-7.

Rall W (1959). Branching dendritic trees and motoneuron membrane resistivity. *Exp Neurol* **1**, 491-527.

Rall W (1969). Time constants and electrotonic length of membrane cylinders and neurons. *Biophys J* **9**, 1483-508.

Rall W, Burke RE, Holmes WR, Jack JJ, Redman SJ & Segev I (1992). Matching dendritic neuron models to experimental data. *Physiol Rev* **72**, S159-86.

Rank MM, Li X, Bennett DJ & Gorassini MA (2007). Role of endogenous release of norepinephrine in muscle spasms after chronic spinal cord injury. *J Neurophysiol* **97**, 3166-80.

Rekling JC, Funk GD, Bayliss DA, Dong XW & Feldman JL (2000). Synaptic control of motoneuronal excitability. *Physiol Rev* **80**, 767-852.

Robinson RB & Siegelbaum SA (2003). Hyperpolarization-activated cation currents: from molecules to physiological function. *Annu Rev Physiol* **65**, 453-80.

Rose CR, Blum R, Kafitz KW, Kovalchuk Y & Konnerth A (2004). From modulator to mediator: rapid effects of BDNF on ion channels. *Bioessays* **26**, 1185-94.

Roy RR, Zhong H, Monti RJ, Vallance KA & Edgerton VR (2002). Mechanical properties of the electrically silent adult rat soleus muscle. Muscle Nerve **26**, 404-12.

Roy RR, Matsumoto A, Zhong H, Ishihara A & Edgerton VR (2007a). Rat alpha- and gamma-motoneuron soma size and succinate dehydrogenase activity are independent of neuromuscular activity level. *Muscle Nerve*

Roy RR, Zhong H, Khalili N, Kim SJ, Higuchi N, Monti RJ, Grossman E, Hodgson JA & Edgerton VR (2007b). Is spinal cord isolation a good model of muscle disuse? *Muscle Nerve* **35**, 312-21.

Russo RE & Hounsgaard J (1996). Burst-generating neurones in the dorsal horn in an in vitro preparation of the turtle spinal cord. *J Physiol* **493 (Pt 1)**, 55-66.

Safronov BV, Wolff M & Vogel W (2000). Excitability of the soma in central nervous system neurons. *Biophys J* **78**, 2998-3010.

Sah P (1996). Ca(2+)-activated K+ currents in neurones: types, physiological roles and modulation. *Trends Neurosci* **19**, 150-4.

Sah P & Faber ES (2002). Channels underlying neuronal calcium-activated potassium currents. *Prog Neurobiol* **66**, 345-53.

Sakmann B (1992). Elementary steps in synaptic transmission revealed by currents through single ion channels. *Biosci Rep* **12** , 237-62.

Sale DG, McComas AJ, MacDougall JD & Upton AR (1982). Neuromuscular adaptation in human thenar muscles following strength training and immobilization. *J Appl Physiol* **53**, 419-24.

Sawczuk A, Powers RK & Binder MD (1995). Spike frequency adaptation studied in hypoglossal motoneurons of the rat. *J Neurophysiol* **73**, 1799-810.

Sawczuk A, Powers RK & Binder MD (1997). Contribution of outward currents to spike-frequency adaptation in hypoglossal motoneurons of the rat. *J Neurophysiol* **78**, 2246-53.

Schwindt P & Crill WE (1977). A persistent negative resistance in cat lumbar motoneurons. *Brain Res* **120**, 173-8.

Schwindt PC (1973). Membrane-potential trajectories underlying motoneuron rhythmic firing at high rates. *J Neurophysiol* **36**, 434-9.

Schwindt PC & Crill WE (1981). Negative slope conductance at large depolarizations in cat spinal motoneurons. *Brain Res* **207** , 471-5.

Schwindt PC & Crill WE (1982). Factors influencing motoneuron rhythmic firing: results from a voltage-clamp study. *J Neurophysiol* **48**, 875-90.

Skydsgaard M & Hounsgaard J (1996). Multiple actions of iontophoretically applied serotonin on motorneurones in the turtle spinal cord in vitro. *Acta Physiol Scand* **158**, 301-10.

Spielmann JM, Laouris Y, Nordstrom MA, Robinson GA, Reinking RM & Stuart DG (1993). Adaptation of cat motoneurons to sustained and intermittent extracellular activation. *J Physiol* **464**, 75-120.

Stauffer EK, McDonagh JC, Hornby TG, Reinking RM & Stuart DG (2007). Historical reflections on the afterhyperpolarization--firing rate relation of vertebrate spinal neurons. *J Comp Physiol A Neuroethol Sens Neural Behav Physiol* **193**, 145-58.

Stephens JA & Usherwood TP (1977). The mechanical properties of human motor units with special reference to their fatiguability and recruitment threshold. *Brain Res* **125**, 91-7.

Suzuki S, Kiyosue K, Hazama S, Ogura A, Kashihara M, Hara T, Koshimizu H & Kojima M (2007). Brain-derived neurotrophic factor regulates cholesterol metabolism for synapse development. *J Neurosci* **27**, 6417-27.

Swett JE, Wikholm RP, Blanks RH, Swett AL & Conley LC (1986). Motoneurons of the rat sciatic nerve. *Exp Neurol* **93**, 227-52.

Taddese A & Bean BP (2002). Subthreshold sodium current from rapidly inactivating sodium channels drives spontaneous firing of tuberomammillary neurons. *Neuron* **33**, 587-600.

Talmadge RJ, Roy RR & Edgerton VR (1996). Distribution of myosin heavy chain isoforms in non-weight-bearing rat soleus muscle fibers. *J Appl Physiol* **81**, 2540-6.

Talmadge RJ, Roy RR, Caiozzo VJ & Edgerton VR (2002). Mechanical properties of rat soleus after long-term spinal cord transection. J Appl Physiol **93**, 1487-97.

Thurbon D, Luscher HR, Hofstetter T & Redman SJ (1998). Passive electrical properties of ventral horn neurons in rat spinal cord slices. *J Neurophysiol* **79**, 2485-502.

Toledo-Rodriguez M, El Manira A, Wallen P, Svirskis G & Hounsgaard J (2005). Cellular signalling properties in microcircuits. *Trends Neurosci* **28**, 534-40.

Ulfhake B & Kellerth JO (1981). A quantitative light microscopic study of the dendrites of cat spinal alpha-motoneurons after intracellular staining with horseradish peroxidase. *J Comp Neurol* **202**, 571-83.

Ulfhake B & Kellerth JO (1982). Does alpha-motoneurone size correlate with motor unit type in cat triceps surae? *Brain Res* **251** , 201-9.

Umemiya M & Berger AJ (1994). Properties and function of low- and high-voltage-activated Ca2+ channels in hypoglossal motoneurons. *J Neurosci* **14**, 5652-60.

Wang MY & Dun NJ (1990). 5-Hydroxytryptamine responses in neonate rat motoneurones in vitro. *J Physiol* **430**, 87-103.

Wolpaw JR & Tennissen AM (2001). Activity-dependent spinal cord plasticity in health and disease. *Annu Rev Neurosci* **24**, 807-43.

Wu N, Enomoto A, Tanaka S, Hsiao CF, Nykamp DQ, Izhikevich E & Chandler SH (2005). Persistent sodium currents in mesencephalic v neurons participate in burst generation and control of membrane excitability. *J Neurophysiol* **93**, 2710-22.

Zeng J, Powers RK, Newkirk G, Yonkers M & Binder MD (2005). Contribution of persistent sodium currents to spike-frequency adaptation in rat hypoglossal motoneurons. *J Neurophysiol* **93**, 1035-41.

Zengel JE, Reid SA, Sypert GW & Munson JB (1985). Membrane electrical properties and prediction of motor-unit type of medial gastrocnemius motoneurons in the cat. *J Neurophysiol* **53**, 1323-44.

Zhang M, Sukiasyan N, Moller M, Bezprozvanny I, Zhang H, Wienecke J & Hultborn H (2006). Localization of L-type calcium channel Ca(V)1.3 in cat lumbar spinal cord--with emphasis on motoneurons. *Neurosci Lett* **407**, 42-7.

CHAPTER 2: FREQUENCY-CURRENT RELATIONSHIPS OF RAT HINDLIMB α-MOTONEURONES

RUNNING TITLE: Frequency-current relationships of motoneurones

KEYWORDS: motoneurone, persistent inward current, f-I relationship, spinal cord, ramp current injection

Chapter 2 is reprinted here with permission (August 23, 2007, The Physiological Society) as it appears in:
Button DC, Gardiner K, Marqueste T, Gardiner PF (2006) Frequency-current relationships of rat hindlimb {alpha}-motoneurones. J Physiol 573:663-77.

MY CONTRIBUTION TO THE PUBLICATION. The technician and I performed the required animal surgeries in preparation for motoneurone electrophysiological recordings. I recorded, measured, and analysed the data included in this publication. After I trained some of the authors on how to record, measure and analyze the data, they also helped with those procedures. During the duration of the experiments I continuously analyzed the data and discussed ideas with my supervisor and the other authors on whether or not more and what type of data was required to complete our project. After collecting and analyzing preliminary data I submitted an abstract, only after consultation with my supervisor and the other authors, on this data for presentation at an annual scientific conference. Once all of the data was collected and analysed I wrote and revised the manuscript in consultation with the other authors. I also discussed with my supervisor the order of authorship for the manuscript. After the manuscript was completed I circulated it to all the authors for their approval on authorship order, the manuscript itself, and editing purposes. Once the manuscript was deemed by all authors, as ready to go to submission, along with my supervisor I selected the Journal in which we submitted the manuscript to and then proceeded with the manuscript submission process. After the reviewer's comments on the manuscript were returned I made all the required revisions and discussed the reasoning for those revisions with the other authors. When the manuscript was accepted I made any further required corrections such as those included in the galley proofs.

ABSTRACT

The purpose of this study was to describe the frequency–current (f–I) relationships of hindlimb α-motoneurones (MNs) in both anaesthetized and decerebrate rats in situ. Sprague–Dawley rats (250–350 g) were anaesthetized with ketamine and xylazine (KX) or subjected to a precollicular decerebration prior to recording electrophysiological properties from sciatic nerve MNs. Motoneurones from KX-anaesthetized rats had a significantly ($P < 0.01$) hyperpolarized resting membrane potential and voltage threshold (Vth), increased rheobase current, and a trend ($P = 0.06$) for a smaller after-hyperpolarization (AHP) amplitude compared to MNs from decerebrate rats. In response to 5 s ramp current injections, MNs could be categorized into four f–I relationship types: (1) linear; (2) adapting; (3) linear + sustained; and (4) late acceleration. Types 3 and 4 demonstrated self-sustained firing owing to activation of persistent inward current (PIC). We estimated the PIC amplitude by subtracting the current at spike derecruitment from the current at spike recruitment. Neither estimated PIC nor f–I slopes differed between fast and slow MNs (slow MNs exhibited AHP half-decay times >20 ms) or between MNs from KX-anaesthetized and decerebrate rats. Motoneurones from KX-anaesthetized rats had significantly ($P < 0.02$) hyperpolarized ramp Vth values and smaller and shorter AHP amplitudes and decay times compared to MNs from decerebrate rats. Pentobarbitone decreased the estimated PIC amplitude and almost converted the f–I relationship from type 3 to type 1. In summary, MNs of animals subjected to KX anaesthesia required more current for spike initiation and rhythmic

discharge but retained large PICs and self-sustained firing. The KX-anaesthestized preparation enables direct recording of PICs in MNs from intact animals

INTRODUCTION

The frequency–current (f–I) relationships of motoneurones (MNs) demonstrate several nonlinearities, which reflect their active properties in response to suprathreshold current injections. The f–I relationship derived from short duration square-wave intracellular current injection can be described by several ranges: (1) primary; (2) secondary; and (3) tertiary (Kernell, 1965b,c; Schwindt, 1973). Longer duration current pulses are accompanied by a decrease in MN firing frequency (FF) known as spike-frequency adaptation, which can be described in three stages: (1) initial; (2) early; and (3) late (Granit et al. 1963; Kernell, 1965a,b; Kernell & Monster, 1981; Sawczuk et al. 1995; Powers et al. 1999; Powers & Binder, 2001; Miles et al. 2005). More recently, square-wave and triangular current pulses have been used to determine MN f–I relationships and the effect of persistent inward currents (PICs) on these relationships (Hounsgaard et al. 1988; Lee & Heckman, 1998a; Bennett et al. 2001).

Persistent inward currents in MNs are depolarizing currents generated by non-inactivating or slowly inactivating voltage-gated Na+ and Ca2+ channels (Lee & Heckman, 1999; Li & Bennett, 2003), when the membrane potential is depolarized above their activation threshold. These currents can mediate a plateau potential that in turn allows the MN to express self-sustained rhythmic firing. A plateau potential can be initiated by a short depolarizing current pulse and remain for a long period of time before being terminated either spontaneously or by brief hyperpolarizing current (Kiehn & Eken, 1998). This property allows a MN to fire for a long period of time. Thus, a MN can behave in a 'bistable' manner, in that it can be toggled between an

active and a quiescent state. Furthermore, a MN PIC can be amplified by a host of neurotransmitters and neuromodulators (Heckman et al. 2004). Neuromodulatory input to a MN via axons originating in the ralphe nucleus and locus coeruleus of the brainstem releases the monoamines serotonin (5-HT; Hounsgaard et al. 1988; Skydsgaard & Hounsgaard, 1996) and noradrenaline (NA; Lee & Heckman, 2000), which can enhance the PIC and render the motoneurone more excitable (Gilmore & Fedirchuk, 2004).

A plateau potential and its underlying PIC that conduct through voltage-gated ion channels have been examined in both in vivo and in vitro animal models through the use of voltage-clamp (Schwindt & Crill, 1977, 1981, 1982; Bennett et al. 2001) and current-clamp techniques (Hounsgaard et al. 1988; Lee & Heckman, 1998a; Bennett et al. 2001) with a concurrent addition of specific voltage-gated ion channel agonists, antagonists and neuromodulators. The current-clamp technique, in the form of a triangular current pulse (referred to as ramp current hereafter), has been used as a tool to determine f–I relationships and to estimate the associated PIC (ePIC) of hindlimb α-MNs in cats in vivo (Hounsgaard et al. 1988; Lee &Heckman, 1998a) and rat tail MNs in vitro (Bennett et al. 2001). However, this technique has not been used to determine the ePIC or describe f–I relationships in rat hindlimb α-MNs in situ. The first purpose of this paper is to determine whether hindlimb α-MNs of our in situ rat preparation demonstrate ePICs and f–I relationship patterns that are comparable with those reported by Bennett et al. (2001).

In previous studies, the ePIC was defined by subtracting the current at which MN rhythmic firing spike derecruitment occurs from the current at which MN

rhythmic firing spike recruitment occurs. The plateau potential or underlying PIC appears as a steep rise in firing frequency in the f–I relationship. In other words, a MN firing pattern elicited by a ramp current illustrates the plateau current as a counter-clockwise f –I hysteresis (Hultborn, 1999). Furthermore, it has been shown that bistable MNs have lower rheobase currents, suggesting that smaller MNs are influenced by PIC in a different manner from bigger MNs (Lee & Heckman, 1998a). Although this technique has been described as a meaningful way to estimate the size of the PIC and to illustrate MN f–I relationships as well as the PIC relationship to passive properties, other important information remains to be uncovered. Some further questions include the following. (1) Does the ePIC correlate with other passive MN properties? (2) Does MN ePIC change owing to the history (e.g. blood pressure, time of day, CO2 levels) of the experimental preparation? (3) Will the ePIC depend on the duration of the glass microelectrode impalement of the MN? (4) Do voltage threshold (Vth), after-hyperpolarization (AHP) amplitude and AHP 3/4 decay time change from spike to spike throughout the ramp? Thus, the second purpose of this paper is to attempt to answer this series of questions pertaining to ePIC.

It has been suggested (Hultborn & Kiehn, 1992; Hultborn, 1999) that, owing to the masking effects of anaesthetics, PICs were not evident in previous experiments in which animals were anaesthetized with barbiturates. More recently, it has been shown that in decerebrate animals compared to animals deeply anaesthetized with pentobarbitone, current generated by stimulation of muscle spindle Ia afferents was amplified four times by active dendritic currents (Lee & Heckman, 2000). Furthermore, when pentobarbitone was added to an in vitro turtle spinal cord slice

preparation, plateau potentials were no longer seen in MNs (Guertin & Hounsgaard, 1999). We wished to determine how the addition of pentobarbitone to an in situ rat preparation would affect the MN ePIC and the f–I relationship.

Finally, we anaesthetized the rat with a ketamine–xylazine (KX) mixture. Xylazine is an α2-adrenoceptor agonist, which should not influence the amplitude or activation of PIC. In contrast, ketamine is an N-methyl-d-aspartate (NMDA) receptor antagonist (Liu et al. 2001). These receptors are present in adult turtle MNs (Guertin & Hounsgaard, 1998) and neonatal rat MNs (Hochman et al. 1994; Palecek et al. 1999; Hsiao et al. 2002). Hochman et al. (1994) demonstrated that NMDA-induced rhythmic membrane voltage oscillations revealed the presence of bistable membrane properties. Little is known about the role of NMDA receptors in MNs of adult mammalian preparations, however, and it has been shown (see above) that, in adult mammalian preparations, PICs conduct through Na^+ and Ca^{2+} channels. Thus, the final purpose of the present paper is to determine whether KX anaesthesia influences rat hindlimb α-MN ePIC and f–I relationship. A portion of these results has been presented elsewhere in abstract form (Button et al. 2005a,b).

METHODS

Treatment of animals. Female Sprague–Dawley rats weighing 275–325 g were obtained from the University of Manitoba (Winnipeg, Manitoba, Canada), and initially housed in groups of two in plastic cages situated in an environmentally controlled room maintained at 23°C and kept on a 12 h–12 h light–dark cycle. The rats were provided with water and food ad libitum throughout the experiment. Rats (n =20)

underwent experimental procedures within 7 days of receipt. All procedures were approved by the animal ethics committee of the University of Manitoba and were in accordance with the guidelines of the Canadian Council of Animal Care.

Surgery. For these terminal experiments, rats were taken from their cages and anaesthetized with ketamine and xylazine (80 and 10 mg kg−1, respectively, i.p.). Each rat also received an intraperitoneal injection (volume 6.6 ml kg−1) of saline containing 5% dextrose and 0.05 mg kg−1 atropine. Briefly, the anaesthetized rat was surgically prepared for electrophysiological recording via impalement of spinal motoneurones following: (1) a tracheotomy; (2) catherization of the femoral artery; (3) an incision to allow stimulation of the sciatic nerve of the left hindlimb; (4) exposure, removal and cleaning of the spinal vertebrae in preparation for the laminectomy; and (5) a laminectomy from T12 to S1. Following the tracheotomy, the rat was ventilated (Harvard Apparatus, Canada) with pure oxygen-enriched room air, at a tidal volume of approximately 2 ml, and a ventilation rate of approximately 60–80 strokes min−1. Expired carbon dioxide levels were measured via a CAPSTAR 100 CO2 analyser (CWE Inc. Ardmore, PA, USA) and were maintained between 3.0 and 4.0%. Mean arterial pressure (MAP; Pressure Monitor BP-1; World Precision Instruments, Sarasota, FL, USA) was also measured and maintained between 80 and 110 mmHg. Anaesthesia was maintained by constant infusion of a physiological saline solution containing ketamine and xylazine (9 and 1mg h−1, respectively) via the femoral artery catheter (Pump 11, Harvard Apparatus). The depth of anaesthesia was verified frequently via MAP and CO2 levels and toe pinch and eye blink reflexes.

Following exposure and cleaning of the spinal vertebrae, the rat was transferred to a stereotaxic unit in preparation for the laminectomy. Rectal temperature was monitored and maintained near 37°C using aHomeothermic Blanket Control Unit (Harvard Apparatus). The head, thoracic and lumbar vertebrae, hips and left foot were immobilized with clamps, and the open leg and back incisions were filled with mineral oil. The dura mater covering the spinal cord was incised, and the large dorsal roots comprising afferents from the left hindlimb were cut and reflected over the right side of the cord. An opening was made in the pia mater just lateral to the entry zone of these roots into the cord, in preparation for introduction of the glass microelectrode. Immediately before beginning the search for motoneurones, a pneumothorax was performed by making a 5mm incision between ribs T5 and T6 on the left side of the thorax.

In another series of experiments, rats were initially anaesthetized with isofluorane and the surgical procedures stated above were performed. In addition to these procedures, the carotid arteries were separated from vagal, aortic and sympathetic nerves and ligated. The carotid arteries were then cannulated towards the head with short saline-filled tubing. The other end of the tubing was connected to a 20 gauge syringe needle used to inject 0.06–0.07 ml of mixed polyvinylsiloxane (PVS; extrude from Kerr or Reprosil from Dentsply Caulk, medium and heavy body) into each carotid artery via a 1 ml syringe. The PVS entered into the external and internal carotid arteries, filling all arteries that these vessels supplied. Once the vessels were filled, a precollicular decerebration was performed (for details of the decerebration procedure see Fouad & Bennett, 1998). Upon the decerebration,

anaesthesia was terminated and the rat was allowed to stabilize for 1 h before electrophysiological recordings began.

Drugs and solutions. To reduce blood pressure and respiration-related movement artifacts and to stabilize the rat for proper electrophysiological recordings, several solutions were injected intravenously, as follows: (1) a solution of 100mm of NaHCO3 (Fisher scientific) and 5% dextrose (Fisher Scientific) dissolved in 25ml of distilled deionized H2O; (2) 300 mosmol l^{-1} of Ficoll 70 (Sigma) dissolved in normal saline, which was used as a plasma expander; and (3) pancuronium bromide (0.2 mg kg^{-1}), as a muscle relaxant. The pancuronium bromide was injected intravenously immediately before the start of electrophysiological recordings and was re-administered upon the reappearance of muscle contraction in response to sciatic nerve stimulation. Upon the addition of pancuronium bromide, depth of anaesthesia was monitored by MAP. In one experiment, sodium pentobarbitone (50 mg kg^{-1}) was administered intravenously to determine the effect, if any, on the PIC (Guertin & Hounsgaard, 1999; Lee & Heckman, 2000).

Measurement of motoneurone properties. Thin-walled glass microelectodes (1.0 mm, World Precision Instruments, USA) were pulled (Kopf Vertical Pipette Puller, David Kopf Instruments, USA), and filled with 2M K citrate. Electrode impedances were approximately 10 MΩ. The tip of the electrode was positioned at a hole in the pia mater and was lowered with an inchworm microdrive system (Burleigh Instruments Inc., USA) into the cord in steps of 10 μm. The sciatic nerve was stimulated with a bipolar silver electrode at a frequency of 1 s^{-1} while the microelectrode was advanced through the cord and the field potential was

continuously monitored. In some experiments, a fine-wire tungsten electrode (World Precision Instruments, USA, 5 MΩ) was used to identify the location and depth in the spinal cord where the field potential was the largest. Evidence of successful impalement of an α-MN was a sudden increase in potential to at least -50 mV, and an antidromic action potential with a spike amplitude of > 55 mV and a reproducible latency of less than 2.5 ms from the stimulation artifact. When recording had stabilized for at least 2 minutes, resting membrane potential was recorded. During recording, an axoclamp intracellular amplifier system (Axoclamp 2B, Axon Instruments Inc., USA) was used, either in bridge or discontinuous current-clamp modes (DCC; 2-3 kHz switching), with capacitance maximally compensated. The following passive MN properties were recorded in bridge mode: antidromic action potential (from an average of 10 spikes), and orthodromic action potential in response to a 0.5-ms current pulse of supramaximal intensity (from an average of 40 spikes). Rheobase current (50-ms square-wave current amplitude resulting in spikes 50% of the time) and cell input resistance (from an average of 60, 1-nA hyperpolarizing pulses each lasting 100 ms) were recorded in DCC mode. From these recordings we determined antidromic spike height and time-course, amplitude and half-decay time of the AHP following an action potential evoked by a 0.5-ms current pulse, resting membrane potential, rheobase current, voltage threshold, and cell input resistance (IR). The half-decay time of the AHP was used to separate "slow" from "fast" MNs, as we have done previously (Beaumont & Gardiner, 2002; Beaumont & Gardiner, 2003).

Measurement of motoneurone f-I relationship. After measuring MN passive properties, cells were then challenged with slow triangular current ramps (range: 0.5-6 nA s^{-1}) and the voltage response was measured in DCC mode. Peak amplitude of the ramp depended entirely on rhythmic threshold of the MNs and an attempt was made to evoke trains of impulses containing 10-75 spikes over a 0.5-2.5 second duration. Ramps were used to determine the MN f-I relationship, evoke voltage-dependent plateaus, and measure the underlying PIC as described previously (Bennett et al., 2001; Hounsgaard et al., 1988; Lee & Heckman, 1998b). During the current ramps, the ePIC producing the plateau and sustaining firing was estimated from the difference in injected current at spike-recruitment compared with spike-derecruitment (see figure 1) (Bennett et al., 2001; Lee & Heckman, 1998b). For computing the average f-I relationship type and ePIC for each MN, we used a series of 3-6 current ramps. Voltage thresholds of the spikes elicited during the ramp were measured at the potential where there was an acceleration in the rate of depolarization to >10 mV/2 ms (modified from Brownstone et al., 1992).

At the end of these measurements, the microelectrode was backed out of the MN in 5-μm steps, and the voltage outside the cell was recorded. Typically, experiments yielded 2 MN with complete complements of data. At the end of the experiment, the rat was killed by an overdose of KCl.

Statistics. Only MNs that responded rhythmically to ramp currents and passed all electrophysiological requirements were used in the analysis (see methods). The MN passive properties and rhythmic properties were subjected to a one-way analysis of variance (ANOVA) for MN type and group (since all of the decerebration

MNs which met the criteria for analysis were the fast type). Motoneurones were designated as fast or slow based on the half-decay time of the AHP (fast < 20 ms, slow > 20 ms). This was done in order to subgroup MNs based on an intrinsic property that covaries highly with muscle fiber type and excitability, and which remains relatively stable in a variety of conditions that evoke changes in other properties (Cormery et al., 2000; Gardiner & Seburn, 1997; Gardiner, 1993; Zengel et al., 1985; Munson et al., 1997). X^2 analysis was used to determine whether significant differences were present in MN f-I relationship type. Some MN rhythmic properties were subjected to a two-way ANOVA procedure on factors of group and spike numbers (see results for details). Where a significant interaction term was present, data were subjected to a Tukey post hoc comparisons test, to determine significant differences among individual means. All data are expressed as mean ± 1 standard deviation.

RESULTS

We recorded data from 29 MNs in 14 rats that were anaesthetized with ketamine/xylazine. The data set is summarized in Table 1. We separated MNs into 'fast' and 'slow', using a half-decay time of the AHP. This is based on previous reports (Cormery et al., 2000; Gardiner, 1993; Cormery et al., 2005) that rat hindlimb MNs with AHP half-decay times equal to or greater than 20 ms innervate slow-twitch muscle fibres.

Motoneurone properties of ketamine/xylazine anethetized rats. The one-way ANOVA test revealed significant main effects of MN type (fast vs. slow) for several electrophysiological properties. Motoneurone passive and f-I relationship

properties are summarized in Table 1 (passive properties are listed from 1-6 and f-I relationship properties 7-12). Fast MNs required 35% more current for spike generation in response to 50-ms square-wave current pulses compared to slow MNs. Input resistance and AHP amplitude were 34 and 45% smaller, respectively for fast MNs compared to slow MNs. During a ramp current, fast MNs required 32% more current to initiate firing and 35% more current to terminate rhythmic firing compared to slow MNs. Furthermore, the minimum instantaneous firing frequencies of fast MNs were significantly higher at spike- recruitment (36%) and derecruitment (42%) compared to slow MNs. The average ePIC was not significantly different between fast and slow MNs.

Types of f-I relationships. We injected ramps of current into the MNs and determined their f-I relationship type (see Table 2 for f-I relationship distributions). This method has been used previously (Bennett et al., 2001; Hounsgaard et al., 1988; Lee & Heckman, 1998b) to determine f-I relationships and as a way to estimate the PIC (see Figure 1). Similar to the four f-I relationship types demonstrated in rat sacral motoneurones in vitro (Bennett et al., 2001), in situ rat hind-limb α–MNs could also be categorized into the same four f-I relationship types. The f-I relationship types are shown in figure 2A-D. Type 1 (n = 7, 17%) MN f-I relationship demonstrated a firing frequency slope (average 24.3 ± 9.5 Hz/nA) that overlaps on the ascending and descending portions of the ramp current (figure 2A). Type 2 (n = 12, 28%) MN f-I relationship demonstrated a clockwise hysteresis (i.e. MN firing rate adaptation) where the firing frequencies were greater during the ascending versus the descending portion of the ramp at any given current and the average slope values of

the up and down portions of the ramp current were 12.6 ± 8.4 Hz/nA and 18.9 ± 10.4 Hz/nA, respectively (figure 2B). Type 3 (n = 19, 43%) MN f-I relationship demonstrated a linear regression line with some self-sustained firing corresponding to tertiary range of firing (Li et al., 2004) (i.e. activation of a PIC) and an average slope of 15.8 ± 6.8 Hz/nA (figure 2C). Type 4 (n = 5, 12%) MN f-I relationship demonstrated a counter-clockwise hysteresis or an acceleration of firing just after spike-recruitment and below the linear regression line (i.e. activation of a PIC) corresponding to the secondary range of firing. None of these MNs demonstrated a primary range of firing but rather started firing in the secondary range followed by shallower sloped tertiary range (see Li et al., (2001) figure 5 for further description of these three firing ranges during a ramp). The type 4 f-I relationship firing frequencies were greater during the descending versus the ascending portion of the ramp at any given current and the average slope values of the up and down portions of the ramp current were 16.7 ± 18.6 Hz/nA (secondary range) and 10.1 ± 2.6 Hz/nA (tertiary range), respectively. There were no significant f-I slope differences among f-I relationships or between MN types. However, there was a trend (P = 0.08) for a decreased slope during the down portion of the ramp in the f-I relationship type 4 compared to the other f-I relationship types.

ePIC amplitudes of f-I relationship types 3 and 4. Frequency-current relationship types 3 and 4 were shown in approximately 60% of MNs we recorded from. These relationship types demonstrate activation of a PIC. During the ePIC, firing frequencies were decreased by approximately 15% in both fast (30 Hz at spike recruitment vs. 25.5 Hz at spike de-recruitment) and slow MNs (15.2 Hz at spike

recruitment vs. 12.9 Hz at spike de-recruitment). Figure 3 illustrates a distribution of average ePIC measured from f-I relationship types 3 and 4. For any given cell, if the initial ramp elicited a PIC, all subsequent ramps did so as well. In most of the motoneurones the ePIC amplitude was consistent from ramp to ramp even when the ramp current was increased or decreased. Although ePIC amplitude did not differ among fast and slow MNs, X^2 analysis revealed a tendency (P = 0.09) for a greater proportion of slow MNs (87%) to demonstrate types 3 and 4 f-I relationships compared to fast MNs (50%).

Lastly, the ePIC was not correlated with the animal's vital signs (blood pressure or CO2 levels) throughout the experiment. However, there was a trend (P = 0.08) for the ePIC to be negatively correlated (-0.44) with time of day during the experiment.

Effect of sodium pentobarbital on MN ePIC amplitude in a ketamine/xylazine anesthetized rat. In one experiment we applied a series of ramps to a MN before and after the intravenous administration of sodium pentobarbital. In total, the MN was impaled for 80 minutes. Prior to the addition of pentobarbital, the ePIC amplitude average over 5 ramps was 0.52 nA. This was significantly (P < 0.001) higher than the ePIC amplitude average over the last 5 ramps recorded 40 – 60 minutes following the first injection of pentobarbital (0.16) (see figure 4A). Furthermore, the f-I relationship type was converting from type 3 to type 1 (see figure 4B). Although ePIC amplitudes decreased, the passive properties (RMP, Vth, rheobase, AHP amplitude and duration) remained similar (not shown) before and after the addition of pentobarbital. Because the MN had been impaled for a long time

prior to the administration of pentobarbital, we wished to demonstrate that the changes in ePIC were due to the drug rather than impalement time. Therefore, in another experiment we impaled a MN for 90 minutes without the addition of pentobarbital and subjected it to a series of ramps. The ePIC amplitude for this neurone was virtually the same at minute 1 (0.55 ± 0.09 nA) and minute 90 (0.56 ± 0.08 nA) (see inset in figure 4A).

Motoneurone RAMP spikes' voltage threshold and AHP properties of ketamine/xylazine anesthetized rats. We also analyzed Vth, AHP amplitude and ¾ decay time of the AHP for the initial 3 spikes during the depolarizing current phase of the ramp, the 3 spikes at the same current during the repolarizing current phase of the ramp, and when applicable the last 3 spikes triggered during the ePIC (see figure 5A and B for details) from 9 fast and 6 slow MNs (which demonstrated all 4 types of f-I relationships). Similar to a short orthodromic spike, the AHP amplitudes and durations of spikes during current ramps were smaller and shorter in fast MNs (see Table 3).

Most importantly, irrespective of MN or f-I relationship type, Vth and AHP properties during a ramp were no different from spike to spike (see figure 6). Figure 6 (which includes all spikes as opposed to the 9 we measured) shows Vths and AHP for all of the ramp shown in figure 5A. For this cell, spike-recruitment was induced at 17.4 nA and spike-derecruitment occurred at 16.1 nA. During this current, the cell generated a total of 19 spikes (12 of which occurred below the current at which spike-recruitment was initiated). Voltage threshold at each spike ranged from -42.7 to -46.5 mV, AHP amplitude ranged from 12 to16 mV, and the AHP ¾ decay time ranged

from 25 to 42 ms. Voltage threshold was consistent throughout. However, the AHP amplitude and duration increased and decreased as ramp current increased and decreased producing a greater range in the AHP properties. The voltage threshold and AHP properties measured at the first and last spikes were very similar in almost every ramp no matter the MN f-I relationship type (see figure 5C). In figure 5C spikes 1, 18, and 19 are at a higher gain then shown in figure 5A and table 4 summarizes Vth and AHP values recorded from the spikes.

The effect of Ketamine/xylazine Vs. decerebration on motoneurone properties. During another set of experiments we recorded from 14 MNs in 6 rats that were subjected to pre-collicular decerebration. All decerebration MNs that met the criteria for analysis were the fast type. This was due to sampling error, since we did record from some decerebrated MNs with AHP ½ decay times greater than 20 ms, and therefore not because of any effect of the decerebration on MN AHP time-course. One limitation in this study is that we compared MNs from an intact anesthetized animal to a non-intact non-anesthetized animal. This limitation could be alleviated in the future by comparing MNs from decerebrate animals to ketamine/xylazine treated decerebrate animals. Nonetheless, the one-way ANOVA revealed significant main effects of group (ketamine/xylazine vs. decerebration) for several electrophysiological properties of fast MNs (see Table 1 for details). Ketamine/xylazine MNs had significantly hyperpolarized (14%) RMP and Vth, required 40% more current for spike triggering and had 45% smaller AHP amplitudes compared to decerebration MNs. During a ramp the ketamine/xylazine MNs required 37 and 38% more current and their instantaneous firing frequencies were 28 and 34%

higher at spike- recruitment and spike-derecruitment respectively compared to decerebration MNs.

Ketamine/xylazine and decerebration MNs demonstrated similar f-I relationship types (see figure 2) and distributions (see Table 2). Furthermore, decerebration (0.7 ± 0.4) and ketamine/xylazine (0.6 ± 0.4) motoneurone mean ePIC amplitudes measured from the MNs demonstrating type 3 and 4 f-I relationships were also similar (see figure 7A). Furthermore, ePIC amplitude did not correlate with MN input resistance in ketamine/xylazine ($P = 0.9$) or decerebration ($P = 0.3$) rats (figure 7B).

Ketamine/xylazine MNs Vths of spikes during current ramps were 11% hyperpolarized, had 9% smaller AHP amplitudes and 45% shorter AHP ¾ decay times compared to decerebration MNs (see table 3 for details). Similar to ketamine/xylazine MNs, decerebration MNs' Vths, and AHP properties during a ramp were no different from spike to spike (see figure 6).

DISCUSSION

The most important finding of this study is that rat hindlimb α–motoneurones injected with ramp currents resulted in four types of f-I relationships, two of which demonstrated a presence of persistent inward current. The four f-I relationship types are similar to those noted previously in vitro using rat sacral MNs (Bennett et al., 2001). Moreover, it appears that the ePIC amplitude is not MN type dependent, which has been indirectly addressed previously in cat lumbar α–MNs (Lee & Heckman, 1998b) and rat sacral-caudal MNs (Bennett et al., 2001). However, f-I relationship types 3 and 4 tend to be more frequent in slow MNs compare to fast. The

presence of this ramp-induced PIC and its amplitude were not altered when the MNs were subjected to the anesthetic mixture of ketamine/xylazine compared to the decerebration preparation which is used to alleviate the effects of anesthetic. This finding is very significant because ketamine/xylazine allows us to estimate PICs in an intact animal (i.e. not decerebrated).

Prior to injecting ramps of current into the MN, we recorded basic properties that have been reported previously (Beaumont & Gardiner, 2003; Beaumont & Gardiner, 2002). Similar to the previous data that were recorded from anaesthetized MNs, no significant differences existed between the passive properties of fast and slow MNs; RMP and Vth, whereas slow MNs had a significantly lower rheobase current. Furthermore, IR, AHP amplitude and AHP ½ decay time were approximately double in slow vs. fast MNs. Thus, our MN passive property findings are comparable to those reported in the literature previously. In addition, during a ramp fast MNs required more current to initiate and stop rhythmic firing compared to the slow MNs. Furthermore, fast MNs had higher instantaneous firing frequencies at spike-recruitment and spike-derecruitment than slow MNs, which is comparable to rhythmic firing for fast and slow MNs in response to square wave pulses of current (Cormery et al., 2005). Similar to cat MNs (Lee & Heckman, 1998a) rheobase was correlated with current and instantaneous firing frequency at spike- recruitment and spike-derecruitment.

Motoneurones could be categorized into four f-I relationship types 1) linear, 2) adapting, 3) linear + self sustained firing, and 4) acceleration. These results are consistent with those previously reported in rat sacral MNs (Bennett et al., 2001). In

the present experiment, frequency-current relationship types 1 and 2 did not demonstrate the presence of a PIC. This may be explained by the fact that motoneurones' PIC amplitude tends to be muscle-dependent in that motoneurones innervating the postural muscles (triceps surae) are more likely to demonstrate PICs (Hounsgaard et al., 1988; Conway et al., 1988) which would be advantageous for maintaining force output during postural tasks (Alaburda et al., 2002). Since sciatic nerve MNs in rat innervate several muscle groups, the MNs demonstrating f-I relationship types 1 and 2 in the present study may have been recorded from MNs innervating muscles that are not required to maintain postural tasks or low forces over long periods of time.

Over 50% of the MNs we recorded from demonstrated type 3 and 4 f-I relationships. It is within these relationships types that the specific PIC voltage gated ion channels are activated (Bennett et al., 2001; Lee & Heckman, 1998a; Hounsgaard et al., 1988). The difference between type 3 and 4 f-I relationships is probably due to the voltage at which the specific voltage gated PIC channels are activated. The PIC in type 3 and 4 may be mediated through persistent Na^{+} and L-type Ca^{++} channels activated prior to the start of rhythmic firing while the PIC in type 4 may be mediated through an L-type Ca^{++} channel activated at a voltage threshold after the start of rhythmic firing (Li & Bennett, 2003). Furthermore, differences in f-I relationship types 3 and 4 may be due to the saturation level of the L-type Ca^{++} channel. Type 3 f-I relationship may activate the calcium PIC in a graded manner upon which additional increases in input result in minimal changes in the Ca^{++} PIC (i.e. it is saturated). However, during a type 4 f-I relationship the calcium PIC is perhaps activated upon

MN recruitment, leading to a steep increase in the firing frequency coinciding with the secondary range of the f-I relationship. Once the Ca^{++} PIC is saturated the slope of the f-I relationship is then reduced, corresponding to the tertiary range of firing (Elbasiouny et al., 2005).

Even though f-I relationship types 3 and 4 demonstrated linear and counter-clockwise relationships respectively, their ePIC magnitude was not different. It has been reported that Na^{+} and Ca^{++} PIC channels contribute approximately equally to the MNs total PIC (Li & Bennett, 2003), thus it is possible that these channels were activated equally in the type 3 and 4 f-I relationships reported here. In addition there was no MN type related ePIC amplitude dominance. This was not surprising since Lee & Heckman (1998a) demonstrated that MN bistability (a property facilitated by PIC) was more pronounced in low vs. high rheobase current (a characteristic of slow vs. fast type MNs, respectively (Beaumont & Gardiner, 2002)), however there was no difference in the initial PIC conductance. The lack of bistability in high rheobase current MNs may be attributed to a faster inactivation of the PIC channels. Bennett et al. (2001) also showed that no difference existed in the amount of PIC between low and high rheobase current sacral-caudal MNs. It also appears that ePIC amplitude is not related to MN type, rheobase current or input resistance in rat hindlimb MNs. Hence, MNs of all sizes have the ability to produce self-sustained firing. Although, the previous statement may be of merit, our data lends some support to a MN type difference in the proportions of MNs demonstrating f-I relationship types 3 and 4. There is a tendency for a greater proportion of slow MNs to have a type 3 or 4 f-I

relationship, which does indeed support the findings (Lee & Heckman, 1998a) that a greater number of smaller MNs demonstrate bistability.

It has been suggested that the F-I function which uses current injected into the soma to fire the cell does not provide a good measure of the enhancement of synaptic input by the PIC (Heckman et al., 2004). However, the ramp technique which is used to determine a MN's F-I function has been successfully used as a way to estimate or at least demonstrate activation of its PIC or a lack thereof. We injected a series of ramp currents into each MN, and unlike earlier reports, averaged all ePICs amplitudes as overall PIC. Interestingly, if the first ramp demonstrated f-I relationship type 3 or 4 (i.e. PIC) all subsequent ramps in the series also demonstrated f-I relationship type 3 or 4 (i.e. PIC). These ramp-induced ePIC amplitudes were similar across the series, with low variability. This was also the case for the other two f-I relationship types. To further illustrate the presence of PIC in types 3 and 4 f-I relationships we injected ramps in a MN before and after the addition of pentobarbital. Pentobarbital was chosen because it abolishes MN PICs (Guertin & Hounsgaard, 1999; Hultborn & Kiehn, 1992; Hultborn, 1999). Motoneurones of animals anesthetized with pentobarbital still retain the ability to rhythmically fire since it does not seem to affect the fast persistent inward current (Na^{++} PIC channel) (Lee & Heckman, 2001). L-type Ca^{++} channels located on MN dendrites do not appear to amplify synaptic Ia currents in pentobarbital cats compared to decerebrate cats (Lee & Heckman, 2000). Thus, it is more likely that pentobarbitol may influence the L-type Ca^{++} channels and subsequently decrease MN bistability. Similarly, our pentobarbital treated MN had a major decrease in ePIC amplitude to a point where its f-I relationship was almost

completely converted from type 3 to type 1. The ePIC was not completely reduced to zero suggesting that perhaps some persistent inward Na^+ current may have not been inhibitied. The MN impalement duration lasted 80 minutes for these recordings, but we later showed that impalement time does not influence the MN's ePIC amplitude or f-I relationship type. These findings reconfirm that ramps evoke PICs which subsequently alter the MN's f-I relationship.

The possibility of an AHP amplitude and duration changing throughout an individual ramp was investigated. Lower firing frequencies at spike-derecruitment where the activated PIC is supposed to help maintain these frequencies might be partially explained by changes in the inter-spike interval AHP amplitude and duration. Perhaps towards the end of motor-unit discharge, a sustained sub-threshold depolarization with the addition of noise may cause the MN to fire one or more times (Kudina, 1999; Matthews, 1996; Gorassini et al., 2002). However, this finding was in human motor-units and perhaps the fluctuation in background noise and spontaneous firing was due to the subject's inadequacy to control their level of voluntary contraction. It has also been suggested in cat spinal MNs that an increased AHP duration contributes to the low firing frequencies at spike-derecruitment (Wienecke et al., 2005). Our data indicate that there were no differences between Vth, AHP amplitude or AHP duration from spike to spike during a ramp for any f-I relation type. Occasionally, the final spike had a longer AHP ¾ decay time compared to the first spike during a ramp which demonstrated a f-I relationship type 3 and 4, but this occurred infrequently. Furthermore, the average number of spikes triggered during the ePIC was 11 (not shown in results) and even if the final spike AHP ¾ decay time

was prolonged, this did not apply to the other 10 spikes. A potential limitation to this finding was that our ramp currents were selected on the bases of only evoking 10 – 75 spikes over a 0.5 – 2.5 second duration (i.e. slow firing rate) and we acknowledge that if we used higher ramp currents the firing frequency would have increased and caused changes to the properties listed above (Schwindt & Crill 1982; Bennett et al. 2001). However, the main purpose of these measurements was to demonstrate that additional spike generation is probably not attributable to changes in these properties but instead to the activated PIC.

Another purpose for our study was to determine the effects of ketamine/xylazine on motoneurone properties. Therefore, we also recorded MN properties from decerebrated rats. It has been suggested recently that anesthetic agents may render the MN as 'sleeping' and may mask some of its important functional properties (Guertin & Hounsgaard, 1999; Delgado-Lezama & Hounsgaard, 1999; Hultborn & Kiehn, 1992; Button et al., 2005a), which are significant in 'awake' MNs. Thus, it was important to determine if MN properties do indeed differ in an anaesthetized versus an unanesthetized rat preparation. Decerebration MNs RMP and Vth were significantly depolarized compared to ketamine/xylazine MNs and required far less rheobase current to reach that threshold. Ketamine has been shown to increase K^+ permeability in synaptosomes (Okun et al., 1986) and block voltage gated Na^+ and K^+ channels in superficial dorsal horn neurones of the lumbar spinal cord thereby reducing their excitability (Schnoebel et al., 2005). Perhaps this also holds true for the MN. An increase in the permeability of K^+ would result in a hyperpolarized RMP in ketamine/xylazine MNs compared to decerebration MNs.

This may suggest that changes in the activation of the ion channels or a change in their conductance that is responsible for these motoneurone properties may occur as a result of ketamine/xylazine. Even though the AHP amplitude was different, AHP duration remained the same. Ketamine has been shown inhibit large conductance Ca^{++}-activated K^{+} channels (BK) in GH3 cells (Denson & Eaton, 1994). BK channel activation is dominant during the big and fast portion of the AHP and if inhibited in the MN by ketamine/xylazine, it would lead to decreased AHP amplitude compared to decerebrate MNs. Since AHP ½ decay times were similar in decerebration and ketamine/xylazine MNs, one could speculate that the ion channels remain open for similar periods of time, but that fewer ion channels open. Similarly, decerebration MNs required less current to initiate and end rhythmic firing and had lower instantaneous firing frequencies at this initiation and end period during rhythmic firing compared to ketamine/xylazine MNs. Overall, based on rheobase current and the amount of current required to initiate rhythmic firing, a ketamine/xylazine mixture appears to render the MN as less excitable, and thus must affect the ion channels that underlie these basic and rhythmic properties.

No difference in ePIC amplitude existed between anaesthetized vs. unanaesthetized MNs. There is no evidence suggesting that ketamine/xylazine affects PIC channels. Xylazine is an alpha 2-adrenoceptor agonist which presumably should not affect PIC channels, whereas ketamine is a NMDA receptor antagonist (Liu et al., 2001). Persistent inward currents are mediated by L-type Ca^{++} channels which are selectively blocked by nimodipine (Li et al., 2004), thus it is not expected that ketamine/xylazine would influence PIC as seen in this study. Although NMDA

receptors have a role in membrane bistability (Hochman et al., 1994) and are present in adult turtle MNs (Guertin & Hounsgaard, 1998) and neonatal rat MNs (Hochman et al., 1994; Hsiao et al., 2002; Palecek et al., 1999), they have no influence on PIC. The decerebration preparation preserves the brainstem and spinal cord in an unanesthetized state which does not negatively influence PIC (Kiehn & Eken, 1998; Kiehn, 1991; Hultborn, 1999; Heckman et al., 2004). Thus, ketamine or xylazine does not affect the major PIC channels in these MNs.

We also described Vth and AHP properties from the ramp technique which, to our knowledge, have not been reported in the literature. Similar to the case with short orthodromic spike, ramp spikes' Vths were depolarized and AHP amplitudes were bigger in decerebrate MNs. Interestingly their AHP ¾ decay time was much longer. Ketamine/xylazine inhibits the small conductance Ca^{++}-activated K^+ channel (SK2) (Dreixler et al., 2000) which is responsible for the slow portion of the AHP and practically the whole AHP during rhythmic firing (Miles et al., 2005). Perhaps ketamine/xylazine partially blocked the MNs small conductance Ca^{++}-activated K^+ channel and its conductance, which lead to a decreased AHP amplitude and duration compared to decerebration MNs. The change in these AHP properties are more than likely the result of a ketamine-induced change to the SK channel that behaves somewhat differently during rhythmic firing compared to an orthodromic spike.

Lastly, the change in firing frequency at spike recruitment vs. spike de-recriutment (types 3 and 4 f-I relationships only – approximately 4 Hz) during ramp currents in our intact anesthetized animal preparation is comparable to that found via paired motor-unit methods in awake rats (Gorassini et al., 1999) and humans

(Gorassini et al., 2002). Motor-units can be de-recruited at lower frequencies than they are initially recruited at during slow triangular muscle contractions, muscle vibration, and sinusoidal muscle stretch. The difference in firing frequency between recruitment and de-recruitment is thought to be provided by the motoneurone's intrinsic PIC. Since these frequencies are comparable, perhaps the ePIC amplitudes found in MNs from our intact anesthetized rat preparation could be used as a starting point for estimating the size of PICs in awake rat and human motor-units.

In conclusion, rat hindlimb α-motoneurones injected with ramp currents can be categorized into one of four different f-I relationship types. Two of these f-I relationships, which were more frequent in slow MNs, demonstrated the existence of persistent inward current. The ePIC amplitude did not differ between f-I relationships type 3 and 4 or between fast and slow MNs. Although the anesthetic mixture of ketamine/xylazine renders the MN as less excitable to initiate spike threshold or rhythmic threshold compared to decerebration MNs, it does not affect the ePIC amplitude, just the voltage and current required to activate these channels and AHP properties during a short spike or a burst of spikes. Ramp current injections activated the PIC channels in MNs of intact animals anesthetized by ketamine/xylazine and decerebrate animals. This statement is supported by the following findings: 1) once a MN demonstrates an ePIC all subsequent ramp currents injected into that same MN also evoke ePICs, 2) the MN f-I relationship remains the same from ramp to ramp 3) the addition of pentobarbital decreases the ramp ePIC as previously shown (Guertin & Hounsgaard, 1999) in turtle MNs, 4) during the ramp the spikes Vth and AHP properties remain unchanged and 5) the ramp technique has been verified as

successful demonstrating the PIC in other animal preparations (Hounsgaard et al., 1988; Lee & Heckman, 1998b; Bennett et al., 2001). Finally, the anesthetic mixture ketamine/xylazine allows us to measure PIC in intact animals which could be administered during future planned experiments to determine how the MN ePIC is influenced by different physiological parameters.

REFERENCE LIST

Alaburda A, Perrier JF, & Hounsgaard J (2002). Mechanisms causing plateau potentials in spinal motoneurones. *Adv Exp Med Biol* **508**, 219-26.

Beaumont E & Gardiner P (2002). Effects of daily spontaneous running on the electrophysiological properties of hindlimb motoneurones in rats. *J Physiol* **540**, 129-38.

Beaumont E & Gardiner PF (2003). Endurance training alters the biophysical properties of hindlimb motoneurons in rats. *Muscle Nerve* **27**, 228-36.

Bennett DJ, Li Y & Siu M (2001). Plateau potentials in sacrocaudal motoneurons of chronic spinal rats, recorded in vitro. *J Neurophysiol* **86** , 1955-71.

Brownstone RM, Jordan LM, Kriellaars DJ, Noga BR & Shefchyk SJ (1992). On the regulation of repetitive firing in lumbar motoneurones during fictive locomotion in the cat. *Exp Brain Res* **90**, 441-55.

Button DB, Gardiner KR, Marqueste T & Gardiner PF (2005a). Frequency-current relationships in anesthetized and decerebrated rat hindlimb motoneurones in situ. *Program No. 750.9. 2005 Abstract Viewer/Itinerary Planner. Washington, DC: Society for Neuroscience, 2005. Online.* (Abstract)

Button DC, Gardiner K, Zhong H, Roy RR, Egerton VR & Gardiner PF (2005b). In Situ Frequency-Current (f-I) Relationships of Hindlimb α-Motoneurones (α-Mns) In Spinal Cord Transected (ST) and Spinal Cord Isolated (SI) Rats. *Canadian Journal of Applied Physiology* **30**, S15(Abstract)

Conway BA, Hultborn H, Kiehn O & Mintz I (1988). Plateau potentials in alpha-motoneurones induced by intravenous injection of L-dopa and clonidine in the spinal cat. *J Physiol* **405**, 369-84.

Cormery B, Beaumont E, Csukly K & Gardiner P (2005). Hindlimb unweighting for two weeks alters physiological properties of rat hindlimb motoneurones. *J Physiol*

Cormery B, Marini JF & Gardiner PF (2000). Changes in electrophysiological properties of tibial motoneurones in the rat following 4 weeks of tetrodotoxin-induced paralysis. *Neurosci Lett* **287**, 21-4.

Delgado-Lezama R & Hounsgaard J (1999). Chapter 5: Adapting motoneurons for motor behavior. In *Peripeheral and spinal Mechanisms in The Neural Control of Movement*, ed. Binder MD, pp. 57-63. Progress in Brain Research: Elsevier.

Denson DD & Eaton DC (1994). Ketamine inhibition of large conductance Ca(2+)-activated K+ channels is modulated by intracellular Ca2+. *Am J Physiol* **267**, C1452-8.

Dreixler JC, Jenkins A, Cao YJ, Roizen JD & Houamed KM (2000). Patch-clamp analysis of anesthetic interactions with recombinant SK2 subtype neuronal calcium-activated potassium channels. *Anesth Analg* **90**, 727-32.

Elbasiouny SM, Bennett DJ & Mushahwar VK (2005). Simulation of Ca+2 Persistent Inward Currents in Spinal Motoneurons: Mode of Activation and Integration of Synaptic Inputs. *J Physiol*

Fouad K & Bennett DJ (1998). Decerebration by global ischemic stroke in rats. *J Neurosci Methods* **84**, 131-7.

Gardiner PF (1993). Physiological properties of motoneurons innervating different muscle unit types in rat gastrocnemius. *J Neurophysiol* **69**, 1160-70.

Gardiner PF & Seburn KL (1997). The effects of tetrodotoxin-induced muscle paralysis on the physiological properties of muscle units and their innervating motoneurons in rat. *J Physiol* **499 (Pt 1)**, 207-16.

Gilmore J & Fedirchuk B (2004). The excitability of lumbar motoneurones in the neonatal rat is increased by a hyperpolarization of their voltage threshold for activation by descending serotonergic fibres. *J Physiol* **558**, 213-24.

Gorassini M, Bennett DJ, Kiehn O, Eken T, & Hultborn H (1999). Activation patterns of hindlimb motor units in the awake rat and their relation to motoneuron intrinsic properties. *J Neurophysiol* **82**, 709-17.

Gorassini M, Yang JF, Siu M & Bennett DJ (2002). Intrinsic activation of human motoneurons: possible contribution to motor unit excitation. *J Neurophysiol* **87**, 1850-8.

Granit R, Kernell D & Shortess GK (1963). Quantitative aspects of repetitive firing of mammalian motoneurones, caused by injected currents. *J Physiol* **168**, 911-31.

Guertin PA & Hounsgaard J (1998). NMDA-Induced intrinsic voltage oscillations depend on L-type calcium channels in spinal motoneurons of adult turtles. *J Neurophysiol* **80**, 3380-2.

Guertin PA & Hounsgaard J (1999). Non-volatile general anaesthetics reduce spinal activity by suppressing plateau potentials. *Neuroscience* **88**, 353-8.

Heckman CJ, Gorassini MA & Bennett DJ (2004). Persistent inward currents in motoneuron dendrites: Implications for motor output. *Muscle Nerve*

Hochman S, Jordan LM & Schmidt BJ (1994). TTX-resistant NMDA receptor-mediated voltage oscillations in mammalian lumbar motoneurons. *J Neurophysiol* **72**, 2559-62.

Hounsgaard J, Hultborn H, Jespersen B & Kiehn O (1988). Bistability of alpha-

motoneurones in the decerebrate cat and in the acute spinal cat after intravenous 5-hydroxytryptophan. *J Physiol* **405**, 345-67.

Hsiao CF, Wu N, Levine MS & Chandler SH (2002). Development and serotonergic modulation of NMDA bursting in rat trigeminal motoneurons. *J Neurophysiol* **87**, 1318-28.

Hultborn H (1999). Plateau potentials and their role in regulating motoneuronal firing. *Prog Brain Res* **123**, 39-48.

Hultborn H & Kiehn O (1992). Neuromodulation of vertebrate motor neuron membrane properties. *Curr Opin Neurobiol* **2**, 770-5.

Kernell D (1965a). The adaptation and the Relation Between Discharge Frequency and Current Strength of Cat Lumbosacral Motoneurones Stimulated by Long-Lasting Injected Currents. *Acta. Physiol. Scand.*

Kernell D (1965b). High-Frequency Repetitive Firing of Cat Lumbosacral Motoneurones Stimulated by Long-Lasting Injected Currents. *Acta. Physiol. Scand.* **65**, 74-86.

Kernell D (1965c). The Limits of Firing Frequency in Cat Lumbosacral Motoneurones Possessing Different Time Course of Afterhyperpolarization. *Acta. Physiol. Scand.* **65**, 87-100.

Kernell D & Monster AW (1981). Threshold current for repetitive impulse firing in motoneurones innervating muscle fibres of different fatigue sensitivity in the cat. *Brain Res* **229**, 193-6.

Kiehn O (1991). Plateau potentials and active integration in the 'final common pathway' for motor behaviour. *Trends Neurosci* **14**, 68-73.

Kiehn O & Eken T (1998). Functional role of plateau potentials in vertebrate motor neurons. *Curr Opin Neurobiol* **8**, 746-52.

Kudina LP (1999). Analysis of firing behaviour of human motoneurones within 'subprimary range'. *J Physiol Paris* **93**, 115-23.

Lee RH & Heckman CJ (1998a). Bistability in spinal motoneurons in vivo: systematic variations in persistent inward currents. *J Neurophysiol* **80**, 583-93.

Lee RH & Heckman CJ (1998b). Bistability in spinal motoneurons in vivo: systematic variations in rhythmic firing patterns. *J Neurophysiol* **80** , 572-82.

Lee RH & Heckman CJ (1999). Paradoxical effect of QX-314 on persistent inward currents and bistable behavior in spinal motoneurons in vivo. *J Neurophysiol* **82**, 2518-27.

Lee RH & Heckman CJ (2000). Adjustable amplification of synaptic input in the dendrites of spinal motoneurons in vivo. *J Neurosci* **20**, 6734-40.

Li Y & Bennett DJ (2003). Persistent sodium and calcium currents cause plateau potentials in motoneurons of chronic spinal rats. *J Neurophysiol* **90**, 857-69.

Li Y, Gorassini MA & Bennett DJ (2004). Role of persistent sodium and calcium currents in motoneuron firing and spasticity in chronic spinal rats. *J Neurophysiol* **91**, 767-83.

Liu HT, Hollmann MW, Liu WH, Hoenemann CW & Durieux ME (2001). Modulation of NMDA receptor function by ketamine and magnesium: Part I. *Anesth Analg* **92**, 1173-81.

Matthews PB (1996). Relationship of firing intervals of human motor units to the trajectory of post-spike after-hyperpolarization and synaptic noise. *J Physiol* **492 (Pt 2)**, 597-628.

Miles GB, Dai Y & Brownstone RM (2005). Mechanisms underlying the early phase of spike frequency adaptation in mouse spinal motoneurones. *J Physiol*

Munson JB, Foehring RC, Mendell LM & Gordon T (1997). Fast-to-slow conversion following chronic low-frequency activation of medial gastrocnemius muscle in cats. II. Motoneuron properties. *J Neurophysiol* **77**, 2605-15.

Okun IM, Aksentsev SL & Konev SV (1986). [Effect of the general anesthetic ketamine on the potassium permeability of plasma membranes of brain synaptosomes]. *Biofizika* **31**, 917-8.

Palecek JI, Abdrachmanova G, Vlachova V & Vyklick L (1999). Properties of NMDA receptors in rat spinal cord motoneurons. *Eur J Neurosci* **11**, 827-36.

Powers RK & Binder MD (2001). Input-output functions of mammalian motoneurons. *Rev Physiol Biochem Pharmacol* **143**, 137-263.

Powers RK, Sawczuk A, Musick JR & Binder MD (1999). Multiple mechanisms of spike-frequency adaptation in motoneurones. *J Physiol Paris* **93**, 101-14.

Sawczuk A, Powers RK & Binder MD (1995). Spike frequency adaptation studied in hypoglossal motoneurons of the rat. *J Neurophysiol* **73**, 1799-810.

Schnoebel R, Wolff M, Peters SC, Brau ME, Scholz A, Hempelmann G, Olschewski H & Olschewski A (2005). Ketamine impairs excitability in superficial dorsal horn neurones by blocking sodium and voltage-gated potassium currents. *Br J Pharmacol* **146**, 826-33.

Schwindt P & Crill WE (1977). A persistent negative resistance in cat lumbar motoneurons. *Brain Res* **120**, 173-8.

Schwindt PC (1973). Membrane-potential trajectories underlying motoneuron rhythmic firing at high rates. *J Neurophysiol* **36**, 434-9.

Schwindt PC & Crill WE (1981). Negative slope conductance at large depolarizations in cat spinal motoneurons. *Brain Res* **207**, 471-5.

Schwindt PC & Crill WE (1982). Factors influencing motoneuron rhythmic firing: results from a voltage-clamp study. *J Neurophysiol* **48**, 875-90.

Skydsgaard M & Hounsgaard J (1996). Multiple actions of iontophoretically applied serotonin on motorneurones in the turtle spinal cord in vitro. *Acta Physiol Scand* **158**, 301-10.

Wienecke J, Zhang M & Hultborn H (2005). The postspike afterhyperpolarization (AHP) following single spikes is prolonged by a preceding spike-train in cat spinal motneurones. Program No. 750.8. *2005. Abstract Viewer/Itinerary Planner.* Washington, DC: Society for Neuroscience, 2005. Online., (Abstract)

Zengel JE, Reid SA, Sypert GW & Munson JB (1985). Membrane electrical properties and prediction of motor-unit type of medial gastrocnemius motoneurons in the cat. *J Neurophysiol* **53**, 1323-44.

ACKNOWLEDGEMENTS.

This research was supported by grants from NSERC Canada, CIHR, and the Canada Research Chairs program. The authors would like to thank Gilles Detillieux, Matt Ellis and Maria Setterbom at University of Manitoba for technical assistance, Farrell Cahill for assistance in data analysis, and Dr. Jayne Kalmar for comments and suggestions during manuscript preparation. P.F.G. is Canada Research Chair in Physical Activity & Health Studies at University of Manitoba.

TABLES

Table 1: Passive and Active Motoneurone Properties.

Motoneurone Property	KX Fast Cells Mean ± SD	KX Slow Cells Mean ± SD	Decerebration Fast Cells Mean ± SD	P value
Rheobase				
1. RMP (mV)	−70.9 ± 6.3	−64.2 ± 5.9	−61.7 ± 7.8	** **0.005**
2. Vth (mV)	−51.6 ± 6.6	−46.1 ± 11.7	−45.6 ± 7.2	** **0.02**
3. Current (nA)	9.8 ± 3.0 n = 21	5.9 ± 4.7 n = 7	6.4 ± 1.8 n = 14	* **0.01** ** **0.01**
4. Input Resistance (MΩ)	1.8 ± 0.6 n = 21	2.7 ± 1.2 n = 7	2.2 ± 0.9 n = 14	* **0.01**
5. AHP Amplitude(mV)	1.5 ± 1.1	2.7 ± 2.1	2.6 ± 2.2	0.06
6. AHP ½ Decay Time (ms)	13.8 ± 1.9 n = 21	27.3 ± 6.6 n = 7	12.7 ± 2.9 n = 14	* **0.00**
7. Current at Spike Recruitment (nA)	11.0 ± 3.1 n = 21	7.4 ± 3.9 n = 7	6.9 ± 4.0 n = 14	* **0.004** ** **0.001**
8. Current at Spike Derecruitment (nA)	10.9 ± 3.1 n = 21	7.0 ± 4.0 n = 7	6.6 ± 4.2 n = 14	* **0.01** ** **0.001**
9. Instantaneous Frequency at Spike Recruitment (Hz)	26.5 ± 7.7 n = 21	16.7 ± 7.2 n = 7	19.0 ± 6.7 n = 14	* **0.003** ** **0.003**
10. Instantaneous Frequency at Spike Derecruitment (Hz)	24.7 ± 6.8 n = 21	14.1 ± 5.6 n = 7	16.3 ± 4.6 n = 14	* **0.000** ** **0.000**
11. Slope (Hz/nA) Depolarizing	17.8 ± 9.7 n = 21	15.3 ± 8.5 n = 7	15.1 ± 11.0 n = 14	0.6
12. ePIC (nA)	0.2 ± 0.6 n = 21	0.4 ± 0.3 n = 7	0.3 ± 0.5 n = 14	0.6

Summary of passive (numbers 1-6 in chart) and active (numbers 7-12 in chart) MN properties. Data are presented as means ± 1 standard deviation for MNs in each group and includes all f-I relationship types. Ketamine/Xylazine (KX), resting membrane current (RMP), voltage threshold (Vth), afterhyperpolarization (AHP), estimated

persistent inward current (ePIC). * Significant difference between KX fast and slow motoneurones. ** Significant difference between KX fast and decerebration fast motoneurones

Table 2: Summary of f-I relationship types.

	Number (n)	f-I Relationship Type							
		Type 1: Overlapping		Type 2: Adapting		Type 3: Linear + sustained		Type 4: Acceleration	
		n	%	n	%	n	%	n	%
All MNs	43	7	17	12	28	19	43	5	12
KX Fast MNs	22	4	18	7	32	11	50	0	0
KX Slow MNs	7	1	15	0	0	4	57	2	28
Decerebration Fast MNs	14	2	14	5	36	4	28	3	22

Table 3: Voltage threshold, AHP amplitude and AHP duration of ramp spikes.

RAMP Motoneurone Property	KX Fast Cells	KX Slow Cells	Decerebration Fast Cells	P value
	Mean ± SD	Mean ± SD	Mean ± SD	
1. Ramp Vth (mV)	–45.1 ± 6.1 n = 9	–45.5 ± 10.6 n = 7	–40.5 ± 5.2 n = 6	** **0.007**
2. Ramp AHP amplitude (mV)	8.6 ± 2.0 n = 9	10.6 ± 2.7 n = 7	9.4 ± 2.3 n = 6	* **0.000** ** **0.02**
3. Ramp AHP ¾ duration time (ms)	19.9 ± 3.3 n = 9	41.8 ± 19.7 n = 7	35.9 ± 14.9 n = 6	* **0.000** ** **0.000**

Data are presented as means ± 1 standard deviation of all MNs in each group and includes all f-I relationship types. Ramp voltage threshold (Vth), ramp afterhyperpolarization (AHP). * Significant difference between KX fast and slow motoneurones. ** Significant difference between KX and decerebration fast motoneurones

Table 4: Voltage threshold, AHP properties and ramp current of first and last two ramp spikes.

	Spike 1	Spike 18	Spike 19
Current required for spike generation (nA)	17.4	16.4	16.1
Vth prior to spike generation (mV)	–42.7	–45.6	–44.0
AHP amplitude (mV)	16.0	13.4	14.3
AHP ¾ duration time (ms)	35.0	34.6	42.0

Data represent the Vth and AHP properties of the ramp spikes in figure 5C.

Afterhyperpolarization (AHP), voltage threshold (Vth).

FIGURES

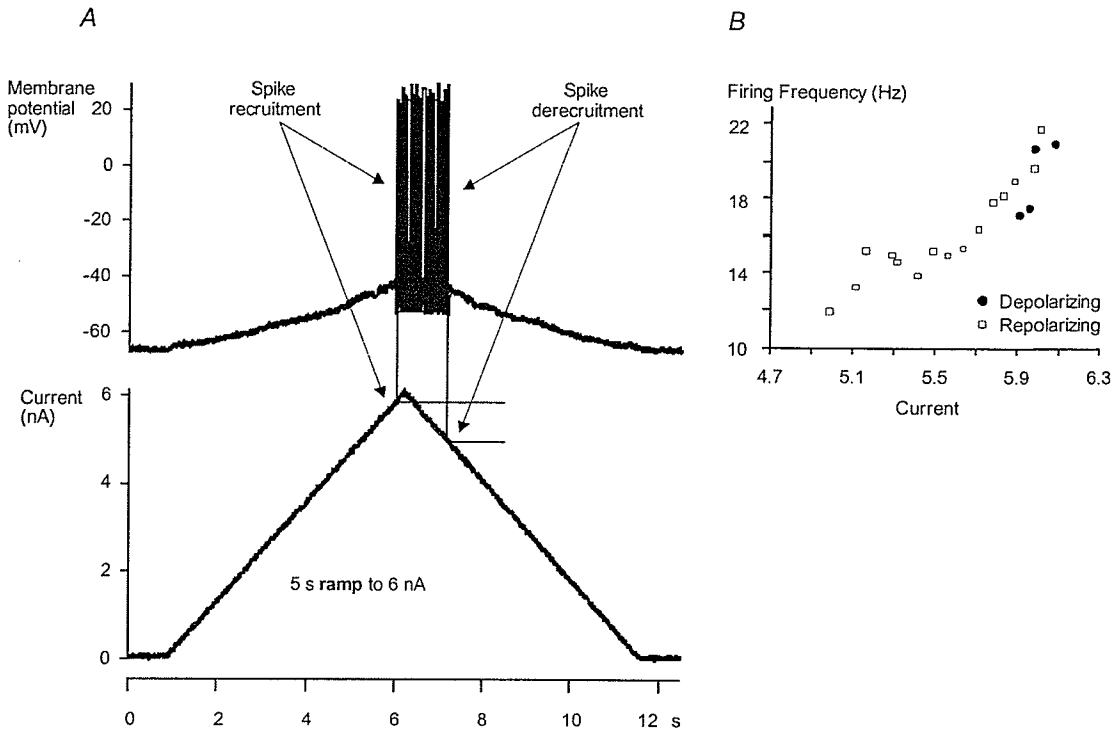

Figure 1. f–I relationships determined by using 5 s up–down ramp injections. A, the top trace is the rhythmic discharge of the MN in response to a ramp current (bottom trace). Arrows point to the current at spike recruitment and spike derecruitment. Estimated PIC (ePIC) was calculated by subtracting the current at spike derecruitment from the current at spike recruitment. B is a plot of the instantaneous firing frequency and current from traces in A. In this example, the f–I relationship was plotted as an counter-clockwise hysteresis.

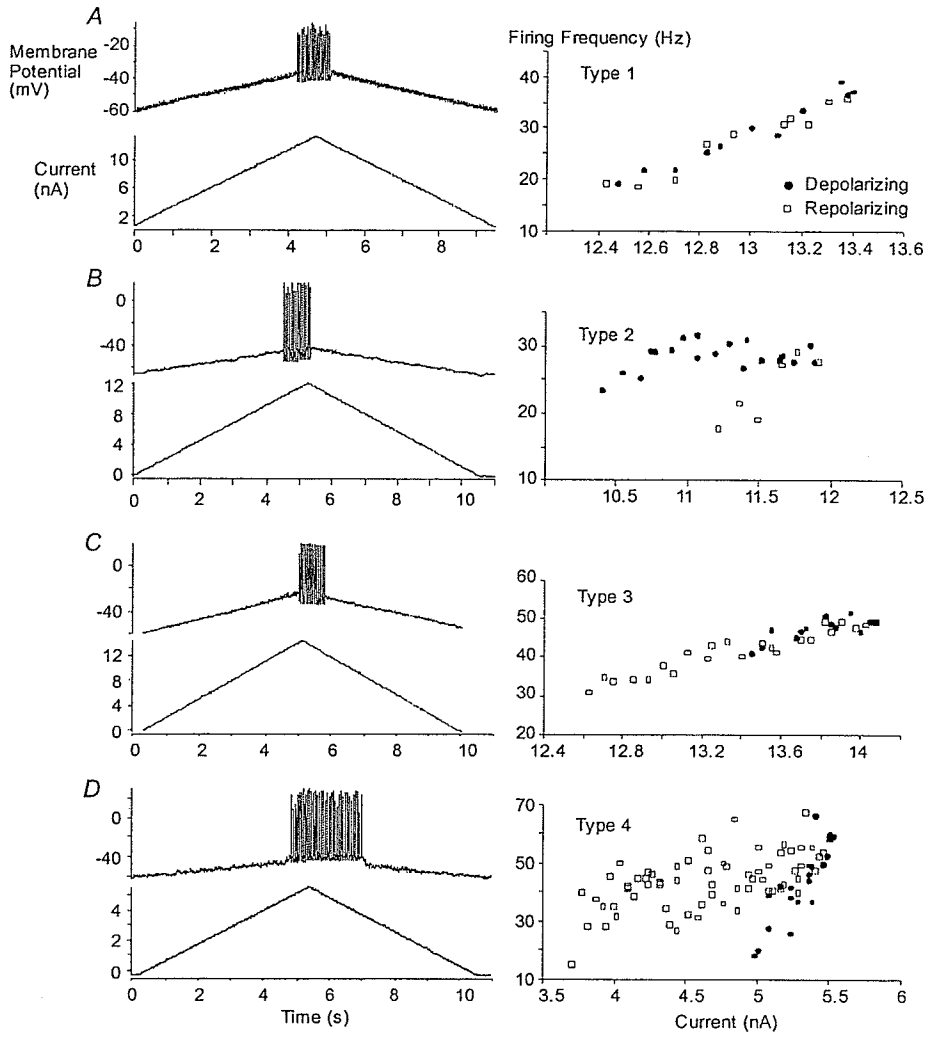

Figure 2. A, B, C and D represent four different ramp-induced f–I relationship types; left is the raw ramp data and right is the plotted f–I relationship. A, type 1MN f–I relationship demonstrates a firing frequency slope that overlaps on the ascending and descending current ramps. B, type 2 MN f–I relationship demonstrates a clockwise hysteresis (MN firing rate adaptation). C, type 3MN f–I relationship demonstrates a linear regression line (upper portion of graph) with some self-sustained firing. D, type 4 MN f–

I relationship demonstrates a counter-clockwise hysteresis or an acceleration of firing just after spike recruitment and below the linear regression line.

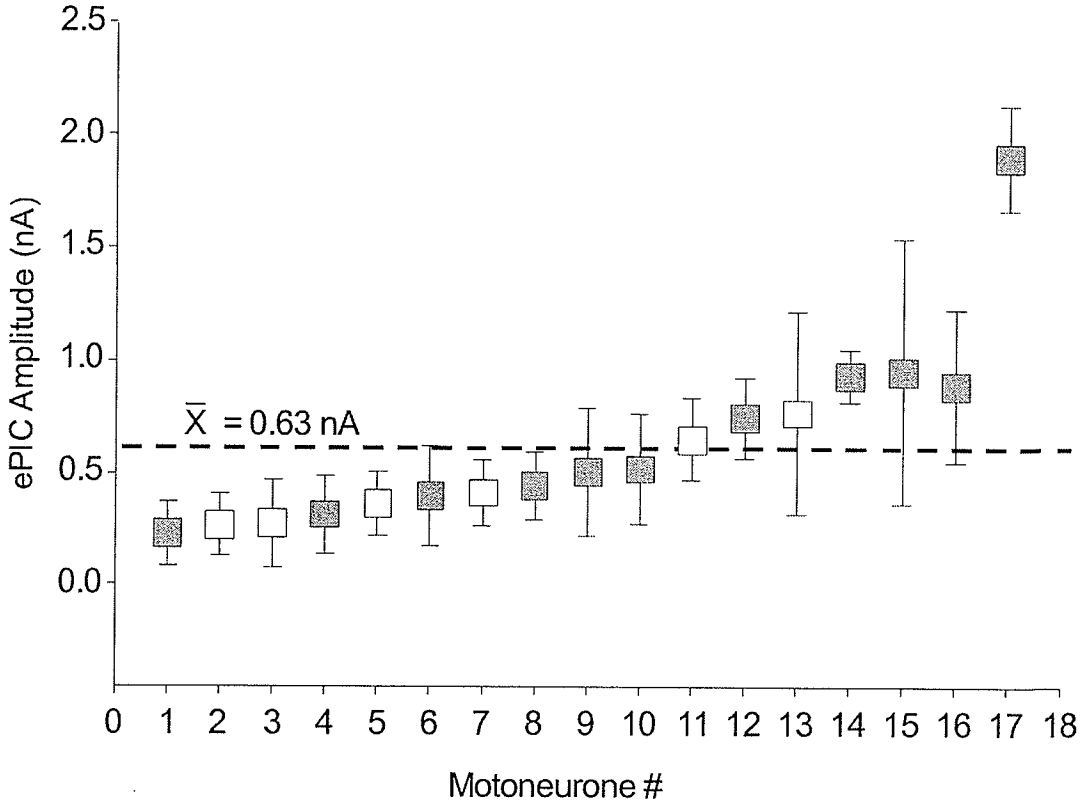

Figure 3. Recordings from MNs demonstrating type 3 and 4 f–I Relationships. Each data point represents the ePIC amplitude of a MN subjected to a series of ramps (minimum of at least three). The grey and white squares represent fast and slow MNs, respectively. The dashed line represents the mean ePIC for all cells. Data points are presented as means ± 1 S.D.

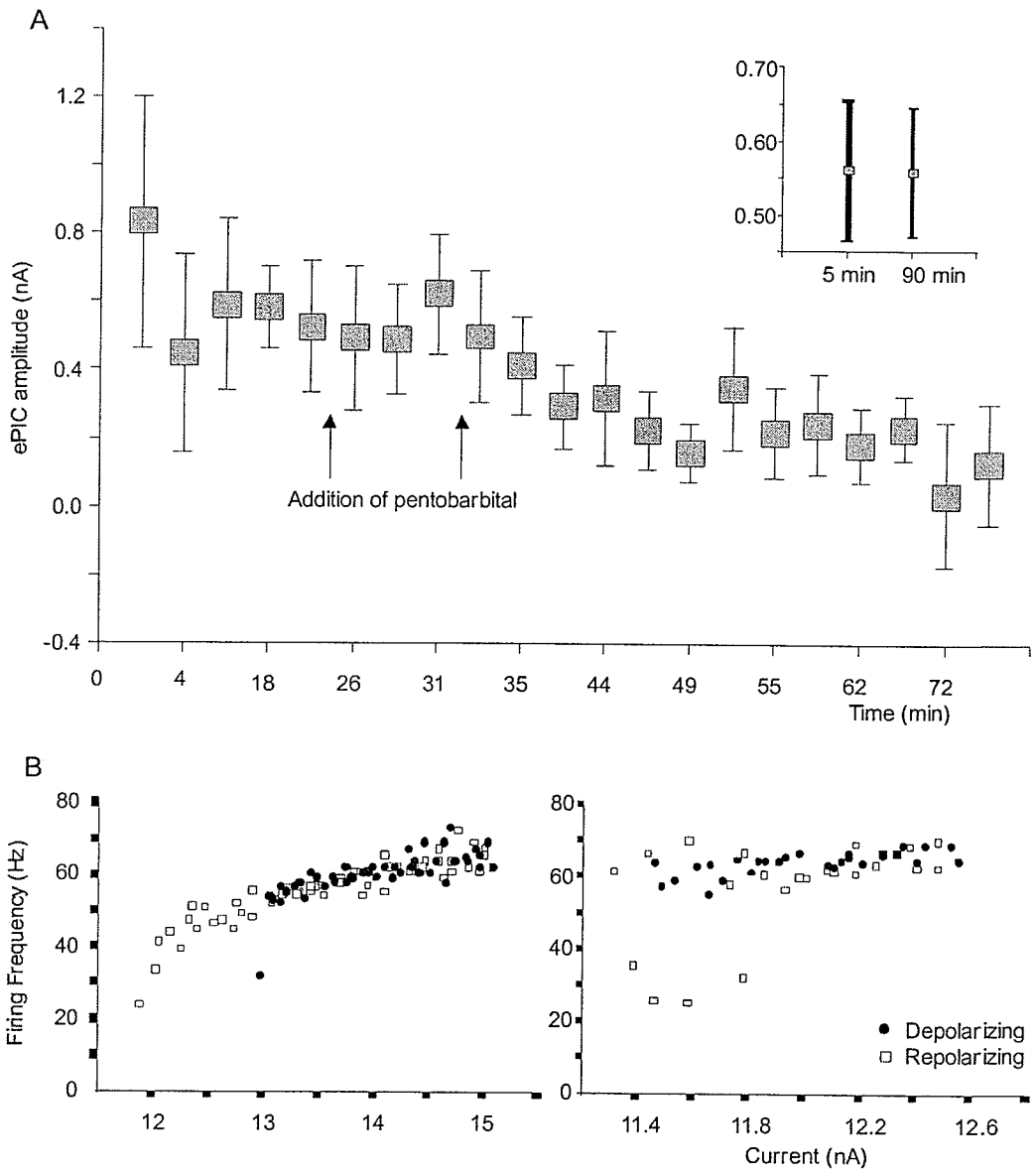

Figure 4. The effect of pentobarbitone on MN ePIC amplitude and f-I relationship. A, data were recorded from one MN. Each data point represents the ePIC amplitude average from of a series of ramps (minimum of at least three) at each time period before and after the addition of pentobarbitone. Arrows indicate when pentobarbitone was injected into the rat. The inset indicates that the ePIC does not

depend on the time course of the glass microelectrode impalement of the motoneurone. B, left is a graph showing the MN f–I relationship (type 3). Its response to a 5 s ramp current injection was measured before the addition of pentobarbitone. Right is a graph demonstrating that upon injection of pentobarbitone, the f–I relationship of the MN is almost converted (within 1 h of motoneurone impalement) from f–I relationship type 3 to type 1.

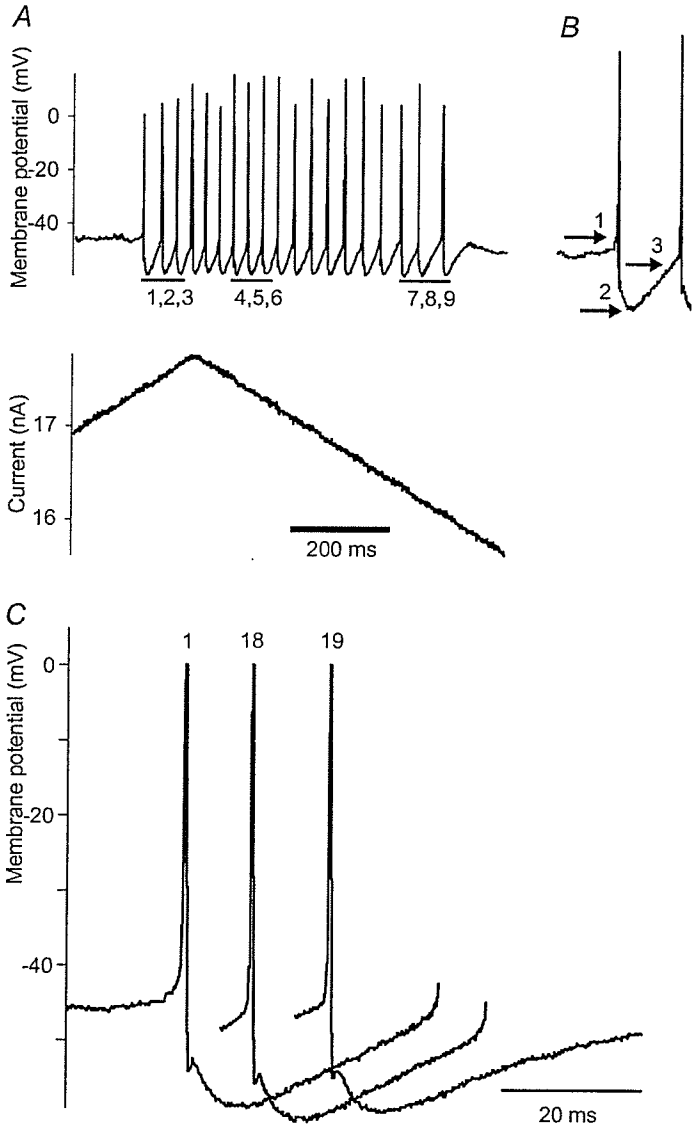

Figure 5. Voltage thresholds, AHP amplitudes and AHP ¾ durations measured during the ramp. A, voltages and currents at which rhythmic firing occurred. The horizontal bars and corresponding numbers below the spikes indicate the spikes that were analysed for the Vth and AHP properties. Only f–I relationship types 3 and 4 (i.e. ePIC) would include a third horizontal bar and corresponding spike numbers. B, the first two spikes from the ramp in A are shown amplified. The voltage threshold was measured at the point indicated by arrow 1, the amplitude of the AHP is indicated

by arrow 2 (the difference between Vth and AHP peak amplitude), and the time it takes for the AHP amplitude to return to ¾ of its baseline valueis indicated by arrow 3. C, illustration of the first and last two spikes (spikes 1, 18 and 19) in the ramp from A. Y axis is the membrane potential, and the spikes are truncated. Spike voltage threshold and after-hyperpolarization values are listed in Table 4.

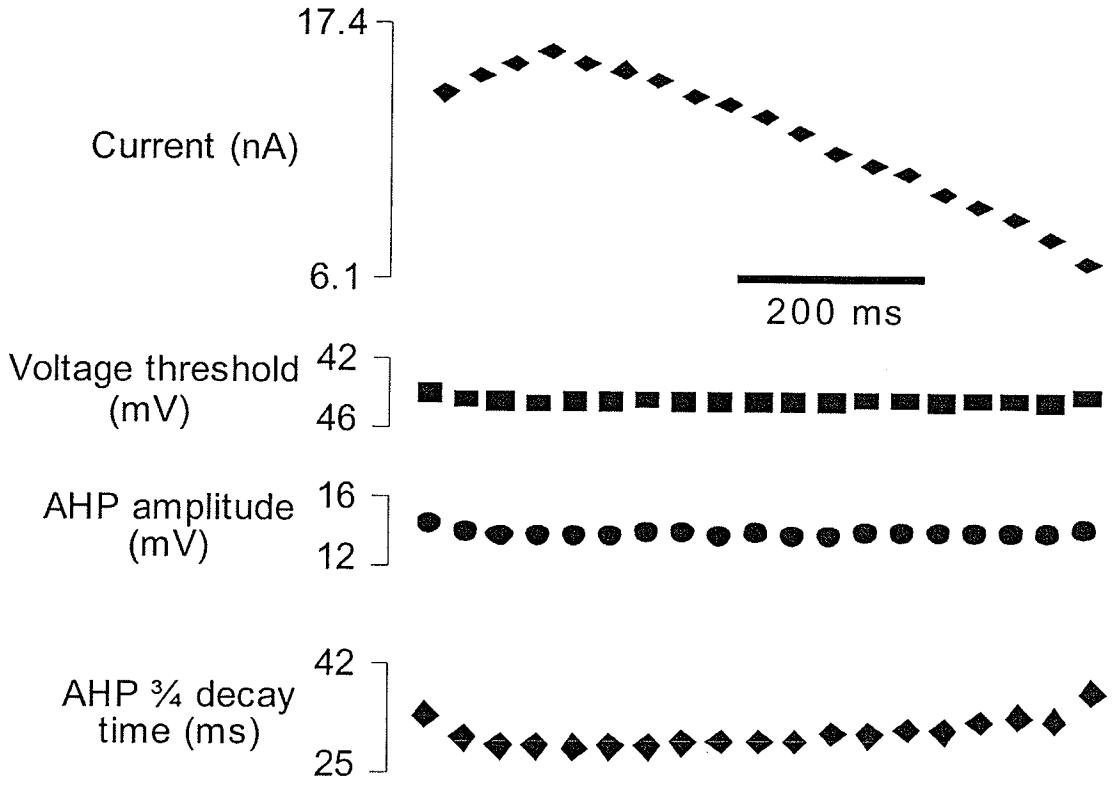

Figure 6. Each data point represents the current and voltage threshold at each spike and its AHP amplitude and AHP ¾ decay time during the subsequent interspike interval (spikes are not shown here) from the example in Fig. 5A. In this ramp, spike recruitment was induced at 17.4 nA and spike derecruitment occurred at 16.1 nA. During this ramp, the MN discharged a total of 19 spikes (12 of which occurred below the current at which spike recruitment was initiated). Voltage threshold at each spike ranged from −42.7 to −46.5 mV, AHP amplitude ranged from 12 to 16 mV, and the AHP 3/4 decay time ranged from 25 to 42 ms.

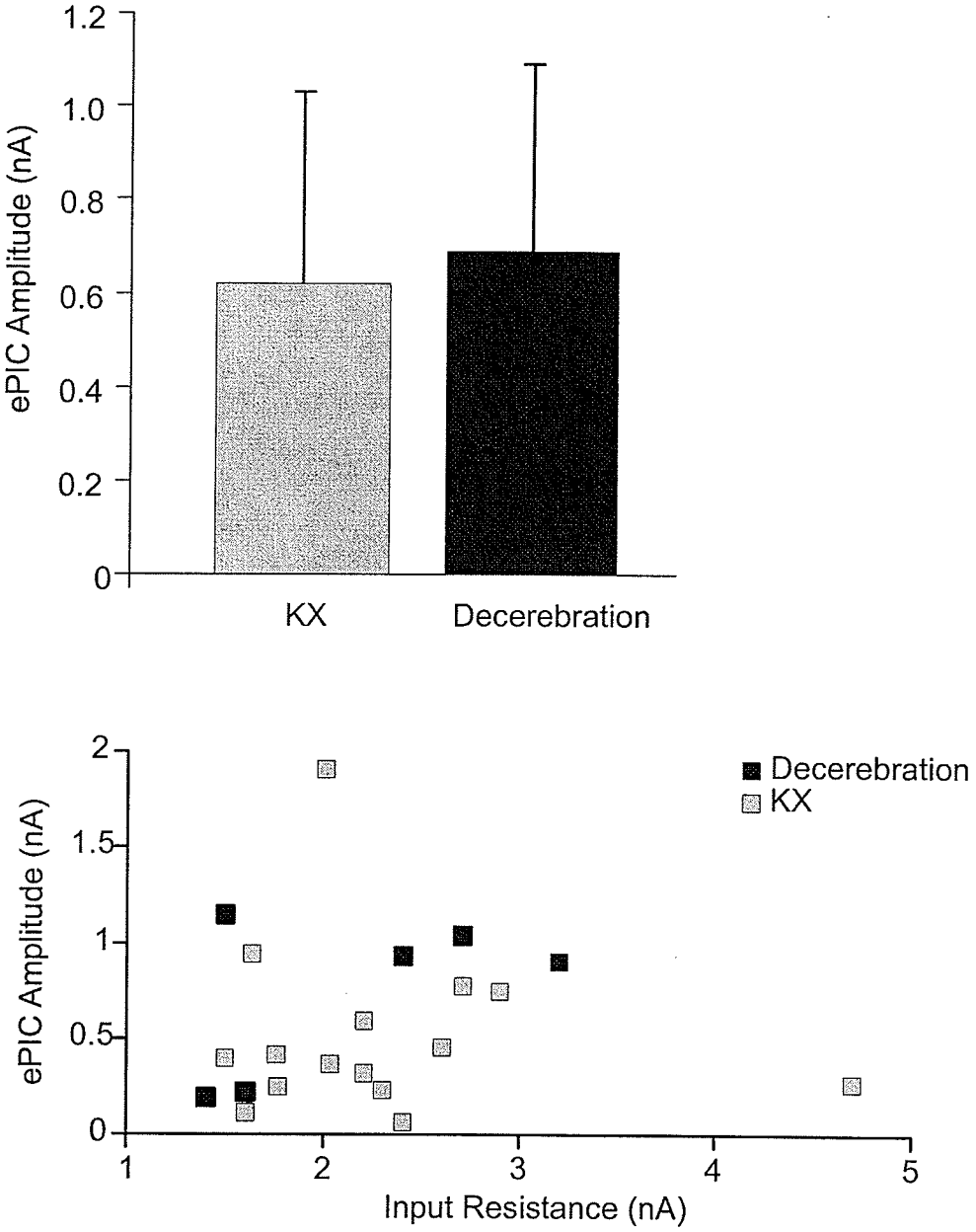

Figure 7. Illustration of average ePIC and its relation to input Resistance. A, comparison of average ePIC amplitude between MNs of KX-anaesthetized and decerebrate rats. Columns represents an average of all ePICs (type 3 and 4 f–I relationships only). Data points are presented as means ± 1 S.D. B, relationship between input resistance and ePIC amplitude.

Each data point represents one motoneurone. Correlation coefficients were 0.5 for MNs from decerebrate rats and 0.01 for MNs from KX-anaesthetized rats.

CHAPTER 3: SPIKE FREQUENCY ADAPTATION OF RAT HINDLIMB MOTONEURONES

RUNNING TITLE: Spike Frequency Adaptation

KEYWORDS: Spinal cord, square-wave pulse injection, persistent inward current

Chapter 3 is reprinted here with permission (August 21, 2007, The American Physiological Society) as it appears in:
Button DC, Kalmar JM, Gardiner K, Cahill F, Gardiner P (2007) Spike frequency adaptation of rat hindlimb motoneurones. J Appl Physiol 102:1041-50.

MY CONTRIBUTION TO THE PUBLICATION. The technician and I performed the required animal surgeries in preparation for motoneurone electrophysiological recordings. I recorded, measured, and analysed the data included in this publication. After I trained some of the authors on how to record, measure and analyze the data, they also helped with those procedures. During the duration of the experiments I continuously analyzed the data and discussed ideas with my supervisor and the other authors on whether or not more and what type of data was required to complete our project. After collecting and analyzing preliminary data I submitted an abstract, only after consultation with my supervisor and the other authors, on this data for presentation at an annual scientific conference. Once all of the data was collected and analysed I wrote and revised the manuscript in consultation with the other authors. I also discussed with my supervisor the order of authorship for the manuscript. After the manuscript was completed I circulated it to all the authors for their approval on authorship order, the manuscript itself, and editing purposes. Once the manuscript was deemed by all authors, as ready to go to submission, along with my supervisor I selected the Journal in which we submitted the manuscript to and then proceeded with the manuscript submission process. After the reviewer's comments on the manuscript were returned I made all the required revisions and discussed the reasoning for those revisions with the other authors. When the manuscript was accepted I made any further required corrections such as those included in the galley proofs.

ABSTRACT

The objective of our study was to resolve two issues pertaining to motoneuron (MN) spike frequency adaptation (SFA): 1) to develop an index of SFA that is sensitive to a wide range in adaptation patterns and would correlate well with MN excitability and 2) to determine if SFA pattern is stimulus current-dependent. Sprague-Dawley rats (250 - 350 g) were anesthetized (ketamine/xylazine) prior to recording electrophysiological properties from sciatic nerve MNs located in the lumbar spinal cord. SFA was measured using 30-s square wave current injections at 1.5, 3.0, and 5.0 nA above estimated rhythmic firing threshold (R_{th}). Discharges per second were significantly ($p < 0.001$) higher for 5 nA versus the 1.5 and 3 nA currents $>R_{th}$ in the first 2 s. SFA was quantified by using ratios of the final to initial number of discharges using 1-s, 2-s, and 5-s bins. The best index of SFA was the percent decline in the number of spikes fired in the 5^{th} 5-s bin relative to the first 5-s bin (1-(bin5/bin1)). Using this index, SFA significantly correlated with several measures of MN excitability, including estimated persistent inward current (PIC) amplitude (r=-0.76), rheobase current (r=0.71), and tended to correlate with input resistance (r=-0.43) and frequency-current (f-I) slope (r=-0.57). This index also showed the widest range of SFA among MNs. In conclusion, a SFA pattern can be ascertained for each MN and becomes more pronounced as MN excitability decreases. Finally, for the first time we report evidence of a relationship between PIC and SFA.

INTRODUCTION

The decline in motoneuron (MN) firing rate during a continuous stimulus is known as spike frequency adaptation (SFA). Motoneuron SFA is characterized by at least three phases: 1) initial adaptation or a linear decrease in spike discharge over the first two or three spikes (Sawczuk et al. 1995; Powers et al. 1999; Zeng et al. 2005; Sawczuk et al. 1997), 2) early adaptation or an exponential decrease in spike discharge over the first couple of seconds (Spielmann et al. 1993; Miles et al. 2005; Granit et al. 1963; Kernell 1965a; Kernell & Monster 1982b), and 3) late adaptation or an exponential decrease in spike discharge over several seconds to minutes (Spielmann et al. 1993; Granit et al. 1963; Kernell 1965a; Kernell & Monster 1982b). Each phase involves several possible mechanisms that contribute to the decrease in spike discharge rate, which are discussed in detail by Sawczuk et al. (1997). The most likely mechanisms underlying SFA in MNs include: 1) summation of the medium afterhyperpolarization (AHP) amplitude (Baldissera & Gustafsson 1974; Brownstone 2006; Powers et al. 1999; Kernell 1972) which is mediated by the Ca^{2+}-activated K^+ channel and 2) slow (persistent Na^+ ion conductance) and fast (transient Na^+ conductance) inactivation of the voltage-gated Na^+ channel (Schwindt & Crill 1982; Brownstone 2006; Miles et al. 2005; Powers et al. 1999).

Motoneuron SFA has been mathematically defined by 1) the time constant of the exponential decay in spike discharge rate during the early and later phases of SFA (Kernell & Monster 1982b; Spielmann et al. 1993; Granit et al. 1963; Gorman et al. 2005) and 2) the decrease in the instantaneous discharge frequency or number of spikes over a given time period (Hornby et al. 2004; Botterman & Cope 1986;

Spielmann et al. 1993; Kernell & Monster 1982b; Gorman et al. 2005). However, there are limitations to both of these approaches. The difficulty in measuring the rate of MN SFA using time constants lies in determining the best number of exponential decays to fit the frequency-time curve. We have found this to be especially problematic in the late phase of adaptation in rat hindlimb motoneurons (unpublished observations from our laboratory). The alternative approach of quantifying the change in firing frequency from the onset to the end of the current injection is easier to execute, but not necessarily more accurate. For example, Kernell & Monster (1982b) defined the time-course of MN late adaptation as the decline in peak discharge frequency from the 2^{nd} s to the 26^{th} s, a method that was later employed by Spielmann et al. (1993). Although this method was successful in determining the rate of adaptation over this time period, it does not reflect the diverse patterns of spike frequency that may occur between 2 and 26 seconds. Furthermore, since SFA patterns vary amongst MNs and because spike frequency changes rapidly in the first 2-3 s of firing (initial and early SFA), a one-second epoch may not provide an accurate estimate of SFA.

The first purpose of this study was to develop a simple method of quantifying SFA that is weighted towards late adaptation with the idea that we could develop an SFA index that would correlate well with membrane properties and be sensitive to a variety of SFA patterns. The second purpose of this study was to determine whether SFA is dependent on current amplitude. Thus for each MN, SFA was recorded in response to three different current amplitudes near the threshold for rhythmic firing.

Because MN SFA is lowest in slow type motor units and greatest in fast fatigable motor units (Kernell & Monster 1982a; Spielmann et al. 1993), a good estimate of MN SFA should significantly correlate with properties that determine MN excitability, such as rheobase current and input resistance (IR). Another property of MNs that modulates membrane excitability is the amplitude of the persistent inward current (PIC). We have demonstrated (Button et al. 2006) that hindlimb MNs of rats anesthetized by a ketamine/xylazine mixture demonstrate the presence of PICs. A recent review by Brownstone (2006) suggested that the inactivation of PIC may relate to MN SFA. Therefore, our *in vivo* rat preparation has allowed us to determine whether or not MN PIC correlates with MN SFA. Previously, this was not possible in in vivo experiments because animals(Spielmann et al. 1993) were anesthetized with pentobarbital (Kernell & Monster 1982b), which abolishes PICs. Some of the data reported here have been presented elsewhere in abstract form (Button at al. 2006).

METHODS

Treatment of animals. Thirteen female Sprague Dawley rats (275-325 g) were obtained from the University of Manitoba (Winnipeg, MB), and housed in plastic cages situated in an environmentally-controlled room maintained at 23 °C and kept on a 12:12-h light-dark cycle. Animals were provided water and food ad libitum and were experimented on within 7 days of receipt. All procedures were approved by the animal ethics committee of the University of Manitoba and were in accordance with the guidelines of the Canadian Council of Animal Care.

Surgery. Animals were anesthetized with ketamine (N-methyl-D-aspartate

receptor antagonist)/xylazine (α2-adrenoceptor agonist) (90/10 mg kg^{-1}, ip). Once anesthetized, atropine (containing saline, 5% dextrose and 0.05 mg kg^{-1} atropine) was administered (volume 6.6 ml kg^{-1}, ip) to minimize airway secretions during the subsequent tracheotomy. The surgical procedures included: 1) insertion of a tracheal tube to ventilate the rat (Harvard Apparatus, Canada) with oxygen-enriched and humidified room air, 2) catheterization of the femoral artery, which allowed continuous monitoring of mean arterial pressure (MAP) and constant infusion of anesthetic (Pump 11, Harvard Apparatus, Canada), 3) exposure of the left hindlimb sciatic nerve for stimulation, 4) exposure and isolation of the spinal vertebrae and laminectomy from T12 to S1 in a stereotaxic unit .

Physiological saline solution containing ketamine/xylazine (9/1 mg hr^{-1}) was infused via the femoral artery to maintain anesthesia and depth of anesthesia was verified continuously via heart rate, MAP, CO_2 levels and bilateral toe pinch. Blood pressure was maintained between 80-110 mmHg and respiration was kept at a tidal volume of 2.0 to 2.5 ml and a ventilation rate of 60-80 strokes min^{-1}. Expired carbon dioxide levels were measured via a CAPSTAR 100 CO_2 analyzer (CWE Inc., USA) and were maintained between 3.0-4.0 % by adjusting tidal volume or ventilation rate. Rectal temperature was monitored and maintained near 37 °C using a feedback Homeothermic Blanket Control Unit (Harvard Apparatus, Canada). The head, thoracic and lumbar vertebrae, hips, and left foot were immobilized with clamps, and the open leg and back incisions were used to make an oil bath around the sciatic nerve and spinal cord respectively. The dura mater covering the spinal cord was incised, and the large dorsal roots comprised of afferents from the left hind-limb were cut and

reflected over the right side of the cord. An opening was made in the pia mater (lumbar spinal cord segments L2 – L4) just lateral to the entry zone of these roots into the cord, in preparation for introduction of the glass microelectrode. Prior to the search for MNs, a pneumothorax was performed on the left side of the thorax.

Drugs and solutions. To reduce blood pressure and respiration-related movement artifacts and to stabilize the animal for optimal electrophysiological recordings, several solutions were administered intravenously. The rat received: 1) a solution of 100 mM $NaHCO_3$ (Fisher scientific) and 5% Dextrose (Fisher Scientific) double distilled H_2O, and 2) pancuronium bromide (0.2 mg kg^{-1}). Pancuronium bromide was injected intravenously in the rat prior to the start of electrophysiological recordings to induce paralysis and was re-administered as needed to maintain paralysis of the respiratory and/or hindlimb muscles.

Measurement of motoneuron properties. Glass microelectodes (1.0 mm thin-walled, World Precision Instruments, USA) were pulled with impedances of approximately 10 MΩ (Kopf Vertical Pipette Puller, David Kopf Instruments, USA), and filled with 2M K citrate. The tip of the electrode was positioned at an incision in the pia mater and was lowered with an inchworm microdrive system (Burleigh Instruments Inc., USA) into the cord in steps of 5-10 μm. The sciatic nerve was stimulated with a bipolar silver electrode at a frequency of 1 pulse·s^{-1} while the microelectrode was advanced through the cord and the field potential was continuously monitored. Evidence of successful impalement of a MN was a sudden decrease in membrane potential to at least $\geq$ 55 mV with an antidromic action potential spike amplitude of > 55 mV with a positive overshoot and a reproducible

latency of less than 2.5 ms from the stimulation artifact. During recording, an axoclamp intracellular amplifier system (Axoclamp 2B, Axon Instruments Inc., USA) was used either in bridge or discontinuous current-clamp modes (DCC; 2-10 kHz switching), with capacitance maximally compensated. Passive MN properties recorded in bridge mode included: antidromic action potential (from an average of 10 spikes), and orthodromic action potential in response to a 0.5-ms current pulse of supramaximal intensity (from an average of 40 spikes). Rheobase current (the amplitude of a 50-ms square-wave current resulting in spikes 50% of the time) and cell IR (from an average of 60, 1-nA hyperpolarizing pulses each lasting 100 ms) were recorded in DCC mode. From these recordings we determined antidromic spike height and time-course, amplitude and half-decay time of the AHP following an action potential evoked by a 0.5 ms current pulse, resting membrane potential (RMP), rheobase current, voltage threshold, and cell IR.

Measurement of frequency-current (f-I) relationship. After completing MN passive properties recordings, the MN's f-I relationship was measured in two different ways. First, cells were challenged with slow triangular current ramps (range: 0.5–6.0 nA s^{-1}), and the voltage response was measured in DCC mode (see (Button et al. 2006) for a complete description of this measurement). Peak amplitude of the ramp depended entirely on the rhythmic threshold of the MN, and an attempt was made to evoke trains of impulses containing 10–75 spikes over 0.5–2.5 s duration. Ramps were used to determine the MN f–I relationship, to evoke voltage-dependent plateaus and to measure the underlying PIC as previously described (Hounsgaard et al. 1988; Lee & Heckman 1998b; Bennett et al. 2001). During the

current ramps, the estimated PIC (ePIC) producing the plateau and sustaining firing was estimated from the difference in injected current at spike recruitment compared with spike derecruitment (see figure. 1 in Button et al. (2006)). Second, cells were challenged with 500 ms square-wave pulse current injections of increasing and then decreasing amplitudes every 1 s and the voltage response was measured in DCC mode. Current was increased in steps until blocking occurred before the end of the 500-ms period, after which current steps of decreasing intensity were administered (see figure 1 in Cormery et al. (2005) for more details). 500-ms square-wave pulse current injections were used to determine minimum and maximum steady-state firing frequencies and current used at those frequencies to determine the MNs frequency-current slope (f-I slope).

Measurement of motoneuron spike-frequency adaptation. Cells were challenged with three 30-s square-wave pulses of current and the voltage response was measured in DCC and bridge mode. The magnitude of current injected into the cell depended on rhythmic firing threshold (the minimum current at which the MN would fire for at least 10 s) of the MNs and an attempt was made to evoke trains of impulses for a 30-s duration. Once the threshold current for rhythmic firing (R_{th}) was determined, three separate square wave pulses of current at 1.5, 3, and 5 nA > R_{th} were injected into the MN for 30 s. Time was allotted after each of the three 30-s current injections for the MNs to repolarize back to resting membrane potential. From these recordings we determined the change in spike frequency over time. Thirty-second current pulses were chosen on the basis that very little MN SFA is seen after this time point (Sawczuk et al. 1995).

At the end of these measurements, the microelectrode was backed out of the MN in 5-μm steps, and the extracellular voltage was recorded. Typically, experiments yielded 1-2 MNs with complete and acceptable complements of data. At the end of the experiment, the animal was euthanized by an overdose of KCl and bilateral pneumothorax.

Analysis of SFA. For each cell we used three different current amplitudes (1.5, 3, and 5 nA > R_{th}) to analyze MN SFA by the following process: 1) we counted the number of discharges in 1-s bins, beginning at the onset of firing such that we had 30 bins (Figure 1B), 2) we normalized these bin counts such that the final bin in the 30-s period of firing always contained 5 spikes, 3) we expressed MN SFA as a the percent decline in the number of spikes discharged between two bins, 4) we repeated this process using 15 bins of 2-s epochs (Figure 1C) as well as 6 bins of 5-s epochs (Figure 1D). These estimates of MN SFA are more sensitive to late adaptation than the initial and early phases of SFA compared to estimates of SFA derived from instantaneous frequency. Many combinations of bins were used to find an index of SFA that 1) correlated the most significantly with other MN properties and 2) demonstrated a wide range of SFA. For example, using 2-s bins, one possible index of SFA is 1-(bin13/bin1). This index expresses the percent decline in the number of spikes discharged in bin13 (25-26s of firing) relative to bin1 (first 2 s of firing) (Figure 1C). Finally, we correlated each index of SFA to other electrophysiological properties including the basic properties listed above as well as the f-I relationships that determine f-I slope and demonstrate the presence of PICs.

Statistics. Only MNs that responded rhythmically for at least 26 s during the 30 s of current injection and passed all electrophysiological requirements were used in the analysis (see Methods). To determine if MN SFA was stimulus current-dependent, we performed a two-way ANOVA (current intensity x time) on the 1-s bin counts. When a significant interaction was present, Tukey post hoc tests were used to detect significant differences among individual means. All data are expressed as mean ± one standard deviation.

RESULTS

We recorded data from 18 MNs (with all properties listed in the Methods) in 13 rats that were anesthetized with ketamine/xylazine. Only MNs with RMPs $\geq$ 55 mV and spike amplitudes (> 55 mV) with positive overshoots were used in the following results. Hereafter, all MN SFA data reported are normalized so that the minimum number of MN spikes discharged in the final second always equaled 5. Although we indexed MN SFA using many different bin combinations (see Methods, Figure 1B,C,D), we report only those indices that estimate a wide range of SFA and that correlate well with other MN properties (i.e. 1-[bin15/bin25]) derived from 1-s bins is not an index that we would report because MN firing rate does not decline significantly between the 15th and 25th s of current injection).

Motoneuron passive and active properties. Motoneuron properties are shown in detail in Table 1. Some of these data were used in previously published work (Button et al. 2006). The data include values that are typically seen in a wide range of MN types. Motoneurons that did not discharge for 30 s had a 65% ($p = 0.03$) higher AHP amplitude compared to MNs that rhythmically discharged for 30 s.

Aside from AHP amplitude, there were no differences in properties between those cells that fired for 30 s and those that did not.

The relationship between motoneuron spike-frequency adaptation and current. A two-way ANOVA test revealed a significant interaction ($p<0.001$) between injected current amplitude and number of spikes discharged during 30 s of rhythmic discharge (Figure 2). Post hoc analysis revealed that this interaction could be attributed to the first two seconds of MN firing when the number of spikes discharged were greater with a current that was 5 nA> R_{th} compared to the 1.5 nA> R_{th} ($p<0.001$) and 3 nA> R_{th} ($p<0.001$) current injections. There were no differences between the 1.5 nA> R_{th} and 3 nA> R_{th} at any time point. After the first 2 seconds of current injection the number of spikes discharged no longer differed between current amplitudes for the duration of the MN rhythmic discharge (Figure 2). Since the 5 nA> R_{th} current injection resulted in increased MN frequency over the first two seconds of MN SFA, these data were excluded and all SFA data reported hereafter is based on an average of 1.5 and 3 nA > R_{th} trials.

Determination of the amount of motoneuron spike frequency adaptation. We used several epochs (1-s, 2-s, and 5-s) of the number of spikes discharged that were near and/or included the time points 2 and 26 s (originally defined by Kernell & Monster (1982b)) to devise an index of SFA. For simplicity, in Table 2 we show only five indices of SFA calculated using different bin combinations using 1-s , 2-s, or 5-s bins. These five indices showed the greatest range of MN SFA and were significantly correlated with other MN properties (Table 3). We found that SFA (the percent decline in the number of spikes discharged from initial to final bin) was significantly

($p < 0.01$) higher for 1-s 1-bin26/bin1 and 2-s 1-bin13/bin2 compared to all other indices.

Motoneuron spike frequency adaptation indices correlate with other motoneuron properties. Linear regression was conducted to determine whether motoneuron SFA indices were correlated (via Pearson Product Moment Correlation procedure) with several MN active and passive properties. Correlation coefficients and levels of significance are presented in Table 3. Interestingly, all indices of SFA were significantly correlated with MN ePIC amplitude, and the following indices were correlated with rheobase; (1-bin 26/bin1) using 1-s bins, (1- bin13/bin1) using 2-s bins, and (1-(bin5/bin1) using 5-s bins. There was a weak but significant correlation between input resistance and the SFA index of 1- bin26/bin2 derived from 1-s bins, and a trend for correlation between input resistance and SFA indices derived from the 2-s and 5-s bins. No significant correlations between any index of SFA and f-I slope, RMP, Vth, AHP amplitude, AHP ½ decay time, or spike height (not shown) were found. Correlation coefficients were not improved by using a multiple regression analysis.

We found that the percent decline in the number of spikes discharged from 5-s bin1 to 5-s bin5 was the best index of SFA. This index (1-bin5/bin1) was significantly correlated to ePIC amplitude and rheobase current and tended to correlate to input resistance and f-I slope, and overall showed the best correlation coefficients and p values. Figure 3 illustrates the relationship between this index and the four properties listed in Table 3. The correlations predict that MNs with lower rheobases and larger ePICs exhibit less MN SFA. We would like to note that the

correlation coefficient for SFA and ePIC (-0.76) in Figure 3D is based on all data points including the eight MNs that demonstrate zero PIC. When these 8 data points are removed and a linear regression is performed the correlation coefficient remains very similar (0.-77). The strength of correlations between motoneuron SFA indices and MN properties was strongest when the high discharge numbers of the initial bins where included in the index of SFA. For example, using indices of SFA derived from 1-s bins, the correlation between these SFA and ePIC decreases from -0.79 to -0.74 to -0.73 to -0.69 when SFA is calculated as (1-bin26/bin1), (1-bin26/bin2), (1-bin26/bin3), and (1-bin26/bin4) , respectively (results not shown for the latter two).

The range of motoneuron types which demonstrate spike frequency adaptation. Only 18 MNs discharged continuously for 30 s or more in response to each of the three different currents. Therefore, we wanted to compare the MN properties of those cells to the properties of cells that did not discharge rhythmically for 30 s to ensure that our sample of rhythmically active cells was representative. In Figure 4, the three MN properties (ePIC, rheobase, and IR) that correlated strongly with the SFA indices (see Table 3) are shown as percentiles for the MNs that could and could not fire rhythmically for 30 s. The group of MNs that rhythmically discharged for 30 s showed a wide range of ePIC amplitudes, rheobase currents and IRs that are comparable to those of a much larger number of MNs that could not rhythmically discharge for 30 s. Furthermore, there were no significant differences between the mean values (see Table 1) for these three properties. The only noticeable difference between the two groups of MNs is in the distribution patterns at the very

low end for rheobase current (Figure 4B) and very high end of IR (Figure 4A). It appears that our MN SFA data set does not include the smallest MNs.

Not only do the rhythmically active MNs have a wide variety of rheobase currents and IRs, they also have a wide range of SFA. This is evident in Figure 5 which plots the number of spikes in 1-s bins for 7 of the MNs which fired for 30 s. Because the number of spikes is normalized to a minimum count of 5 spikes, the differences in the magnitude and pattern of SFA among these MNs is quite evident. Table 2 also demonstrates that different MNs exhibit very different magnitudes of SFA. For example, the number of spikes discharged by one motoneuron declined by 86% within 26 s of firing compared to a 42% decline in another MN.

Finally, two MNs were excluded (referred to as $MN_{excluded}$ hereafter) from the SFA data set because their rhythmic discharge behaved differently than all other MNs. Their number of spikes discharged increased over the first second or two followed by no change in the number of spike discharge for the remainder of the time (i.e. no SFA). Due to the initial increase in MN spike discharge during the first two seconds, all SFA indices which included this time were negative (i.e. no adaptation). These MNs had passive properties typical of the other 16 MNs. For example one $MN_{excluded}$ had; 1) a resting membrane potential of -66 mV which returned to 0 mV upon backing out of the cell, 2) a rheobase current of 4 nA that would have been the lowest of the data set, 3) an input resistance of 2.9 MΩ that would have been the third highest in our data set and 4) an ePIC amplitude of 0.75 nA that would have been the highest in the data set. The other $MN_{excluded}$ had the highest input resistance (3.7 MΩ) of the data set.

DISCUSSION

Motoneurons injected with a suprathreshold square-wave current exhibit a decline in firing rate that is referred to as spike frequency adaptation. Intracellular injections of different current amplitudes have been used for years to study MN SFA. However, it is not clear whether the overall pattern of MN SFA is dependent on stimulus current amplitude. Furthermore, a standardized method of quantifying SFA that is sensitive to the wide range in SFA patterns among cells and correlates with motoneuronal properties is lacking in the present literature. In the present study, we found that rat hindlimb motoneurons injected with 30-s square wave currents at amplitudes 1.5, 3, and 5 nA above the threshold for rhythmic firing elicit similar patterns of MN SFA. Using the index of motoneuron SFA described here, SFA is only stimulus current-dependent in the first 2-s of MN firing, when the number of discharges is significantly greater with the 5 nA > R_{th} than at the two lower current amplitudes. After normalizing the number of spikes discharged in 1-s, 2-s, or 5-s bins to a minimum bin count of 5 spikes for each MN, we found that using 5-s bins, the SFA index 1-bin5/bin1 provided the greatest range of MN SFA between cells and was best correlated with other MN properties. These correlations predict that MNs with lower rheobase and larger ePICs exhibit less MN SFA.

Our observation that MN SFA is stimulus current-dependent only in the first two seconds of firing is consistent with previous literature. Similar results can be seen in the sixth figure presented in a MN SFA study by Granit et al. (1963). In this figure (Granit et al. 1963), the patterns of MN SFA in response to current intensities ranging from 5.7-32.2 nA are similar, whereas the highest current (48 nA) evokes a

pattern of MN SFA that seems to differ from the others. Consistent patterns of motoneuron SFA throughout a range of current intensities can also be seen in cat hindlimb (Kernell & Monster 1982b) and forelimb (Botterman & Cope 1986), hypoglossal (Sawczuk et al. 1995) and rat facial nucleus (Magarinos-Ascone et al. 1999) motoneurons. If the data from these earlier studies were analyzed using the normalized method we propose in the present study, the frequency-time curves generated at different current amplitudes near the threshold for rhythmic firing would likely overlap. Furthermore, it has been shown that higher currents evoke greater initial instantaneous firing frequencies (Granit et al. 1963; Baldissera & Gustafsson 1974; Botterman & Cope 1986). In the present study, the initial phase of MN SFA adds only 1-3 extra spikes to the first bin count, thus the drastic change in instantaneous firing frequency that occurs within the first 2 to 3 spikes does not have a major influence on the overall pattern of MN SFA.

In the cat, motoneuron f-I relationships can be observed by recording the firing frequencies evoked by a series of 500-ms square-wave current injections of increasing amplitude. The resulting f-I curve is characterized by a primary, secondary, and tertiary range of firing frequencies (Kernell 1965b; Kernell 1965c; Schwindt 1973). Briefly, as the intracellularly-injected current increases there is an initial linear increase in the MN firing frequency (primary range) followed by a sudden and sharp increase in slope (secondary range). There is also evidence that rat motoneurons can also fire in primary and secondary ranges when subjected to 500-ms current pulses (Cormery et al. 2003) and ramp currents (Bennett et al. 2001; Button et al. 2006). Thus, the current-dependence of SFA in the first few seconds seen in

Granit et al. (1963) original work and the present study could be due to a shift from the secondary to primary range during the first few seconds of a prolonged current injection. The lower current amplitudes (1.5 and 3 nA above rhythmic threshold) may not have been high enough to induce the secondary range of MN firing in the present study.

Once we determined a range of intracellularly injected current intensities that did not influence the pattern of MN SFA we used these currents to develop a method of "quantifying" MN SFA. The method employed here was a modified version of that used by Kernell & Monster (1982b) and Spielmann et al. (1993). Indices of SFA were used to reflect the decline in the number of spikes within the first 26 s of current injection using bins of several sizes (1-s, 2-s, and 5-s). Indices of SFA derived from small bins (1 or 2 s) and that include the first second of firing yield the greatest estimate of SFA. This is not unexpected, since the majority of MN SFA occurs during the initial and early phases (Granit et al. 1963; Kernell 1965b; Kernell 1972; Kernell & Monster 1982b) which combined can last up to approximately two seconds (Spielmann et al. 1993; Miles et al. 2005; Granit et al. 1963; Kernell 1965a; Kernell & Monster 1982b). Thus, one would expect that an index which includes the first second of firing should provide the highest estimate of SFA. However, using 5-s bins, an SFA index of 1-bin5/bin1 provides not only a high magnitude of SFA magnitude (81%) but the greatest range (42-81%) of MN SFA compared to other indices. This is most likely because this estimate of SFA includes the first 5 s of MN firing (all of the early adaptation phases and some of the late adaptation phase) which captures the greatest time block (all three phases) of MN SFA.

An increased rate of adaptation has been previously shown to correlate with motor unit properties that are seen in motoneurons with higher rheobase currents and lower input resistances (Zengel et al. 1985). On a recruitment continuum from type slow to type fast the conduction velocity increases, fatigue index decreases, twitch contraction times decrease and peak tetanic forces increase (Burke et al. 1973; Burke 1967) all of which have been found to also correlate with the rate of MN SFA (Kernell & Monster 1981; Spielmann et al. 1993; Kernell & Monster 1982a). Kernell & Monster (1982a) also showed that fast motor units demonstrate much greater rates of SFA and fatigue, compared to slow motor units. All of these factors are consistent with our finding that motoneurons with higher rheobases and lower input resistances demonstrate faster rates of SFA.

All five indices of SFA were significantly correlated with ePIC amplitude, a MN active property. The finding that MNs with greater ePIC had less SFA was surprising since Zeng et al. (2005) recently demonstrated that blocking the persistent Na^+ channel during 30 s of sustained constant-current steps had no effect on the pattern of MN SFA. They suggested that ion channels other than the persistent Na^+ channel work concomitantly in motoneurons to ensure maintenance of sustained firing. Furthermore, persistent Na^+ channels need to be active in order for spinal motoneurons to sustain rhythmic firing (Lee & Heckman 2001; Harvey et al. 2006). In earlier work, Lee & Heckman (1998a) demonstrated that MN bistability (a property facilitated by PIC) was more pronounced in low vs. high rheobase current MNs, but there was no difference in the initial PIC conductance. The lack of bistability in high rheobase current MNs may be attributed to a faster inactivation of

the PIC channels. In the present study, approximately 50% of the MN ePIC amplitude may be due to the Na^+ PIC channel (Li & Bennett 2003). As the persistent Na^+ channel inactivates, the MNs ability to sustain rhythmic firing decreases (Lee & Heckman 2001). Perhaps the motoneurons with lower ePIC amplitudes reported here have faster inactivation rates of the persistent Na^+ channel which possibly leads to differences in SFA patterns amongst the MNs. In addition, during constant current stimulation MNs which innervate fast muscle fibers have high initial firing frequencies and tend to adapt the most (25). The high initial firing frequencies occur due to very fast AHP time courses (23) and adapt quickly due to a summation of these AHPs over the first few spikes (2,5,24,35) . However, we now have some evidence suggesting that these MNs may also have faster inactivation of PIC channels which along with the AHP time course contributes to greater SFA.

On the other hand, MNs with high PIC amplitudes have less inactivation and therefore less SFA. Decreased PIC inactivation may be extremely important during behavioral tasks such as posture (Alaburda et al. 2002) and fictive locomotor activity (Brownstone et al. 1992). For instance, during fictive locomotion MN repetitive firing does not exhibit SFA. Actually, the rate of repetitive firing is high and constant throughout each burst, suggesting that in this situation PIC channels may be turned on and off in an all-or-none fashion. All PIC channels are activated leading to a continuous non-SFA burst of activity during excitation and are inactivated between excitation episodes or they are somehow modulated in a different way (Brownstone et al. 1992; Brownstone 2006).

The SFA index 1-bin5/bin1, derived from 5-s bins was better correlated to ePIC, rheobase current, input resistance, f-I slope than other indices. Estimates of SFA that excluded the earliest phases of adaptation did not correlate well with ePIC, rheobase, or IR, illustrating the importance of using the first 1-2 seconds of MN discharge when correlating SFA to other MN properties. On the other hand, none of the indices correlated with the AHP amplitude, AHP ½ decay time or the f-I slope. We would not expect a relationship between MN SFA rates and f-I slopes since the f-I slope is not dependent on motoneuron type (Cormery et al. 2005). In addition, the cat model but not the rat model has been used to show the relationship between SFA and motor unit type. Cat motor unit type can be predicted from MN passive properties much more easily (Zengel et al. 1985) than in rat (Gardiner 1993). Therefore, our finding of a lack of rat MN AHP amplitude and AHP ½ decay time correlating to our SFA indices were not surprising.

We used percentile distributions to compare rheobase, input resistance and ePIC amplitude of the cells that discharged rhythmically for 30 s to cells that did not and found that the distributions did not differ between the two groups. Also, there were many different patterns of SFA (see Figure 5) and a wide range SFA among the MNs providing further evidence that our sample of MNs is representative of a wide variety of MN types and sizes. However, the least SFA that we report for any cell was 42%. In comparison, Kernell & Monster (1982a) demonstrated that MNs innervating slow twitch muscle had very little adaptation, much less than shown here. Therefore, it is possible that the absolute slowest types of MNs, with the lowest rheobase and highest input resistance, may not be completely represented in our

sample of rhythmically active MNs (see Figure 4). Another possibility is that the rat may not have hindlimb MNs that demonstrate very little SFA.

Two motoneurons ($MNs_{excluded}$) had a frequency-time relationship that showed an increase in firing frequency at the onset of current injection followed by a slight decline in firing rates (i.e. no SFA by our measure). Furthermore, these MNs had high ePIC amplitudes and low rheobase currents. Interestingly, the SFA profiles of the $MNs_{excluded}$ conform very similar patterns to fatigue myogram patterns of rat fast-fatigue resistant (FR) motor units (Gardiner & Olha 1987), suggesting that these MNs innervate FR units. Since excitable cells tend to be more bistable (Button et al. 2006), or capable of toggling between active and quiescent states, compared to low excitable cells (Lee & Heckman 1998a), SFA may be related to MN bistability. The PIC may have activated a plateau potential that in turn allowed $MN_{excluded}$ to express self-sustained rhythmic firing at a fairly constant frequency and remain firing for a long period of time (Kiehn & Eken 1998; Guertin & Hounsgaard 1999). The $MNs_{excluded}$ SFA pattern can be seen in a turtle interneuron that has a plateau potential (Gorman et al. 2005). Furthermore, Sawczuk et al. (1995) also showed that some hypoglossal MNs have a similar MN SFA pattern as our $MNs_{excluded}$ (see figure 2B in Sawczuk et al. (1995)). However, an explanation for this pattern of SFA has not been provided. Perhaps, some bistable rat hindlimb MNs show a SFA pattern similar to our $MNs_{excluded}$, but this is speculative at the present.

Kernell & Monsters (1982b) method to quantify MN late adaptation assumes that MN late adaptation patterns are similar across all MNs and that SFA is negligible upon 2 s of rhythmic discharge. Our method of using normalized bin counts to index

MN SFA has illustrated that SFA patterns are widely disseminated among MNs and that these SFA patterns vary quite extensively even after 3 or more seconds of rhythmic discharge (Figure 5). The 5-s bin SFA index (1-bin5/bin1) results in the greatest range of MN SFA values, which is probably due to capturing a greater time-course of the different MN SFA phases. Using a longer duration bin counts to estimate SFA demonstrates that significant changes in MN output do indeed occur after 2 s of a 30 s rhythmic discharge. Spike frequency adaptation (measured by injecting current pulses intracellularly) patterns probably vary among MNs due to differences in their; 1) relative number, density and distribution of ion channels, 2) relative number, density and distribution of membrane receptors, 3) ion channel and receptor sub-unit type, 4) the muscle fiber type they innervate, 5) dendritic and somata morphology. All of these factors may play a role in determining the onset-time and duration of each of the MN SFA phases (initial, early and late), thus providing a non-universal MN SFA pattern which requires a longer as opposed to short duration spike discharge bincount for its measurement.

In conclusion, rat hindlimb MNs show similar SFA patterns when injected with prolonged intracellular square-wave current injections of various intensities. The magnitude of SFA is only stimulus current-dependent within the first two seconds of current injection, perhaps due to a shift from the secondary to primary range of the f-I relationship. As such, any current near threshold may be used to elicit SFA rendering the time-consuming process of measuring SFA at several currents unnecessary. We estimated the amount of SFA using the decline in the normalized number of spikes discharged in 1-s, 2-s, and 5-s bins over 26s of firing. In so doing,

we found that quantifying SFA as the percent decline in number of spikes discharged from the first 5 s (bin1) to the last 5 s (bin5) during 26s of sustained firing was a good index of SFA. This index (1-bin5/bin1) produced the widest range of SFA amongst MNs and the most significant correlation between SFA and ePIC amplitude, rheobase current, input resistance, and f-I slope. These correlations are consistent with the notion that larger MNs exhibit greater SFA. Lastly, and perhaps most importantly, we have developed a simple method of estimating MN SFA rates that may be applied to our altered activity models to study the adaptability of MN properties.

ACKNOWLEDGEMENTS

This research was supported by grants from NSERC Canada, Canadian Institute for Health Research, and the Canada Research Chairs program. The authors would like to thank Gilles Detillieux, Matt Ellis and Maria Setterbom at University of Manitoba for technical assistance.

REFERENCE LIST

Alaburda A, Perrier JF & Hounsgaard J (2002). Mechanisms causing plateau potentials in spinal motoneurones. *Adv Exp Med Biol* **508**, 219-26.

Baldissera F & Gustafsson B (1974). Firing behaviour of a neurone model based on the afterhyperpolarization conductance time course and algebraical summation. Adaptation and steady state firing. *Acta Physiol Scand* **92**, 27-47.

Bennett DJ, Li Y & Siu M (2001). Plateau potentials in sacrocaudal motoneurons of chronic spinal rats, recorded in vitro. *J Neurophysiol* **86**, 1955-71.

Botterman BR & Cope TC (1986). Discharge properties of motoneurons supplying distal forelimb muscles in the cat. *Brain Res* **379** , 192-5.

Brownstone RM (2006). Beginning at the end: repetitive firing properties in the final common pathway. *Prog Neurobiol* **78**, 156-72.

Brownstone RM, Jordan LM, Kriellaars DJ, Noga BR & Shefchyk SJ (1992). On the regulation of repetitive firing in lumbar motoneurones during fictive locomotion in the cat. *Exp Brain Res* **90**, 441-55.

Burke RE (1967). Motor unit types of cat triceps surae muscle. *J Physiol* **193**, 141-160.

Burke RE, Levine DN, Tsairis P & Zajac FE 3rd (1973). Physiological types and histochemical profiles in motor units of the cat gastrocnemius. *J Physiol* **234**, 723-48.

Button DB, Kalmar JM, Gardiner KR, Cahill F & Gardiner PF (2006). Spike frequency adaptation of rat hindlimb alpha motoneurons. *Program No. 55.14. 2006 Abstract Viewer/Itinerary Planner. Atlanta, GA: Society for Neuroscience, 2006. Online.* (Abstract)

Button DC, Gardiner K, Marqueste T & Gardiner PF (2006). Frequency-current relationships of rat hindlimb {alpha}-motoneurones. *J Physiol* **573**, 663-77.

Cormery B, Beaumont E, Csukly K & Gardiner P (2005). Hindlimb unweighting for 2 weeks alters physiological properties of rat hindlimb motoneurones. *J Physiol* **568**, 841-50.

Cormery B, Beaumont E & Gardiner P (2003). Rhythmic discharge properties of rat hindlimb motoneurones in response to sustained current injections, and the effects of increased voluntary exercise. *Can.J.Appl.Physiol.* **28**,

Gardiner PF (1993). Physiological properties of motoneurons innervating different muscle unit types in rat gastrocnemius. *J Neurophysiol* **69**, 1160-70.

Gardiner PF & Olha AE (1987). Contractile and electromyographic characteristics of rat plantaris motor unit types during fatigue in situ. *J Physiol* **385**, 13-34.

Gorman RB, McDonagh JC, Hornby TG, Reinking RM & Stuart DG (2005). Measurement and nature of firing rate adaptation in turtle spinal neurons. *J Comp Physiol A Neuroethol Sens Neural Behav Physiol* **191**, 583-603.

Granit R, Kernell D & Shortess GK (1963). Quantitative aspects of repetitive firing of mammalian motoneurones, caused by injected currents. *J Physiol* **168**, 911-31.

Guertin PA & Hounsgaard J (1999). Non-volatile general anaesthetics reduce spinal activity by suppressing plateau potentials . *Neuroscience* **88**, 353-8.

Harvey PJ, Li Y, Li X & Bennett DJ (2006). Persistent sodium currents and repetitive firing in motoneurons of the sacrocaudal spinal cord of adult rats. *J Neurophysiol* **96**, 1141-57.

Hornby TG, Heckman CJ, Harvey RL & Rymer WZ (2004). Changes in voluntary torque and electromyographic activity following oral baclofen. *Muscle Nerve* **30**, 784-95.

Hounsgaard J, Hultborn H, Jespersen B & Kiehn O (1988). Bistability of alpha-motoneurones in the decerebrate cat and in the acute spinal cat after intravenous 5-hydroxytryptophan. *J Physiol* **405**, 345-67.

Kernell D (1965a). The adaptation and the Relation Between Discharge Frequency and Current Strength of Cat Lumbosacral Motoneurones Stimulated by Long-Lasting Injected Currents. *Acta. Physiol. Scand.* 65-73.

Kernell D (1965b). High-Frequency Repetitive Firing of Cat Lumbosacral Motoneurones Stimulated by Long-Lasting Injected Currents. *Acta. Physiol. Scand.* **65**, 74-86.

Kernell D (1965c). The Limits of Firing Frequency in Cat Lumbosacral Motoneurones Possessing Different Time Course of Afterhyperpolarization. *Acta. Physiol. Scand.* **65**, 87-100.

Kernell D (1972). The early phase of adaptation in repetitive impulse discharges of cat spinal motoneurones. *Brain Res* **41**, 184-6.

Kernell D & Monster AW (1981). Threshold current for repetitive impulse firing in motoneurones innervating muscle fibres of different fatigue sensitivity in the cat. *Brain Res* **229**, 193-6.

Kernell D & Monster AW (1982a). Motoneurone properties and motor fatigue. An intracellular study of gastrocnemius motoneurones of the cat. *Exp Brain Res* **46**, 197-204.

Kernell D & Monster AW (1982b). Time course and properties of late adaptation in spinal motoneurones of the cat. *Exp Brain Res* **46**, 191-6.

Kiehn O & Eken T (1998). Functional role of plateau potentials in vertebrate motor neurons. *Curr Opin Neurobiol* **8**, 746-52.

Lee RH & Heckman CJ (1998a). Bistability in spinal motoneurons in vivo: systematic variations in persistent inward currents. *J Neurophysiol* **80**, 583-93.

Lee RH & Heckman CJ (1998b). Bistability in spinal motoneurons in vivo: systematic variations in rhythmic firing patterns. *J Neurophysiol* **80**, 572-82.

Lee RH & Heckman CJ (2001). Essential role of a fast persistent inward current in action potential initiation and control of rhythmic firing. *J Neurophysiol* **85**, 472-5.

Li Y & Bennett DJ (2003). Persistent sodium and calcium currents cause plateau potentials in motoneurons of chronic spinal rats. *J Neurophysiol* **90**, 857-69.

Magarinos-Ascone C, Nunez A & Delgado-Garcia JM (1999). Different discharge properties of rat facial nucleus motoneurons. *Neuroscience* **94**, 879-86.

Miles GB, Dai Y & Brownstone RM (2005). Mechanisms underlying the early phase of spike frequency adaptation in mouse spinal motoneurones. *J Physiol* **15**, 519-532.

Powers RK, Sawczuk A, Musick JR & Binder MD (1999). Multiple mechanisms of spike-frequency adaptation in motoneurones. *J Physiol Paris* **93**, 101-14.

Sawczuk A, Powers RK & Binder MD (1995). Spike frequency adaptation studied in hypoglossal motoneurons of the rat. *J Neurophysiol* **73**, 1799-810.

Sawczuk A, Powers RK & Binder MD (1997). Contribution of outward currents to spike-frequency adaptation in hypoglossal motoneurons of the rat. *J Neurophysiol* **78**, 2246-53.

Schwindt PC (1973). Membrane-potential trajectories underlying motoneuron rhythmic firing at high rates. *J Neurophysiol* **36**, 434-9.

Schwindt PC & Crill WE (1982). Factors influencing motoneuron rhythmic firing: results from a voltage-clamp study. *J Neurophysiol* **48**, 875-90.

Spielmann JM, Laouris Y, Nordstrom MA, Robinson GA, Reinking RM & Stuart DG (1993). Adaptation of cat motoneurons to sustained and intermittent extracellular activation. *J Physiol* **464**, 75-120.

Zeng J, Powers RK, Newkirk G, Yonkers M & Binder MD (2005). Contribution of persistent sodium currents to spike-frequency adaptation in rat hypoglossal motoneurons. *J Neurophysiol* **93**, 1035-41.

Zengel JE, Reid SA, Sypert GW & Munson JB (1985). Membrane electrical properties and prediction of motor-unit type of medial gastrocnemius motoneurons in the cat. *J Neurophysiol* **53**, 1323-44.

TABLES

Table 1: Passive and Active Motoneuron Properties.

Motoneuron Property	rhythmic firing for 26 s	does not fire for 26 s	P value
1. RMP (mV)	–70.3 ± 6.1 (15)	–67.4 ± 8.0 (56)	0.13
2. Vth (mV)	–48.8 ± 6.2 (15)	–48.8 ± 9.0 (56)	0.98
3. Rheobase Current (nA)	11.1 ± 4.9 (15)	9.0 ± 4.0 (56)	0.14
4. Input resistance (MΩ)	1.9 ± 0.9 (17)	2.0 ± 1.1 (59)	0.7
5. AHP amplitude(mV)	1.3 ± 0.5 (17)	2.0 ± 1.8 (42)	**0.03**
6. AHP ½ decay time (ms)	13.5 ± 3.4 (17)	14.9 ± 5.5 (46)	0.2
7. Spike height (mV)	78.6 ± 13.5 (15)	73.0 ± 10.3 (46)	0.15
8. f/I slope (Hz/nA)	7.1 ± 2.8 (12)	7.5 ± 2.5 (27)	0.43
9. ePIC (nA)	0.4 ± 0.2 (8)	0.5 ± 0.3 (15)	0.2

Summary of passive (numbers 1-7) and active (numbers 8-9) MN properties. Data are presented as means ± SD (n) for all MNs. Resting membrane current (RMP), voltage threshold (Vth), afterhyperpolarization (AHP), estimated persistent inward current (ePIC). Notice that ePIC only has an n of 8, this is because the other 8 MNs demonstrated a type 1 or type 2 f-I relationship (i.e. f-I relationship types of MNs that do not demonstrate the presence of PIC (10)).

Table 2: Distribution of Motoneuron Spike Frequency Adaptation.

	SFA (Decline in Number of Spikes over Time)				
	1-s bins		2-s bins		5-s bins
MN #	1-(bin26/bin1)	1-(bin26/bin2)	1-(bin13/bin1)	1-(bin13/bin2)	1-(bin5/bin1)
1	N/A	N/A	N/A	N/A	N/A
2	0.84	0.81	0.81	0.77	0.70
3	0.71	0.68	0.71	0.63	0.66
4	0.83	0.78	0.79	0.70	0.72
5	0.78	0.75	0.75	0.70	0.69
6	N/A	N/A	N/A	N/A	N/A
7	0.72	0.66	0.71	0.64	0.65
8	0.82	0.78	0.78	0.73	0.72
9	0.57	0.65	0.62	0.60	0.58
10	0.76	0.72	0.73	0.66	0.64
11	0.84	0.76	0.81	0.70	0.81
12	0.82	0.78	0.81	0.71	0.73
13	0.86	0.81	0.84	0.76	0.76
14	0.83	0.76	0.80	0.69	0.71
15	0.80	0.75	0.79	0.70	0.72
16	0.55	0.54	0.55	0.50	0.50
17	0.53	0.49	0.52	0.47	0.42
18	0.81	0.78	0.81	0.75	0.73
Mean	*0.76	0.72	*0.74	0.67	0.67
SD	0.11	0.09	0.10	0.09	0.10
Range	0.54-0.86	0.49-0.82	0.52-0.84	0.47-0.77	0.42-0.81

Summary of 5 different indices of SFA derived from the normalized number of spikes in 1-s bins, 2-s bins and 5-s bins. For example, for MN #9 the index of SFA derived from bin13 relative to 2-s bin1 = 0.62, indicating that there was 62% decline in the number of spikes fired from bin 1 (time 0-2 s) to bin 13 (time 25-27 s). The indices shown in this table were selected because they were sensitive to a wide range of MN SFA and were significantly correlated with other MN properties. Motoneurons 1 and 6 are not applicable (NA) because they demonstrated a SFA pattern typical of that

seen when a MN is stimulated extracellularly, thus they were excluded from the data set. Columns denoted by * are significantly different ($p < 0.001$) than all other columns .

Table 3: Correlations between spike frequency adaptation indices and other motoneuron properties.

Bin size	SFA index	Correlation Coefficients			
		ePIC	Rheobase	IR	f-I Slope
1-s	1-bin26/bin1	**-0.79, p<0.01**	**0.60, p=0.01**	-0.33, p=0.21	-0.38, p=0.27
	1-bin26/bin2	**-0.74, p<0.001**	0.37, p=0.16	**-0.55, p<0.05**	-0.35, p=0.31
2-s	1-bin13/bin1	**-0.77, p<0.01**	**0.61, p<0.01**	-0.48, p=0.06	-0.45, p=0.19
	1-bin13/bin2	**-0.72, p<0.01**	0.47, p=0.07	-0.27, p=0.31	-0.31, p=0.38
5-s	1-bin5/bin1	**-0.76, p<0.001**	**0.71, p<0.01**	-0.43, p=0.09	-0.57, p=0.09

Summary of the relationship between different indices of SFA and other MN properties. Correlation coefficients and level of significance are presented for each of the correlations between SFA ratio and estimated persistent inward current amplitude (ePIC), rheobase current, input resistance (IR) and frequency-current slope (f-I slope).

FIGURES

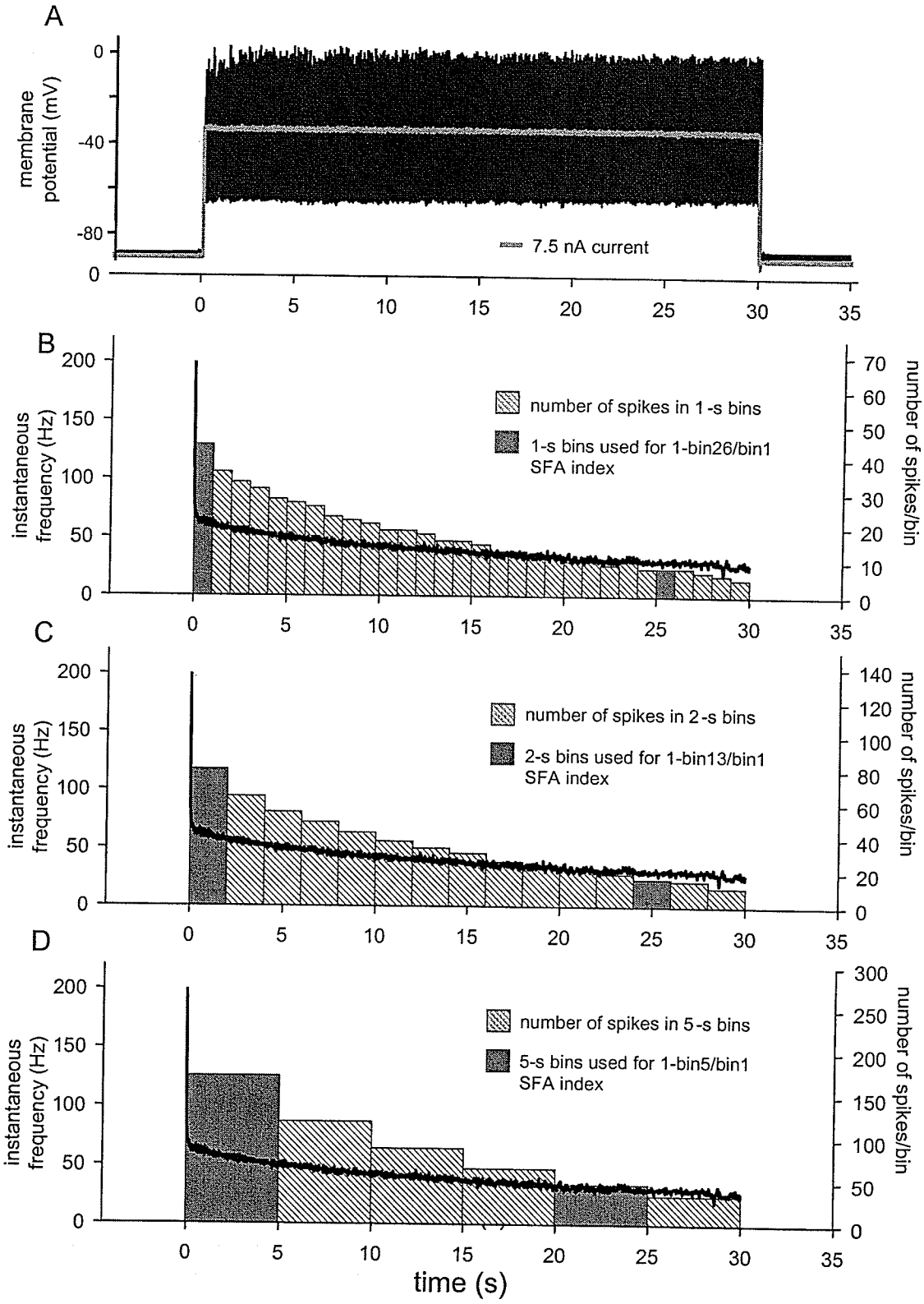
A
membrane potential (mV)
0
-40
-80
7.5 nA current
0 5 10 15 20 25 30 35
B
instantaneous frequency (Hz)
number of spikes in 1-s bins
1-s bins used for 1-bin26/bin1 SFA index
number of spikes/bin
C
instantaneous frequency (Hz)
number of spikes in 2-s bins
2-s bins used for 1-bin13/bin1 SFA index
number of spikes/bin
D
instantaneous frequency (Hz)
number of spikes in 5-s bins
5-s bins used for 1-bin5/bin1 SFA index
number of spikes/bin
time (s)

Figure 1. Motoneuron spike frequency adaptation analysis method. A 30-s sustained injection of supra-threshold current results in sustained firing that gradually decreases (spike frequency adaptation). **A**, shows current injected and spikes (voltage measured in DCC mode). **B**, shows the instantaneous firing frequency (black line, left axis) and the normalized number of spikes discharged in 1-s bins (hatched vertical bars, right axis). The 1-s bins were normalized such that the final bin in the 30-s period of spike discharge always contained 5 spikes. The normalized number of spikes was also counted in 2-s (**C**) and 5-s (**D**) bins. The solid grey vertical bars represent bins used in three different indices of SFA including 1-bin26/bin1 using 1-s bins (B), 1-bin13/bin1 using 2-s bins (C), and 1-bin5/bin1using 5-s bins (D). The indices depicted by the solid grey boxes in A, B, and C are found in Table 2, MN # 8. This figure is an example of a MN with a medium SFA adaptation.

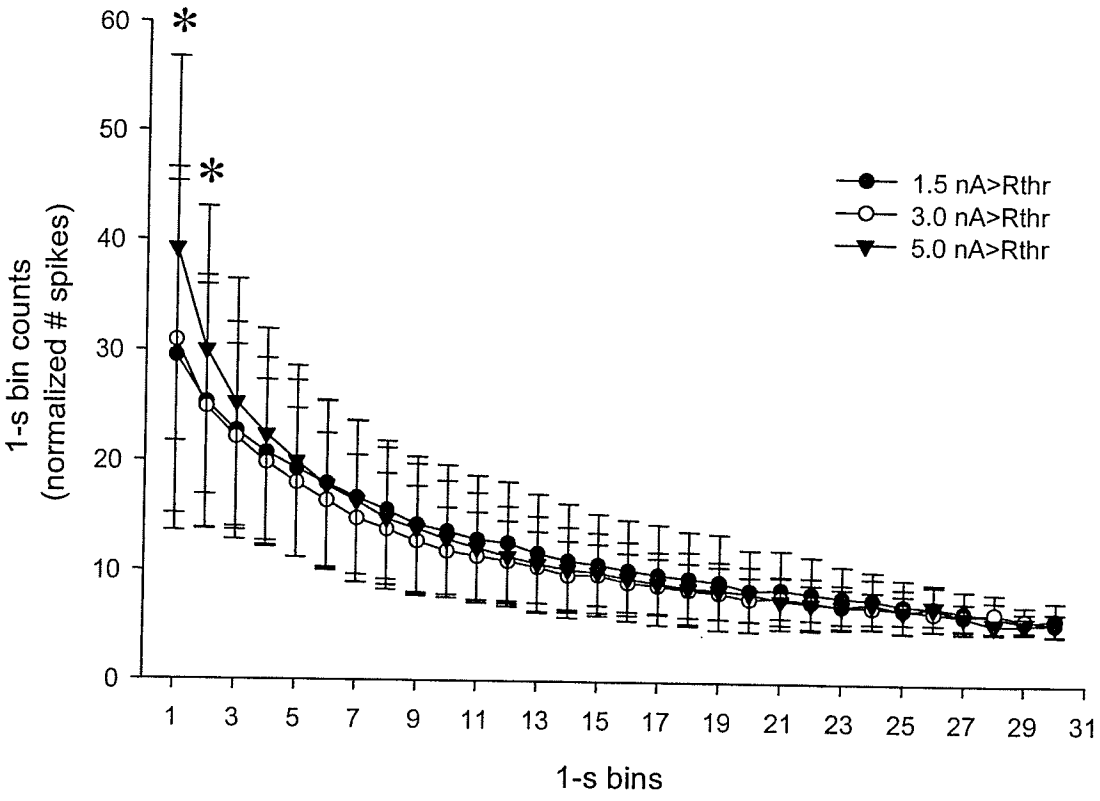

Figure 2. Motoneuron spike frequency adaptation when injected with 3 currents above the threshold for rhythmic firing. With exception for the first 2 s of MN rhythmic discharge, MN SFA was not stimulus current-dependent. The number of spikes discharged in the 1st and 2nd second of rhythmic discharge were 25% and 19% higher and 16% and 16% higher with an injected current of 5 nA>R_{th} compared to 1.5 and 3 nA >R_{th} current injections, respectively. * Represent a significant difference ($p < 0.001$) for the number of spikes discharged during 5 nA > R_{th} of current injection compared to 1.5 and 3 nA > R_{th} currents. Data points and vertical bars represent means ± SD.

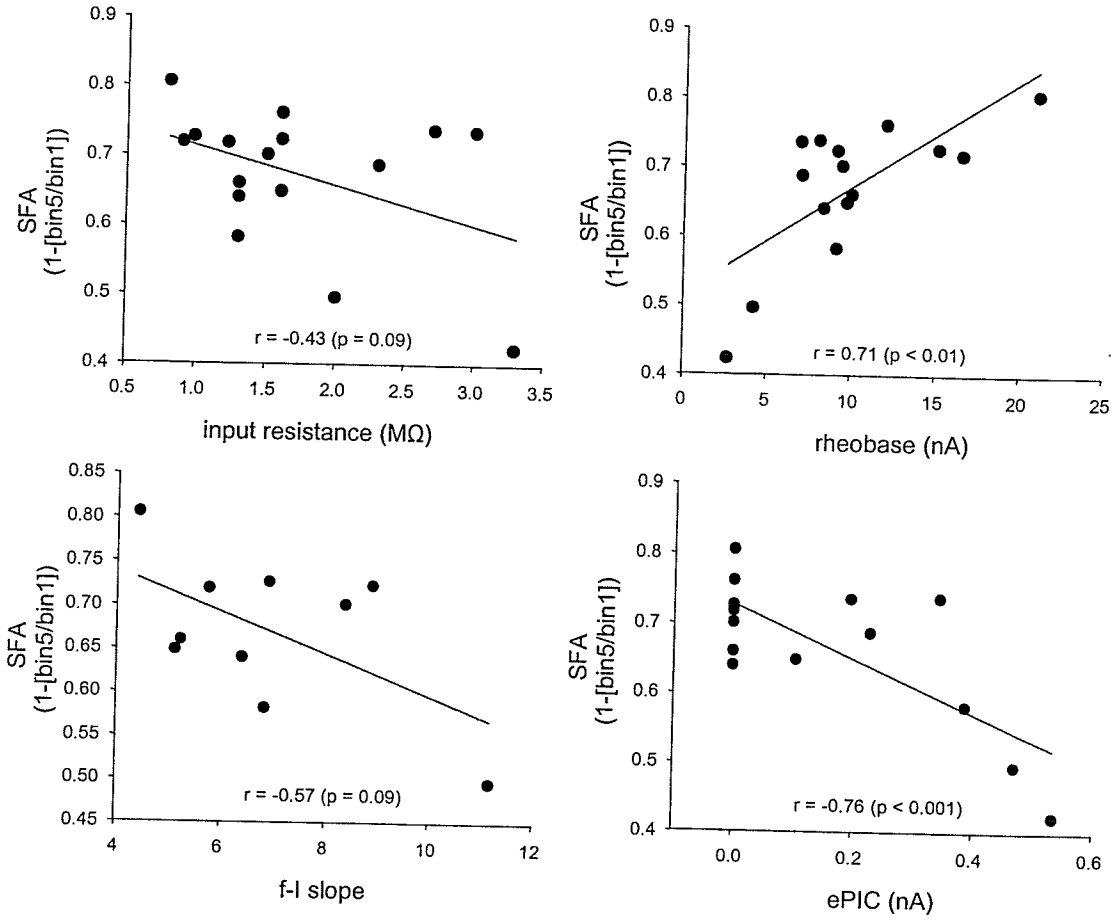

Figure 3. Correlations between the MN SFA index 1-(bin5/bin1) and other motoneurone properties. SFA is calculated as 1-(bin5/bin1) using 5-s bins. Therefore, a motoneuron with a SFA index of 0.4 demonstrates a 40% reduction in the number of spikes fired in bin5 (21-25s) relative to bin1 (1-5 s). A and B are passive properties of the MN and C and D are active properties of the MN. The r and p values are shown in each. On the X-axis are the MN properties and on the Y-axis is the 5-s 1-bin5/bin1 SFA index. **A**, input resistance, **B**, rheobase current, **C**, frequency-current slope (f-I slope) and **D**, estimated persistent inward current amplitude (ePIC). Note that the r and p values in D include points for 8 MNs that did not demonstrate a PIC (see Table 1 and Results).

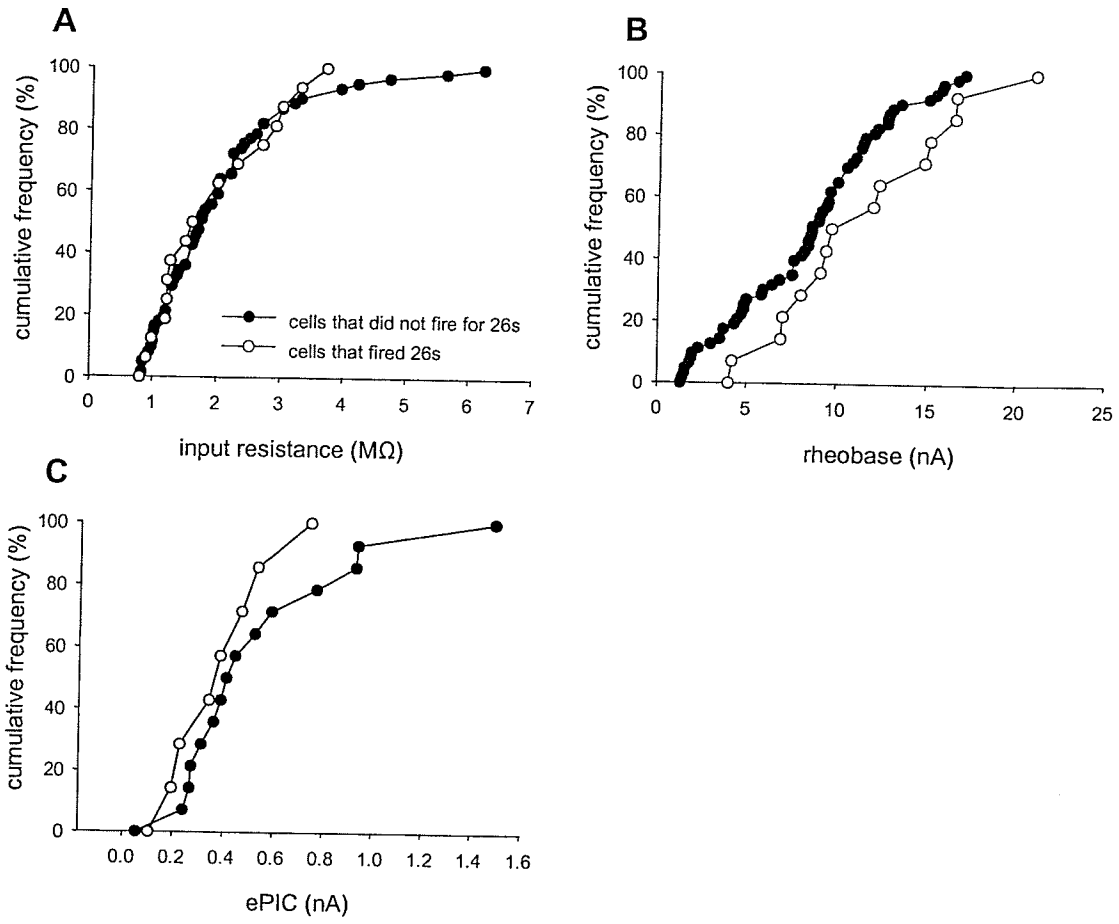

Figure 4. Percentile distributions for **A**, IR, **B**, rheobase, and **C**, ePIC amplitude, between the group of motoneurons which discharged for 26 s and ones that did not. Mean MN values in A,B, and C for each group were not significantly different from one another and are listed in Table 1.

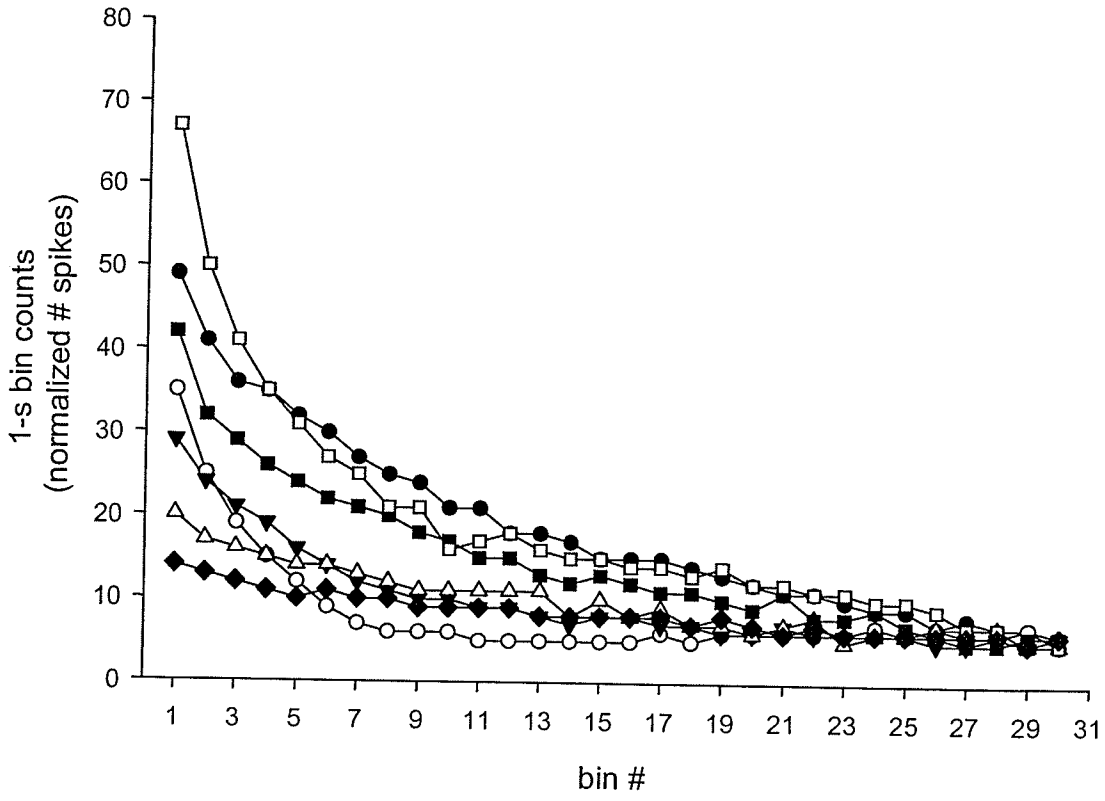

Figure 5. Differences in spike frequency adaptation among motoneurons. Shown are 7 MNs and their corresponding normalized SFA curves. Only SFA curves of 7 MNs are illustrated for clarity. Furthermore, the 7 SFA curves in this figure include the MNs with the greatest and least amount of SFA. Motoneurons 1 and 6 from Table 2 are not included.

CHAPTER 4: DOES ELIMINATION OF AFFERENT INPUTS MODIFY THE CHANGES IN RAT MOTONEURONE PROPERTIES THAT OCCUR FOLLOWING CHRONIC SPINAL CORD TRANSECTION?

RUNNING TITLE: Motoneurone properties following spinal cord isolation

KEYWORDS: Firing frequency, spike frequency adaptation, chronic spinal cord isolation, persistent inward current

Chapter 4 is reprinted here with permission as it appears in:
Button DC, Kalmar JM, Gardiner K, Marqueste T, Zhong H, Roy RR, Edgerton VR and Gardiner PF (2007). Does elimination of afferent input modify the changes in rat motoneurone properties that occur following chronic spinal cord transection? J. Physiol.

MY CONTRIBUTION TO THE PUBLICATION. This work was part of collaboration with the Edgerton Lab, UCLA, who are experts in the SI and ST procedures. They performed the SI and ST procedures on the rats and shipped them to my supervisor's lab where we did the terminal experiments. The SI and ST animals required a lot of day-to-day maintenance which I took part in. The technician and I performed the required animal surgeries in preparation for motoneurone electrophysiological recordings. I recorded, measured, and analysed the data included in this publication. During the duration of the experiments I continuously analyzed the data and discussed ideas with my supervisor and the other authors on whether or not more and what type of data was required to complete our project. After collecting and analyzing preliminary data I submitted an abstract, only after consultation with my supervisor and the other authors, on this data for presentation at an annual scientific conference. Throughout the SI and ST data collection, I constituted a communication link between the Gardiner and Edgerton labs, summarizing on-going data trends and making suggestions as to the need for more data, etc. Once all of the data was collected and analysed I wrote and revised the manuscript in consultation with the other authors. I also discussed with my supervisor the order of authorship for the manuscript. After the manuscript was completed I circulated it to all the authors for their approval on authorship order, the manuscript itself, and editing purposes. Once the manuscript was deemed by all authors, as ready to go to submission, along with my supervisor I selected the Journal in which we submitted the manuscript to and then proceeded with the manuscript submission process. After the reviewer's comments on the manuscript were returned

I made all the required revisions and discussed the reasoning for those revisions with the other authors. When the manuscript was accepted I made any further required corrections such as those included in the galley proofs.

ABSTRACT

The purpose of this study was to determine the effects of 6-8 weeks of chronic spinal cord isolation (SI, removal of descending, ascending and afferent inputs), compared to the same duration of spinal cord transection (ST, removal of descending input only) on hindlimb motoneurone biophysical properties. Adult female Sprague-Dawley rats were placed into three groups: 1) Con (no removal of inputs), 2) ST, and 3) SI. The electrophysiological properties from sciatic nerve motoneurones were recorded from deeply anesthetized rats. Motoneurones in SI rats had significantly ($p < 0.01$) lower rheobase currents and higher spike afterhyperpolarization amplitudes and input resistances compared to motoneurones in Con rats. A higher percentage (Chi-square, $p = 0.01$) of motoneurones in SI than Con rats demonstrated frequency-current (f-I) relationships consistent with activation of persistent inward currents. Motoneurone steady state f-I slopes determined by increasing steps of 500-ms current pulses were significantly lower ($p < 0.02$) in SI than Con rats. Motoneurone spike frequency adaptation measured using 30-s square-wave current injections (1.5 - 3.0 nA above the estimated rhythmic firing threshold), was similar for Con and SI motoneurones. Changes in motoneurone properties following SI did not differ from ST. These findings indicate that the removal of afferent and ascending inputs along with descending inputs has little additional affect on motoneurone properties than removal of descending inputs alone. This study is the first to demonstrate that intact ascending and afferent input does not modify the effects of spinal transection on basic and rhythmic firing properties of rat hindlimb motoneurones.

INTRODUCTION

Spinal cord transection eliminates supraspinal input to motoneurones below the transection site. Although voluntary drive to the motoneurone is eliminated, the afferent connections remain intact. Excitation of these afferents can lead to the activation of intact segmental reflexes (Li & Bennett 2003), exciting the motoneurones and subsequently generating involuntary muscle contractions (Alaimo et al. 1984; Ishihara et al. 2002). For example, muscle electromyography activity after spinal cord transection (ST) is reduced only by ~50-75% (Ishihara et al. 2002). These involuntary contractions following ST may reflect the accentuation of voltage-dependent persistent inward currents (PIC) (Bennett et al. 2001b) that enhance motoneurone excitability and, in the absence of inhibition from supraspinal systems, may contribute to periodic prolonged muscle contractions (spasticity) (Li et al. 2004; Li & Bennett 2003; Bennett et al. 2001a; Bennett et al. 2001b). Furthermore, fully-developed spasticity after ST results in partial recovery of muscle atrophy and reversion back from a higher percentage of fast-type muscle fibers to the more comparable proportions of slow and fast fibers seen in controls (Harris et al. 2007). Although some biophysical properties of motoneurones below the site of ST may undergo significant changes such as depolarization of resting membrane potential and voltage threshold (Beaumont et al. 2004; Hochman & McCrea 1994; Cope et al. 1986), decreased afterhyperpolarization (AHP) duration (Czeh et al. 1978; Hochman & McCrea 1994; Cope et al. 1986) and a rightward shift in the frequency-current (f-I) relationship (Beaumont et al. 2004), a large degree of heterogeneity is maintained. Thus, like muscle, afferent-induced activation of segmental reflexes after ST may

help maintain, to a certain degree, the biophysical properties of the affected motoneurones. The question remains, would a lack of afferent and ascending input to motoneurones in addition to ST induce further changes in motoneurone biophysical properties compared to ST alone?

To address this issue, we use the spinal cord isolation (SI) model which combines ST with surgical ablation of afferent and ascending inputs (Grossman et al. 1998). The SI model abolishes segmental reflexes (Pierotti et al. 1991) and the hindlimb muscles are almost completely quiescent such that the integrated electromyography of the soleus muscle of SI rats is < 1% of normal control values (Roy et al. 2007b; Gomez-Pinilla et al. 2004). Unlike chronic ST, spasticity does not develop following chronic SI, myofibers undergo severe atrophy and remain atrophied, and myofiber types are transformed to predominantly fast-type without reverting back to those seen in controls (Harris et al. 2007). Furthermore, SI has a more pronounced affect on muscular force properties and different myosin heavy chain proportions than ST (Roy et al. 2002; Talmadge et al. 2002; Grossman et al. 1998). Despite the known effects of SI on muscle, the effect of SI on motoneurone biophysical properties remains unknown. However, it is known that two to three weeks after ST along with a bilateral deafferentation, which is very similar to the SI model, motoneurone electrotonic lengths in cats decreased and input resistances (R_{in}) and excitatory post synaptic potentials increased, suggesting an overall atrophy of motoneurones (Gustafsson et al. 1982), although recent evidence shows that motoneurone soma size may be unaffected after SI (Roy et al. 2007a; Chalmers et al. 1992). Furthermore, following ST, the decreased slope of the f-I relationship of

motoneurones below the lesion can be prevented by one month of daily passive cycling exercise (Beaumont et al. 2004). Perhaps this demonstrates the importance of regular afferent input in determining the properties of motoneurones.

Finally, neurotrophins are important for motoneurone survival and maintenance and may modulate the expression of ion channel subunits that render the motoneurone more or less excitable (Lesser et al. 1997; Rose et al. 2004). After SI the ventral horn has lower levels of brain-derived neurotrophic factor and neurotrophin 3 proteins and mRNA (Gomez-Pinilla et al. 2004). A decrease in neurotrophins after spinal cord injury may affect the number, density, composition, activation, and/or location of the motoneurone ion channels thereby altering their conductance and subsequently eliciting changes in motoneurone electrophysiological properties. Since neurotrophins are located in both efferent and afferent pathways (Mitsumoto & Tsuzaka 1999), SI may induce greater change to neurotrophin expression in the lumbar spinal cord and consequently to motoneurone electrophysiological properties compared to ST.

The purpose of the present study was to assess and compare the effects of ST and SI on the biophysical properties of rat hindlimb motoneurones. We hypothesized that, in SI, the ablation of ascending and afferent inputs in addition to the spinal transection would have a more pronounced effect on motoneurones than the lack of descending inputs induced by ST alone. We compared a series of active and basic motoneurone properties and found that ST and SI motoneurones have decreased f-I slopes, increased incidence of bistability but not PIC amplitude, and similar spike frequency adaptation (SFA) patterns compared to Con motoneurones. Furthermore,

ST and SI motoneurones have lower rheobase currents and higher R_{in}s and spike afterhyperpolarization (AHP) amplitudes compared to Con motoneurones. No differences existed between ST and SI motoneurone properties. These findings suggest that afferent and ascending inputs do not preserve the biophysical properties of motoneurones following ST. Preliminary results have been published elsewhere (Button et al. 2005; Button et al. 2006 a, c).

METHODS

Experimental animals. Adult female Sprague-Dawley rats were used in this study. Con animals (275-325 g, n=33) were from the University of Manitoba (Winnipeg, MB). The ST (250-350 g, n=15) and SI (225-300 g, n=14) animals received surgery at the University of California, Los Angeles (UCLA). Animals were maintained at UCLA for 30 days after surgery and then shipped to the University of Manitoba. All animals were housed individually with 12:12-h light-dark cycle and provided water and food *ad libitum*. The room temperature was maintained at ~25°C. When electrophysiological recordings were made from the SI and ST animals, rats had been chronically spinal isolated or spinal transected for approximately 6-8 weeks. Con rats were approximately the same age when electrophysiological recordings were made, but did not undergo SI or ST. All procedures were approved by the animal ethics committee of the University of Manitoba and the UCLA Chancellor's Animal Research Committee and were in accordance with the guidelines of the Canadian Council of Animal Care and followed the American Physiological Society Animal Care Guidelines.

ST and SI surgical procedures. These procedures were performed at the University of California, Los Angeles. Animals were acclimated to the laboratory conditions for one week prior to the surgical procedures and maintained at the University of California, Los Angeles for 30 days post-operatively prior to shipment to the University of Manitoba. The rats were deeply anesthetized with ketamine hydrochloride/xylazine (100/5 mg kg^{-1} body weight, i.p.). A surgical level of anesthesia was maintained with supplements of ketamine as needed. All surgical procedures were performed under aseptic conditions.

The spinal cord of the ST rats was completely transected at a mid-thoracic level as described previously (Talmadge et al. 2002). Briefly, a dorsal midline incision was made, muscles overlying the spinal column from T6-T9 were separated from the spinal column, and a partial laminectomy was performed at T7-T8. Two to three drops of lidocaine (2%) were applied to the exposed spinal cord and the spinal cord was completely transected with micro-dissection scissors. The cut ends of the spinal cord were lifted gently to verify the completeness of the transection. Gelfoam was packed between the cut ends of the cord. The fascia and muscles surrounding the spinal column were sutured (4-0 chromic gut) over the transection site and the skin incision was closed (4-0 Ethilon sutures).

The SI procedure for rats has been described in detail elsewhere (Grossman et al. 1998). Briefly, rats in the SI group were subjected to complete spinal cord transections at mid-thoracic (~T7) and upper sacral (~S1) levels with a complete bilateral dorsal rhizotomy between the two transection sites. A longitudinal midline skin incision was made dorsal to the spinal column from the T6 to the S2 vertebral

levels and the muscles overlying the spinal column were separated from the spinal column. A partial laminectomy was performed to remove the spinous processes, a trough (~2 mm wide) was made in the midline of the column between vertebral levels T7 and S2, and the dura mater was opened longitudinally along the midline. Once the above procedures were successfully completed the dorsal roots from T7 to S2 were cut bilaterally as close to the spinal cord as possible, retracted to their point of exit, and then cut as close to the exit site as possible. Following the dorsal rhizotomy, the spinal cord was completely transected at approximately T7–T8 and S1–S2 and a complete transection was verified as described above. The transection sites were packed with Gelfoam. A strip of gelfilm was placed along the length of exposed spinal cord to minimize adhesions between the spinal cord and the overlying tissues. The paravertebral muscles and fascia surrounding the spinal column and the skin incision were sutured as described above. A schematic illustration of the SI surgery and details of post-operative care have been published previously (Hyatt et al. 2003; Roy et al. 1992).

An antibiotic (Baytril - enrofloxacin) was administered orally (2 ml/125 ml water) for the first 5 days. An analgesic was administered (Buprenex - buprenorphin, 0.05 mg kg^{-1}, s.c.) twice daily for the first 2 days. During recovery, the rats were housed individually in polycarbonate cages (26 cm x 48 cm) in a room maintained at 26 ± 1°C, with a 12:12-h light:dark cycle. Post-surgical care involved manual expression of the bladder three times per day for the first 2 weeks and two times per day for the remainder of the study. Following ST and SI surgery, the rats used their forelimbs to move around their cages to access food and water ad libitum. Although

we did not measure electromyographic activity of muscles following ST or SI, the hindlimbs of SI animals were completely flaccid and exhibited no reflex activity (no muscle spasms, withdrawal reflexes or toe spread responses) at any point during the one-month recovery period indicating that the transections and dorsal rhizotomy were complete. The hindlimbs of SI and ST rats were manipulated passively through a full range of movement once per day to maintain joint flexibility. Animal health, based on factors such as body weight, appearance, grooming, and quantity and quality of expressed urine, was assessed daily for both the SI and ST rats and cage bedding was changed to prevent skin infections. Con animals were confined to standard plastic cages for the same time period. The procedures for the care and maintenance of spinal injured animals have been detailed previously (Roy et al. 1992).

Surgery for electrophysiological experiments. Approximately one month after the ST or SI surgeries, the rats were shipped to the University of Manitoba for *in situ* electrophysiology experiments. Animals were anesthetized with ketamine/xylazine (90/10 mg kg^{-1}, i.p.) and atropine (0.05 mg kg^{-1} atropine in a 5% dextrose physiological saline vehicle, i.p.) was administered to minimize airway secretions during the subsequent tracheotomy. The surgical procedures included: 1) insertion of a tracheal tube for ventilation (Harvard Apparatus, Canada), 2) catheterization of the femoral artery for continuous monitoring of mean arterial pressure (MAP) and constant infusion of anaesthetic (Pump 11, Harvard Apparatus, Canada), 3) exposure of the left hindlimb sciatic nerve for electrical stimulation, and 4) exposure of the spinal vertebrae and laminectomy from T12 to S1 in a stereotaxic unit.

Physiological saline solution containing ketamine/xylazine (9/1 mg h^{-1}) was infused via the femoral artery to maintain anesthesia. The depth of anesthesia was verified continuously via heart rate, MAP, expired CO_2 levels, and bilateral toe pinch. Blood pressure was maintained between 80-110 mm Hg and respiration was kept at a tidal volume of 2.0 to 2.5 ml and a ventilation rate of 60-80 strokes min^{-1}. Expired CO_2 levels were measured via a CAPSTAR 100 CO_2 analyzer (CWE Inc., USA) and maintained between 3-4% by adjusting tidal volume and/or ventilation rate. Rectal temperature was monitored and maintained near 37°C using a feedback Homeothermic Blanket Control Unit (Harvard Apparatus, Canada). The head, thoracic and lumbar vertebrae, hips, and left foot were immobilized with clamps, and the open leg and back incisions were used to make an oil bath around the sciatic nerve and spinal cord, respectively. The dura mater covering the spinal cord was incised, and the large dorsal roots comprised of afferents from the left hind-limb in Con and ST rats were cut and reflected over the right side of the cord. An opening was made in the pia mater just lateral to the entry zone of these roots into the cord to allow penetration of the glass microelectrode for intracellular recording. Since SI rats had their dorsal roots removed, a greater medial to lateral opening in the pia matter was made along the L2-L4 vertabrae approximately where the dorsal roots were found in ST and Control animals. Prior to the search for motoneurones, respiratory movement was minimized by performing a left unilateral pneumothorax.

Additional drugs and solutions. To reduce blood pressure and respiration-related movement artifacts and to stabilize the animal for optimal electrophysiological recordings, several additional solutions were administered intravenously. The rat

received: 1) a solution of 100 mM $NaHCO_3$ (Fisher scientific) and 5% Dextrose (Fisher Scientific) in double-distilled H_2O, and 2) pancuronium bromide (0.2 mg kg^{-1}). Pancuronium bromide was injected prior to the start of the electrophysiological recordings and then re-administered as needed to maintain paralysis of the respiratory and hindlimb muscles, a requirement for optimal intracellular recordings.

Measurement of motoneurone basic properties. Glass microelectodes (1.0 mm thin-walled, World Precision Instruments, USA) were pulled with impedances of approximately 10 MΩ (Kopf Vertical Pipette Puller, David Kopf Instruments, USA), and filled with 2M K^+ citrate. The tip of the electrode was positioned over the incision in the pia mater and lowered into the cord with an inchworm microdrive system (Burleigh Instruments Inc., USA) in steps of 5-10 μm. The sciatic nerve was stimulated with a bipolar silver chloride electrode at a frequency of 1 pulse·s^{-1} (0.1-0.2 mA for 0.1 ms) while the microelectrode was advanced through the cord and the field potential was monitored continuously. Evidence of successful impalement of a motoneurone was indicated by 1) a sudden increase in membrane potential to at least 50 mV; 2) an antidromic action potential spike amplitude greater than 55 mV with a positive overshoot and, 3) a reproducible latency of less than 2.5 ms from the stimulation artifact. During recording, an Axoclamp intracellular amplifier system (Axoclamp 2B, Axon Instruments Inc., USA) was used either in a bridge or a discontinuous current-clamp mode (DCC; 2-10 kHz switching), with capacitance maximally compensated. Basic motoneurone properties recorded from resting membrane potential in bridge mode included: resting membrane potential, spike height, AHP amplitude and half-decay time of orthodromic action potentials evoked

by brief (0.5 ms) supramaximal intracellular current injections (averaged from at least 40 spikes). Rheobase current (the minimum amplitude of a 50-ms square-wave current required to elicit an action potential 50% of the time), voltage threshold (membrane voltage at which a spike was triggered 50% of the time), and cell R_{in} (averaged from 60, 1-nA hyperpolarizing current pulses each lasting 100 ms) were determined in the DCC mode.

Measurement of motoneurone frequency-current (f-I) relationship. After measuring the basic properties, the motoneurone f-I relationship was measured in two ways. First, cells were challenged with slow current ramps (range: 0.5-6.0 nA s^{-1}), and the voltage response was measured in DCC mode (see Button et al. (2006b) for a complete description of this measurement). Peak amplitude of the ramp depended on the rhythmic threshold of the motoneurone and an attempt was made to evoke trains of impulses containing 10-75 spikes over a 0.5-2.5-s duration. The ramps were used to determine the motoneurone f–I relationship, to evoke voltage-dependent plateaus, and to estimate the underlying PIC as previously described (Hounsgaard et al. 1988; Lee & Heckman 1998b; Bennett et al. 2001b) (Fig. 1). Since PICs are activated at membrane potentials depolarized greater than -60 mV (Li & Bennett 2003), only those cells with a resting membrane potential of -60 mV were used to determine f-I relationships. During the current ramps, PIC was estimated from the difference in injected current at spike recruitment compared with spike derecruitment (Fig. 1C and D on left). Second, cells were challenged with an incremental series of 500-ms square-wave pulse current injections and the voltage response was measured in DCC mode. Current was gradually increased and decreased by 1-5 nA steps from

minimum to maximum steady state firing until blocking occurred before the end of the 500-ms period, after which current steps of decreasing intensity were administered (see Cormery et al. 2005). 500-ms square-wave pulse current injections were used to determine minimum and maximum steady-state firing frequencies (SSFF) (Fig. 2A). The f-I slope for each motoneurone was determined by plotting the relationship between the minimum current and mean firing frequency of the last 3 inter-spike intervals during the 500 ms square-wave pulse current injection and the maximum current and the mean firing frequency of the last 3 inter-spike intervals and the slope of the line was calculated (Fig 2B).

Measurement of motoneurone spike-frequency adaptation (SFA). To evoke rhythmic firing, cells were injected with 30-s square-wave current pulses at an amplitude exceeding rhythmic firing threshold (the minimum current at which the motoneurone would fire for at least 10 s). From these recordings we determined the change in spike frequency over time. A 30-s current pulse was chosen on the basis that very little motoneurone SFA is seen after this time point (Sawczuk et al. 1995). Once the threshold current for rhythmic firing was determined, a square-wave pulse of current was injected into the motoneurone for 30 s (Button et al. 2007) and the membrane voltage was measured in DCC and bridge mode (Fig. 3A). Time was allotted after each 30-s current injection for the motoneurone to repolarize back to the resting membrane potential prior to the next attempt. For each cell we used one to two current amplitudes that ranged from 1.5–3 nA > threshold current for rhythmic firing and analyzed motoneurone SFA by the following process: 1) we counted the number of discharges in 1-s bins beginning at the onset of firing (Fig. 3B), 2) we

normalized the number of spikes in each 1-s bin such that the final bin in the 30-s period of firing always contained 5 spikes, 3) these 1-s bins were pooled into six 5-s bins, and 4) [1-(bin5/bin1)] ratio was used as an index of SFA. The rationale for using this measure of SFA and a more detailed description of the methods have been published (Button et al. 2007).

After recording all basic and active properties of the motoneurone, the microelectrode was backed out of the motoneurone in 5-μm steps, and the extracellular voltage was recorded. Typically, experiments yielded 2 - 4 motoneurones with complete and acceptable complements of data. At the end of the experiment, the rat was killed by an overdose of KCl and a bilateral pneumothorax.

Statistics. Only motoneurones that passed all electrophysiological requirements were used for the statistical analyses (see Methods). We performed a one-way ANOVA to determine if motoneurone basic and active properties differed between the Con, ST, and SI groups. A Tukey post hoc analysis was used where significant main effects were present. Pearson Product Moment Correlation was used to determine relationships between several properties. Chi-square analysis was used to determine whether significant differences were present in motoneurone f-I relationship type determined by ramp current injections between Con, ST, and SI motoneurones. Data are expressed as either mean ± SD or as a distribution.

RESULTS

Overall, we recorded the basic and active properties of 96 motoneurones from 33 Con rats, 71 motoneurones from 15 ST rats, and 57 motoneurones from 14 SI rats. Typically, each rat yielded 1-5 motoneurones with acceptable data (see Methods). Some of the Con motoneurone data reported here have been published elsewhere (Button et al. 2006b; Button et al. 2007). In the present study, the elimination of supraspinal input via spinal transection altered the basic properties and rhythmic firing behaviour of rat hindlimb motoneurones. Surprisingly, the elimination of afferent input in addition to spinal transection (spinal isolation) had no further effect on the biophysical properties of the motoneurone.

Basic motoneurone properties after SI and ST. Basic and active motoneurone properties are summarized in Table 1. Con and SI motoneurones had similar resting membrane potentials and voltage thresholds. On the other hand, motoneurones in SI rats had 27% lower rheobase current and 42% higher R_{in} than motoneurones in Con rats (Fig. 4A and B, respectively). SI had no effect on mean spike height and AHP ½ decay time, but increased AHP amplitude by 56% compared to Con motoneurones (Fig. 4C) (see Table 1, Basic Properties). The distributions for rheobase current, R_{in}, spike AHP amplitude and AHP duration are shown in Fig. 5. Con and SI motoneurones had similar maximum and minimum values for each of the three basic properties (Fig. 5A-C), but different distributions between these values for rheobase current (Fig. 5A), R_{in} (Fig. 5B), and AHP amplitude (Fig. 5C). However, motoneurone AHP duration distributions were very similar (Fig. 5D). The relationship between rheobase current and R_{in} (Fig. 6) was maintained following Con

(slope = -0.14, r = -0.56), ST (slope = -0.24, r = -0.64), and SI (slope = -0.23, r = -0.52). In all cases, the correlation for each group was significant ($p < 0.0001$, data not shown). There were no significant differences between SI and ST motoneurones for any basic property (Table 1; Figs. 4, 5, and 6).

Active motoneurone properties after SI and ST.

F-I relationship and PIC amplitude determined by ramp current injections. To determine motoneurone PIC amplitude, we plotted the motoneurone f-I relationships of ramp current injections from 44 Con, 40 ST, and 30 SI motoneurones. This procedure has been used in our (Button et al. 2006b) and other (Hounsgaard et al. 1988; Lee & Heckman 1998b; Bennett et al. 2001b) laboratories to estimate motoneurone PIC amplitude. Only those motoneurones with a minimum resting membrane potential of -60 mV were used in the PIC analysis. Motoneurone f-I relationships plotted from ramp current injections could be categorized into four distinct types based on spike recruitment and derecruitment thresholds from the ascending and descending portions of the ramp currents (Fig. 1A-D). These f-I types have been described in detail previously (Button et al. 2006b), and include: a) type 1 overlapping, b) type 2 adapting, c) type 3 linear + sustained, and d) type 4 acceleration. All four f-I relationship types were observed in motoneurones from all groups of rats (Fig. 1 and 7).

The PIC can be estimated from f-I relationship types 3 and 4 by subtracting the current at spike-derecruitment from the current at spike-recruitment (Fig. 1C and D). The average PIC amplitudes (see Table 1, f-I relationship) of Con and SI motoneurones were similar. Furthermore, the frequency distributions of types 3 and 4

f-I relationships (which indicate the presence of an PIC) of Con and SI motoneurones overlapped (Fig. 7 inset). However, Chi-square analysis revealed that there was a significant difference in the distribution of f-I relationship types between Con and SI motoneurones; more SI motoneurones demonstrated f-I relationships that indicated the presence of PIC (types 3 and 4), compared to Cons (Fig. 7). The average motoneurone PIC amplitude and frequency distribution of motoneurones exhibiting PIC in ST rats were similar to those of SI rats (Fig. 7 inset). Similar to the case for SI rats, however, there was a greater percentage of motoneurones demonstrating f-I relationships that indicate the presence of PIC (types 3 and 4) (Fig. 1C and D) in ST compared to Con rats (Fig. 7). There was no correlation found between motoneurone PIC amplitude and resting membrane potential in each group (Con, ST, and SI groups, data not shown). Other ramp properties (current and firing frequency at spike-recruitment and spike derecruitment) were similar in Con, ST and SI rats. The similarity in the effects of ST and SI suggest that a loss of descending input plays a larger role in determining motoneurone bistability than the loss of afferent and ascending inputs.

The effect of SI or ST on motoneurone f-I relationship properties determined by 500-ms current injections. We determined the motoneurone f-I relationship by injecting 500-ms square-wave pulses into 37 Con, 26 ST, and 31 SI motoneurones. This allowed us to determine the minimum and maximum SSFFs, the minimum current required evoking these SSFFs, and ultimately the f-I slope for each motoneurone (Fig. 2). These 500-ms current injections have been employed previously to describe changes in motoneurone f-I relationships following two to four

weeks of ST (Beaumont et al. 2004) and 2 weeks of hindlimb unloading (Beaumont et al. 2004; Cormery et al. 2005). Motoneurone SSFF Min was 19% lower and SSFF Max was 24% lower in SI than Con rats (see Table 1, f-I Relationship, Fig. 8A), as might be expected based on the higher spike AHP amplitudes (measured by short 0.5 ms suprathreshold current injections at resting membrane potential) for the motoneurones from SI than Con rats and the increased incidence of the number of motoneurones demonstrating PIC (see Discussion for details). Motoneurone f-I slopes also were ~20% lower in SI than Con rats (Fig. 8B). In addition, the distribution of each of the aforementioned three motoneurone properties was shifted significantly to the left in SI compared to Con rats (Fig. 9).

In general, motoneurones in ST and SI rats had similar f-I relationship properties recorded from 500-ms current injections. Motoneurone SSFF Min was 26% and f-I slopes ~20% lower in ST than Con rats (Fig. 8B). Unlike in SI rats, however, the motoneurone SSFF Max was unaffected in ST rats. All mean values (Fig. 8) and distributions (Fig. 9) of the 500-ms f-I relationship properties were similar for the SI and ST groups. Once again, the similarity in the effects of ST and SI suggests that a loss of descending input plays a larger role in determining the gain of motoneurone f-I relationship than the loss of afferent and ascending inputs.

The effect of SI or ST on motoneurone spike frequency adaptation.

To determine whether motoneurone spike frequency adaptation is influenced by ST or SI, we injected 30-s square-wave current pulses into 21 Con, 14 ST, and 14 SI motoneurones. The average number of spikes discharged in 1-s bins was plotted over 30 s for each group of motoneurones (Fig. 10). These spike counts are normalized to

a frequency of 5 spikes per second in the final 1-s bin to more clearly visualize differences in SFA patterns between groups. When 1-s bins are pooled into six 5-s bins, the decline in the number of spikes discharged from the first to the second last 5-s of firing (1-[bin5/bin1]) provides a sensitive index of SFA (Button et al. 2007). One-way ANOVA showed no difference in the mean SFA index among the three groups. In addition, the distributions were similar among the groups (Fig. 10, inset). Thus, neither ST nor SI significantly influenced motoneurone SFA patterns.

DISCUSSION

It is reasonable to expect that the change in the biophysical properties of motoneurones seen after ST would be more pronounced after SI. Motoneurone adaptations would be expected to occur in association with the dramatic decrease in muscle fiber size and shift towards "faster" myosin heavy chain phenotypes reported in the hindlimb muscles of SI rats (Roy et al. 2002; Grossman et al. 1998) and because SI has a greater effect on muscle tension related properties than ST (Roy et al. 2002; Talmadge et al. 2002). However, the population of hindlimb motoneurones in SI rats maintained a degree of heterogeneity for both basic and active properties as illustrated by a range of values and measures of variation that were comparable to those observed in motoneurones of Con and ST rats. Thus, there is an unusual dissociation between the effects of spinal isolation on muscle fibers and motoneurone properties. This illustrates that despite the more pronounced changes in muscle properties following SI compared to ST, SI does not appear to have a greater influence on motoneurone properties. Furthermore, the aforementioned results clearly show that a lack of descending input (ST) alone affects active and basic

properties of motoneurones caudal to the site of the transection. Removing the afferent and ascending inputs to the motoneurones in addition to the descending input (SI) had no further effect on their basic or active properties.

SI and ST motoneurones have lower rheobase currents and higher R_{in}s. Rheobase current and R_{in} are indices of motoneurone size and excitability. Specifically, motoneurones with a low rheobase and high R_{in} are easily excited, relatively small, and are more likely to innervate slow-twitch muscle fibers (Zengel et al. 1985), and are therefore classified as slow motoneurones. Conversely, motoneurones with a high rheobase and low R_{in} are less easily excited, relatively large, and usually innervate fast-twitch muscle fibers and are classified as fast motoneurones. After ST and SI, rheobase and R_{in} shifted towards values typically seen in slower and more excitable cells. There are several possible explanations for this. The most obvious is motoneurones become smaller after ST or SI. Morphologically, motoneurone soma sizes show either no change after ST and SI (Chalmers et al. 1992) or become reduced after ST (Kitzman 2005). There is a loss, however, in the number of primary, secondary, and tertiary dendrites following ST (Kitzman 2005; Gazula et al. 2004) and spinal cord contusion (Bose et al. 2005); however, effects of SI on dendritic structure remain unknown. Due to a trimming of the dendritic tree after spinal cord injury, the overall motoneurone size may become smaller whether or not the soma size is affected. The reported reductions in rat motoneurone cell capacitance following ST (Beaumont et al. 2004) and decrease in electrophysiologically-calculated motoneurone diameter of cat motoneurones following ST with a partial dorsal rhizotomy surgery very similar to SI (Gustafsson et

al. 1982), further suggest that chronic inactivity may diminish overall motoneurone size.

An alteration in ion channel expression could have caused motoneurone rheobase and R_{in} to change in the 6-8 week period following ST and SI. Neurotrophins are important for motoneurone survival and maintenance and may modulate the expression of ion channel sub-units that render the motoneurone more or less excitable (Lesser et al. 1997; Rose et al. 2004). Neurotrophins are transported from the muscle to the motoneurone (retrograde) and from the motoneurone to the muscle (anterograde) (Mitsumoto & Tsuzaka 1999). After ST or SI (or spinal cord injury) the ventral horn has lower levels of brain-derived neurotrophic factor and neurotrophin 3 proteins and mRNA (Gomez-Pinilla et al. 2004). Furthermore, motoneurone properties in ST rats are maintained near control values when fetal tissue, which contains and may continue to secrete neurotrophins, is transplanted into the spinal cord immediately after the transection (Beaumont et al. 2004). Thus, a decrease in neurotrophin activity in the spinal cord after ST or SI may affect the number, density, composition, activation, and/or location of the motoneurone ion channels thereby altering the conductances that underly rheobase and R_{in}. However, it remains unknown whether or not neurotrophin levels are differentially altered following SI compared to ST. It is likely that a combination of these factors contributed to the changes in motoneurone rheobase and R_{in} after ST or SI.

Descending but not afferent and ascending inputs have greater influence on motoneurone properties. Muscle spasms observed after ST may be due to a number of factors including afferent input, enhanced interneuronal excitability, and

persistent inward currents (PIC) that are sufficient to activate motoneurones in the absence of descending inhibition. Because EMG activity is nearly eliminated and spasms are not observed after SI (Roy et al. 2007b; Gomez-Pinilla et al. 2004), it may be assumed that increased excitability of interneurones is insufficient to activate motoneurons in the absence of sensory feedback. Therefore, we expected motoneurons deprived of sensory input for 6-8 weeks (chronic SI) to have different properties than motoneurones with intact sensory input (chronic ST) for 6-8 weeks. This, however, was not the case suggesting that motoneurone properties are primarily dependent upon descending inputs after ST. Monoaminergic inputs increase motoneurone excitability (Hounsgaard et al. 1988; Heckman et al. 2003; Gilmore & Fedirchuk 2004; Perrier et al. 2003). This excitability is especially apparent from the work of Harvey et al (2006 a,b,c) illustrating the effects of monoamines on MN basic properties, PICs, and firing frequency rates after acute and chronic ST. Thus, the lack of descending monoaminergic input to the motoneurones following chronic ST and SI and the chronic adaptation to the loss of these inputs seems to be a major contributor to the change in motoneurone properties in the current study.

Similar to ST, a higher percentage of SI motoneurones demonstrate the presence of PIC. An increase in the presence of PIC is another indication that motoneurone ion channel profiles and other receptors may have changed after ST or SI. PICs are depolarizing currents generated by voltage-gated Na^{+} and Ca^{++} channels that slowly inactivate (Li & Bennett 2003; Lee & Heckman 1999) when the membrane potential is depolarized above activation threshold. These currents can mediate plateau potentials that allow self-sustained rhythmic firing and bistability

(Kiehn & Eken 1998). Bistable motoneurones tends to have relatively lower rheobase currents, suggesting that small motoneurones are influenced by PIC differently than large motoneurones (Lee & Heckman 1998a). The shift towards lower rheobase currents in ST and SI motoneurones may contribute to the increased number of motoneurones exhibiting PICs. Alternatively, ST and SI motoneurones may be more sensitive to serotonin (5-HT) and noradrenaline (NA). Serotonergic and NA input to motoneurones via projections from the raphe nucleus and locus coerulus, respectively of the brainstem (Hounsgaard et al. 1988; Heckman et al. 2003), enhances PIC and renders the motoneurone more excitable (Gilmore & Fedirchuk 2004; Heckman et al. 2003). After acute ST, descending input from the brainstem is eliminated and facilitation of the PIC by 5-HT and NA is compromised. Four weeks later, ST motoneurones become supersensitive to 5-HT and NA and such that small amounts of exogenous 5-HT and NA are sufficient to activate motoneuronal 5-HT receptors (Harvey et al. 2006a; Rank et al. 2007). There is also an increase in motoneurone sensitivity to residual endogenous 5-HT in the spinal cord (Harvey et al. 2006b) which enhances PIC and increases motoneurone bistability. Similar effects should be expected after SI. The increase in motoneurone PIC and subsequently bistability plays a role in the development of spasticity following ST (Li et al. 2004; Li & Bennett 2003; Bennett et al. 2001a; Bennett et al. 2001b).

There is no difference between Con, ST and SI motoneurone PIC amplitudes. Acute and chronic ST motoneurones have distinct differences in their ability to activate PIC channels and PIC size. Very little PIC is seen after acute ST compared to chronic ST (Bennett et al. 2001b; Harvey et al. 2006c; Li et al. 2007).

However, a direct comparison of PIC amplitude between normal control (no transection) motoneurones and chronic ST motoneurones has not been previously reported. Because we found no difference between Con, ST and SI motoneurone PIC amplitudes, there may be an increase in 5-HT and NA receptor sensitivity to residual endogenous monoamines in the 6-8 week period following chronic ST and SI (Harvey et al. 2006b; Harvey et al. 2006a), which is enough to maintain motoneurone PICs to match PIC amplitudes seen in those motoneurones where the monoaminergic systems are left intact (Con motoneurones).

In the present study, PIC amplitude following ST was smaller than previously reported by others who also studied this lesion (Bennett et al. 2001b). One of the major differences in our measurement of motoneurone PIC was the use of anaesthetics (ketamine/xylazine) and the time period following ST at which motoneurone recordings were made. It has been suggested (Hultborn & Kiehn 1992; Hultborn 1999) and found (Guertin & Hounsgaard 1999; Button et al. 2006b) that PICs are substantially decreased when animals are anaesthetized with barbiturates. We previously reported (Button et al. 2006b) that PICs recorded from motoneurones of unaesthetized decerebrated rats did not differ from PICs recorded from motoneurones of rats anesthetized with a mixture of ketamine (an N-methyl-D-aspartate receptor antagonist) and xylazine (an alpha 2-adrenoceptor agonist). Thus, the discrepancy between PIC amplitude reported here and elsewhere is probably not due to the use of our anaesthetic. In the present study, PIC amplitudes were recorded from motoneurones following 6-8 weeks of ST, where as in Bennett et al. (2001b) PIC amplitudes were recorded from motoneurones following 1.5 – 7 months of ST.

A period of six to eight weeks following ST may not be long enough to allow for full development of spasticity, which may explain the smaller PIC amplitudes seen here. Perhaps, PICs in rat lumbar motoneurones are actually somewhat smaller than those of sacral-caudal motoneurones. The functions of the rat hindlimb (Button et al. 2006b) *vs.* tail (Bennett et al. 2001b) are quite different, and may be accompanied by differences in motoneurone PIC amplitude. Finally, although changes in neurotrophin levels occur following ST and SI (Gomez-Pinilla et al. 2004), which can significantly alter motoneurone properties (Gonzalez & Collins 1997), their involvement in the mechanisms underlying PIC is probably limited.

Motoneurone f-I slopes are decreased similarly after SI and ST. We found a reduction in f-I slopes following ST or SI that indicates a decreased input-output gain of the motoneurone suggestive of a change of ion channel profiles. Because, a decrease in AHP amplitude increases the f-I slope (Hounsgaard et al. 1988; Hounsgaard & Kiehn 1989; Hultborn et al. 2004), the most logical explanation for the smaller motoneurone f-I slope following ST and SI was an increase in AHP amplitude, which has been reported for motoneurones of ST rats previously (Petruska et al. 2007; Beaumont et al. 2004). These properties, however, reverted towards control values after fetal tissue transplants and/or passive cycling exercise (Beaumont et al. 2004), or step training (Petruska et al. 2007), probably because of increased neurotrophin levels below the transection (Beaumont et al. 2004; Gomez-Pinilla et al. 2001). SI results in decreased neurotrophin levels in the spinal cord (Gomez-Pinilla et al. 2004) which may increase motoneurone AHP amplitudes generated by large (BK) and small (SK2) Ca^{2+}-activated K^+ channel conductances (Powers & Binder

2001), and subsequently diminish the motoneurone gain. In addition, motoneurones with high R_{in}s tend to have large AHP amplitudes (Gardiner 1993; Cormery et al. 2005).

The decrease firing frequencies after ST and SI may be due to a greater percentage of motoneurones demonstrating the presence of PIC. It has been demonstrated by Li et al. (2004) that both an increase in membrane conductance as a result of the activation of Na^+ and Ca^{++} PIC channels and a subthreshold oscillation of the Na^+ PIC leads to slow motoneurone firing rates in ST motoneurones. Furthermore, when Na PIC is increased in ST motoneurones by increased 5-HT_2 receptor activation firing frequency is significantly reduced (Harvey et al. (2006a).

SI and ST do not affect motoneurone SFA. Spike frequency adaptation is a time-dependent decrease in motoneurone firing frequency that can be further broken down into initial, early, and late adaptation phases. Until now, the effects of SI or ST on motoneurone SFA were unknown. Previously, our laboratory reported that the firing rate declines to a lesser extent during a 30-s current injection (less SFA) in motoneurones that exhibit a high PIC and low rheobase (Button et al. 2007). Given previous evidence of the tendency for smaller, more excitable motoneurones to exhibit less SFA in Con animals (Kernell & Monster 1982; Spielmann et al. 1993), one might expect the more easily excitable motoneurones from SI and ST rats to exhibit less SFA. Instead, SFA was unaffected by SI or ST despite the apparent increase in motoneurone excitability. SFA, however, was measured using currents injected into the motoneurone that were just above that required for rhythmic discharge. At higher currents motoneurone SFA patterns start to differ (Button et al.

2007), and perhaps after ST and SI, SFA patterns could have been distinguished from those in Con rats at higher currents. Nonetheless, like Con, ST and SI motoneurones were able to fire for prolonged periods ($\geq$ 30 s) without any measurable change in SFA pattern.

On a continuum from slow to fast-type motoneurones, the rate of SFA covaries with the rate of fatigue of the innervated muscle fibers. For example, fast motor units demonstrate much greater rates of SFA and fatigue, compared to slow motor units (Kernell & Monster 1982). Following 6 months of ST and 60 days of SI soleus muscle fibers become faster and there is approximately a 40% reduction in soleus fatigue resistance compared to control (Roy et al. 2002; Talmadge et al. 2002). Even after prolonged ST where there is reversion back from a higher percentage of fast-type muscle fibers to the more comparable proportions of slow and fast fibers seen in controls, muscle fatigue resistance remains suppressed (Harris et al. 2006). Since the SFA patterns reported here showed no difference between Con, ST and SI motoneurones, the matching of SFA and muscle fatigue within motor units may be lost following ST and SI.

There is dissociation between the effect of SI on motoneurones and muscle fiber type. Following SI, muscle fiber types are severely atrophied and converted to mainly express type 2 myosin heavy chains (Grossman et al. 1998; Harris et al. 2007). It has been reported previously that muscle type can influence motoneurone type. For example cross-reinnervation of the MG nerve onto the soleus muscle for 9 – 11 months leads to motoneurone biophysical property changes such that MG motoneurones behave more like soleus motoneurones (Foehring et al. 1987).

Furthermore, chronic electrical stimulation of cat MG nerve for 2-3 months converts all muscles fibers to slow, with some of the innervating motoneurones changing their properties to those of motoneurones normally innervating soleus (Munson et al. 1997). In the present study, motoneurone properties following SI maintained heterogeneity and did not match the changes that are known to take place in muscle fiber type (motoneurones did not change to become more "fast"-like in properties). Unfortunately, the motoneurone properties reported here were after only 6-8 weeks of SI, which may not be enough time for changes in motoneurones to be significantly influenced by their target muscle – indeed, this time factor may explain the rather limited change in motoneurone properties that occurs following chronic muscle stimulation (Munson et al. 1997). Efferent innervation of muscle is left intact after SI enabling uptake of trophic substances by the motoneurone, which may be enough to maintain motoneurone properties. Furthermore, with the exception of motoneurone size, dorsal rhizotomy only has minimal effects on motoneurone properties (Kuno et al. 1974; Gustafsson et al. 1982). Therefore, the current results do not support a significant effect of muscle-derived substances on motoneurone properties following spinal cord transection.

In conclusion, we show that following six to eight weeks of chronic ST or chronic SI, motoneurone Rin, rheobase current, spike AHP amplitude, and bistability tend to become like those observed in more excitable motoneurones. ST and SI motoneurones also have decreased f-I slopes and minimum firing frequencies but retain ability to discharge for short and long durations in response to an electrical input. Even though SI and ST motoneurones have a greater tendency to be bistable,

overall PIC amplitude is not greater than Con motoneurones, maybe owing to increased monoaminergic receptor sensitivity. Although the SI procedure is one of the most "severe" experimental models of spinal cord injury, the range of values for basic and active motoneurone properties indicate that the heterogeneity among motoneurones is relatively maintained. Finally, unlike muscle, it appears that the development of spasticity is not required (for at least up to 6 – 8 weeks) to maintain motoneurone biophysical properties.

REFERENCES

Alaimo MA, Smith JL, Roy RR & Edgerton VR (1984). EMG activity of slow and fast ankle extensors following spinal cord transection. J Appl Physiol **56**, 1608-13.

Beaumont E, Houle JD, Peterson CA & Gardiner PF (2004). Passive exercise and fetal spinal cord transplant both help to restore motoneuronal properties after spinal cord transection in rats. Muscle Nerve **29**, 234-42.

Bennett DJ, Li Y, Harvey PJ & Gorassini M (2001a). Evidence for plateau potentials in tail motoneurons of awake chronic spinal rats with spasticity. J Neurophysiol **86**, 1972-82.

Bennett DJ, Li Y & Siu M (2001b). Plateau potentials in sacrocaudal motoneurons of chronic spinal rats, recorded in vitro. J Neurophysiol **86**, 1955-71.

Bose P, Parmer R, Reier PJ & Thompson FJ (2005). Morphological changes of the soleus motoneuron pool in chronic midthoracic contused rats. Exp Neurol **191**, 13-23.

Button DC, Gardiner K, Marqueste T & Gardiner PF (2006b). Frequency-current relationships of rat hindlimb {alpha}-motoneurones. J Physiol **573**, 663-77.

Button DC, Gardiner K, Zhong H, Roy RR, Egerton VR & Gardiner PF (2005). In situ frequency-current (f-I) relationships of hindlimb α-motoneurons (α-Mns) in spinal cord transected (ST) and spinal cord isolated (SI) rats. Canadian Journal of Applied Physiology **30**, S15.

Button DC, Gardiner KR, Cahill F, Marqueste T, Zhong H, Roy RR, Egerton VR & Gardiner PF (2006a). The effects of spinal cord isolation (SI) on rat hindlimb α-motoneurone (α-Mns) electrophysiological properties. The FASEB Journal, **20**, A1415-c.

Button DC, Kalmar JM, Gardiner K, Cahill F & Gardiner P (2007). Spike frequency adaptation of rat hindlimb motoneurones. J Appl Physiol **102**, 1041-50.

Button DC, Kalmar KM, Gardiner K, Cahill F, Zhong H, Roy RR, Egerton VR & Gardiner PF (2006c). Do spinal cord isolation and spinal cord transection

differentially influence rat hindlimb alpha-motoneurone properties?. Applied Physiology, Nutrition, and Metabolism
31, S15.

Chalmers GR, Roy RR & Edgerton VR (1992). Adaptability of the oxidative capacity of motoneurons. Brain Res **570**, 1-10.

Cope TC, Bodine SC, Fournier M & Edgerton VR (1986). Soleus motor units in chronic spinal transected cats: physiological and morphological alterations. J Neurophysiol **55**, 1202-20.

Cormery B, Beaumont E, Csukly K & Gardiner P (2005). Hindlimb unweighting for 2 weeks alters physiological properties of rat hindlimb motoneurones. J Physiol **568**, 841-50.

Czeh G, Gallego R, Kudo N & Kuno M (1978). Evidence for the maintenance of motoneurone properties by msucel activity. J Physiol **281**, 239-52.

Foehring RC, Sypert GW & Munson JB (1987). Motor-unit properties following cross-reinnervation of cat lateral gastrocnemius and soleus muscles with medial gastrocnemius nerve. I. Influence of motoneurons on muscle. J Neurophysiol **57**, 1210-26.

Gardiner PF (1993). Physiological properties of motoneurons innervating different muscle unit types in rat gastrocnemius. J Neurophysiol **69**, 1160-70.

Gazula VR, Roberts M, Luzzio C, Jawad AF & Kalb RG (2004). Effects of limb exercise after spinal cord injury on motor neuron dendrite structure. J Comp Neurol **476**, 130-45.

Gilmore J & Fedirchuk B (2004). The excitability of lumbar motoneurones in the neonatal rat is increased by a hyperpolarization of their voltage threshold for activation by descending serotonergic fibres. J Physiol **558**, 213-24.

Gomez-Pinilla F, Ying Z, Opazo P, Roy RR & Edgerton VR (2001). Differential regulation by exercise of BDNF and NT-3 in rat spinal cord and skeletal muscle. Eur J Neurosci **13**, 1078-84.

Gomez-Pinilla F, Ying Z, Roy RR, Hodgson J & Edgerton VR (2004). Afferent input modulates neurotrophins and synaptic plasticity in the spinal cord. J Neurophysiol **92**, 3423-32.

Gonzalez M & Collins WF 3rd (1997). Modulation of motoneuron excitability by brain-derived neurotrophic factor. *J Neurophysiol* **77**, 502-6.

Grossman EJ, Roy RR, Talmadge RJ, Zhong H & Edgerton VR (1998). Effects of inactivity on myosin heavy chain composition and size of rat soleus fibers. Muscle Nerve **21**, 375-89.

Guertin PA & Hounsgaard J (1999). Non-volatile general anaesthetics reduce spinal activity by suppressing plateau potentials. Neuroscience **88**, 353-8.

Gustafsson B, Katz R & Malmsten J (1982). Effects of chronic partial deafferentiation on the electrical properties of lumbar alpha-motoneurones in the cat. Brain Res **246**, 23-33.

Harris RL, Bobet J, Sanelli L & Bennett DJ (2006). Tail muscles become slow but fatigable in chronic sacral spinal rats with spasticity. *J Neurophysiol* **95**, 1124-33.

Harris RL, Putman CT, Rank M, Sanelli L & Bennett DJ (2007). Spastic tail muscles recover from myofiber atrophy and myosin heavy chain transformations in chronic spinal rats. J Neurophysiol **97**, 1040-51.

Harvey PJ, Li X, Li Y & Bennett DJ (2006a). 5-ht2 receptor activation facilitates a persistent sodium current and repetitive firing in spinal motoneurons of rats with and without chronic spinal cord injury. J Neurophysiol **96**, 1158-70.

Harvey PJ, Li X, Li Y & Bennett DJ (2006b). Endogenous monoamine receptor activation is essential for enabling persistent sodium currents and repetitive firing in rat spinal motoneurons. J Neurophysiol **96**, 1171-86.

Harvey PJ, Li Y, Li X & Bennett DJ (2006c). Persistent sodium currents and repetitive firing in motoneurons of the sacrocaudal spinal cord of adult rats. J Neurophysiol **96**, 1141-57.

Heckman CJ, Lee RH & Brownstone RM (2003). Hyperexcitable dendrites in motoneurons and their neuromodulatory control during motor behavior. Trends Neurosci **26**, 688-95.

Hochman S & McCrea DA (1994). Effects of chronic spinalization on ankle extensor motoneurons. II. Motoneuron electrical properties. J Neurophysiol **71**, 1468-79.

Hounsgaard J, Hultborn H, Jespersen B & Kiehn O (1988). Bistability of alpha-motoneurones in the decerebrate cat and in the acute spinal cat after intravenous 5-hydroxytryptophan. J Physiol **405**, 345-67.

Hounsgaard J & Kiehn O (1989). Serotonin-induced bistability of turtle motoneurones caused by a nifedipine-sensitive calcium plateau potential. J Physiol **414**, 265-82.

Hultborn H (1999). Plateau potentials and their role in regulating motoneuronal firing. Prog Brain Res **123**, 39-48.

Hultborn H, Brownstone RB, Toth TI & Gossard JP (2004). Key mechanisms for setting the input-output gain across the motoneuron pool. Prog Brain Res **143**, 77-95.

Hultborn H & Kiehn O (1992). Neuromodulation of vertebrate motor neuron membrane properties. Curr Opin Neurobiol **2**, 770-5.

Hyatt JP, Roy RR, Baldwin KM & Edgerton VR (2003). Nerve activity-independent regulation of skeletal muscle atrophy: role of MyoD and myogenin in satellite cells and myonuclei. Am J Physiol Cell Physiol **285**, C1161-73.

Ishihara A, Roy RR, Ohira Y & Edgerton VR (2002). Motoneuron and sensory neuron plasticity to varying neuromuscular activity levels. Exerc Sport Sci Rev **30**, 152-8.

Kernell D & Monster AW (1982). Motoneurone properties and motor fatigue. An intracellular study of gastrocnemius motoneurones of the cat. *Exp Brain Res* **46**, 197-204.

Kiehn O & Eken T (1998). Functional role of plateau potentials in vertebrate motor neurons. Curr Opin Neurobiol **8**, 746-52.

Kitzman P (2005). Alteration in axial motoneuronal morphology in the spinal cord injured spastic rat. Exp Neurol **192**, 100-8.

Kuno M, Miyata Y & Munoz-Martinez EJ (1974). Properties of fast and slow alpha motoneurones following motor reinnervation. J Physiol **242**, 273-88.

Lee RH & Heckman CJ (1998a). Bistability in spinal motoneurons in vivo: systematic variations in persistent inward currents. J Neurophysiol **80**, 583-93.

Lee RH & Heckman CJ (1998b). Bistability in spinal motoneurons in vivo: systematic variations in rhythmic firing patterns. J Neurophysiol **80**, 572-82.

Lee RH & Heckman CJ (1999). Paradoxical effect of QX-314 on persistent inward currents and bistable behavior in spinal motoneurons in vivo. J Neurophysiol **82**, 2518-27.

Lesser SS, Sherwood NT & Lo DC (1997). Neurotrophins differentially regulate voltage-gated ion channels. Mol Cell Neurosci **10**, 173-83.

Li X, Murray K, Harvey PJ, Ballou EW & Bennett DJ (2007). Serotonin facilitates a persistent calcium current in motoneurons of rats with and without chronic spinal cord injury. J Neurophysiol **97**, 1236-46.

Li Y & Bennett DJ (2003). Persistent sodium and calcium currents cause plateau potentials in motoneurons of chronic spinal rats . J Neurophysiol **90**, 857-69.

Li Y, Gorassini MA & Bennett DJ (2004). Role of persistent sodium and calcium currents in motoneuron firing and spasticity in chronic spinal rats. J Neurophysiol **91**, 767-83.

Mitsumoto H & Tsuzaka K (1999). Neurotrophic factors and neuro-muscular disease: II. GDNF, other neurotrophic factors, and future directions. Muscle Nerve **22**, 1000-21.

Munson JB, Foehring RC, Mendell LM & Gordon T (1997). Fast-to-slow conversion following chronic low-frequency activation of medial gastrocnemius muscle in cats. II. Motoneuron properties. J Neurophysiol **77**, 2605-15.

Perrier JF, Alaburda A & Hounsgaard J (2003). 5-HT1A receptors increase excitability of spinal motoneurons by inhibiting a TASK-1-like K+ current in the adult turtle. *J Physiol* **548**, 485-92.

Petruska JC, Ichiyama RM, Jindrich DL, Crown ED, Tansey KE, Roy R, Edgerton VR & Mendell LM (2007). Changes in motoneuron properties and synaptic inputs related to step training after spinal cord transection in rats. J Neurosci **27**, 4460-71.

Pierotti DJ, Roy RR, Bodine-Fowler SC, Hodgson JA & Edgerton VR (1991). Mechanical and morphological properties of chronically inactive cat tibialis anterior motor units. J Physiol **444**, 175-92.

Powers RK & Binder MD (2001). Input-output functions of mammalian motoneurons. Rev Physiol Biochem Pharmacol **143**, 137-263.

Rank MM, Li X, Bennett DJ & Gorassini MA (2007). Role of endogenous release of norepinephrine in muscle spasms after chronic spinal cord injury. J Neurophysiol **97**, 3166-80.

Rose CR, Blum R, Kafitz KW, Kovalchuk Y & Konnerth A (2004). From modulator to mediator: rapid effects of BDNF on ion channels. Bioessays **26**, 1185-94.

Roy RR, Hodgson JA, Lauretz SD, Pierotti DJ, Gayek RJ & Edgerton VR (1992). Chronic spinal cord-injured cats: surgical procedures and management. Lab Anim Sci **42**, 335-43.

Roy RR, Matsumoto A, Zhong H, Ishihara A & Edgerton VR (2007a). Rat alpha- and gamma motoneuron soma size and succinate dehydrogenase activity are independent of neuromuscular activity level. Muscle Nerve March 22, 2007; 10.1002/mus.20810.

Roy RR, Zhong H, Khalili N, Kim SJ, Higuchi N, Monti RJ, Grossman E, Hodgson JA & Edgerton VR (2007b). Is spinal cord isolation a good model of muscle disuse? Muscle Nerve **35**, 312-21.

Roy RR, Zhong H, Monti RJ, Vallance KA & Edgerton VR (2002). Mechanical properties of the electrically silent adult rat soleus muscle. Muscle Nerve **26**, 404-12.

Sawczuk A, Powers RK & Binder MD (1995). Spike frequency adaptation studied in hypoglossal motoneurons of the rat. J Neurophysiol **73**, 1799-810.

Spielmann JM, Laouris Y, Nordstrom MA, Robinson GA, Reinking RM & Stuart DG (1993). Adaptation of cat motoneurons to sustained and intermittent extracellular

activation. *J Physiol* **464**, 75-120.

Talmadge RJ, Roy RR, Caiozzo VJ & Edgerton VR (2002). Mechanical properties of rat soleus after long-term spinal cord transection. J Appl Physiol **93**, 1487-97.

Zengel JE, Reid SA, Sypert GW & Munson JB (1985). Membrane electrical properties and prediction of motor-unit type of medial gastrocnemius motoneurons in the cat. J Neurophysiol **53**, 1323-44.

ACKNOWLEDGEMENTS

This research was supported by grants from NSERC, CIHR, the Canada Research Chairs program, and NIH (NS 16333). Financial support for DB, JK and TM was provided by NSERC PGSB and Manitoba Health Research Council (MHRC), NSERC PDF, and MHRC PDF, respectively. The authors would like to thank Farrell Cahill, Gilles Detillieux and Matt Ellis at University of Manitoba for technical assistance.

TABLES

Motoneurone Property	Con	Spinal Cord Transected	Spinal Cord Isolated	P value
Basic Properties				
1. Resting membrane potential (mV)	–66.4 ± 9.3 (60)	–66.9 ± 8.1 (47)	–68.0 ± 7.3 (43)	0.61
2. voltage threshold (mV)	–48.0 ± 8.5 (60)	–49.7 ± 8.3 (47)	–50.6 ± 9.0 (44)	0.31
3. Rheobase Current (nA)	9.6 ± 4.4 (59)	7.3 ± 4.0 (47)	7.0 ± 4.3 (44)	***< 0.01** ***< 0.02**
4. Input resistance (MΩ)	1.9 ± 1.1 (56)	2.3 ± 1.4 (47)	2.7 ± 1.9 (43)	***< 0.05** 0.32
5. AHP amplitude(mV)	1.6 ± 1.5 (60)	2.6 ± 1.5 (47)	2.5 ± 1.7 (44)	***< 0.05** ****< 0.01**
6. AHP ½ decay time (ms)	14.8 ± 5.4 (60)	14.4 ± 3.9 (47)	14.9 ± 5.0 (44)	0.88
7. Spike height (mV)	73.2 ± 12.7 (53)	74.5 ± 17.1 (41)	74.6 ± 15.3 (40)	0.88
f-I Relationship				
8. Estimated PIC (nA)	0.49 ± 0.4 (44)	0.53 ± 0.4 (40)	0.55 ± 0.3 (30)	0.83
9. SSFF Min Current (nA)	11.3 ± 3.8 (37)	9.8 ± 5.2 (26)	9.3 ± 4.4 (31)	0.13
10. SSFF Max Current (nA)	20.6 ± 5.9 (37)	24.4 ± 10.7 (26)	20.9 ± 10.7 (31)	0.3
11. SSFF (Min) (Hz)	34.8 ± 11.1 (37)	25.7 ± 6.3 (26)	28.1 ± 10.4 (31)	***< 0.001** ****< 0.001**
12. SSFF (Max) (Hz)	104.3 ± 35.0 (37)	84.2 ± 31.2 (26)	78.8 ± 40.3 (31)	***< 0.01** 0.21
13. SSFF f-I slope (Hz/nA)	6.5 ± 2.4 (37)	5.0 ± 1.8 (26)	5.1 ± 2.5 (31)	***< 0.02** ****< 0.02**
Spike Frequency daptation				
14. SFA 5-s bincount Ratio [1 – (bin5/bin 1)]	0.69 ± 0.11 (21)	0.63 ± 0.14 (14)	0.68 ± 0.09 (14)	0.5

Table 1: A summary of basic (numbers 1-7) and active (numbers 8-14) motoneurone properties for Con, ST, and SI groups. Throughout the table, values are presented as means $\pm$ SD with the number of motoneurones (N) recorded from. Afterhyperpolarization (AHP), persistent inward current (PIC), steady state firing frequency (SSFF), firing frequency (FF), spike frequency adaptation (SFA). Number 8 only includes PICs of f-I relationship types 3 and 4. * and ** denotes a significant difference between Con *vs.* SI and Con *vs.* ST, respectively. A Tukey post hoc analysis was used where a significant main effect ($p < 0.05$) was present. There were no significant differences between ST *vs.* SI for any measure.

FIGURES

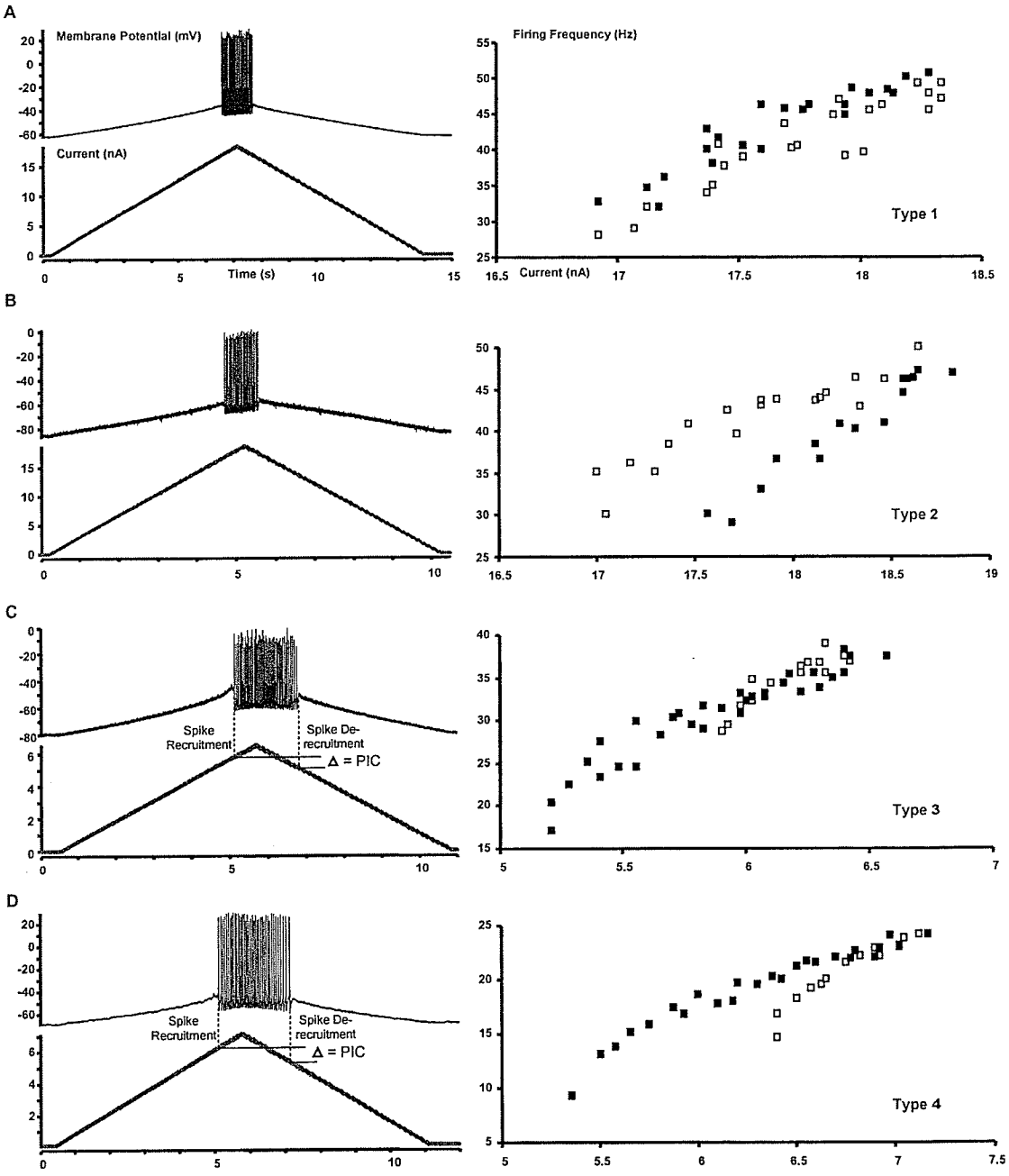

Figure 1. F-I relationships for Con, ST and SI motoneurones were determined by using 5-second up-down ramp injections. The left portion of A, B, C, and D illustrate the rhythmic discharge of the motoneurone in response to a ramp current (bottom trace). In C and D the dashed lines indicate the

current at spike recruitment and spike de-recruitment. Estimated PIC was calculated by subtracting the current at spike de-recruitment from the current at spike recruitment. The right portion of A, B, C, and D is the plotted f-I relationship which show a plot of the instantaneous firing frequency and current from traces on the left. White and black squares represent up and down phases of the ramp, respectively. **A)** type 1 motoneurone f-I relationship demonstrated a firing frequency slope that overlaps. **B)** type 2 motoneurone f-I relationship demonstrated a clockwise-hysteresis. **C)** type 3 motoneurone f-I relationship demonstrated a linear regression line with some self-sustained firing. **D)** type 4 (bottom) motoneurone f-I relationship demonstrated a counter-clockwise hysteresis. Ramp data shown here were recorded from 4 different Con motoneurones.

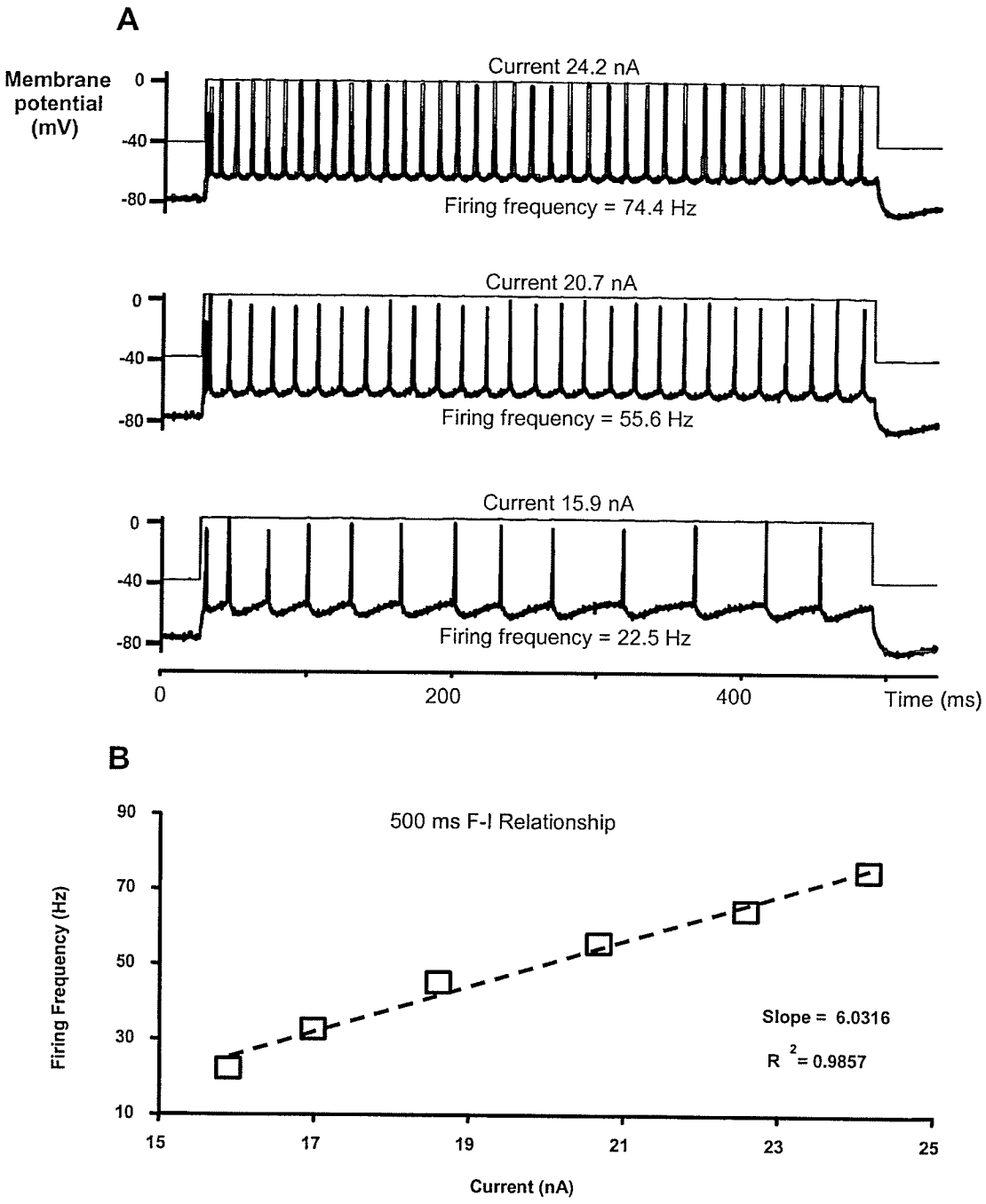

Figure 2. motoneurones from Con, ST and SI groups were capable of discharging rhythmically when injected with sustained 500 ms current pulses. **A)** For each motoneurone the intensity of the 500 ms current pulses was gradually increased until steady-state firing occurred, and was increased further in approximately 1-5 nA steps

until blocking began to take place. At that time, current was decreased by approximately the same current steps until the cell stopped firing. Not all 500 ms current pulses are shown. **B)** The f-I relationship plotted from the 500 ms current pulses in **A** was used to determine the minimum and maximum SSFFs (mean of last 3 intervals during 500 ms of current injection), current required to evoke SSFFs and slope. Each data point represents the SSFF and current intensity for each 500 ms current pulse injected into the motoneurone.

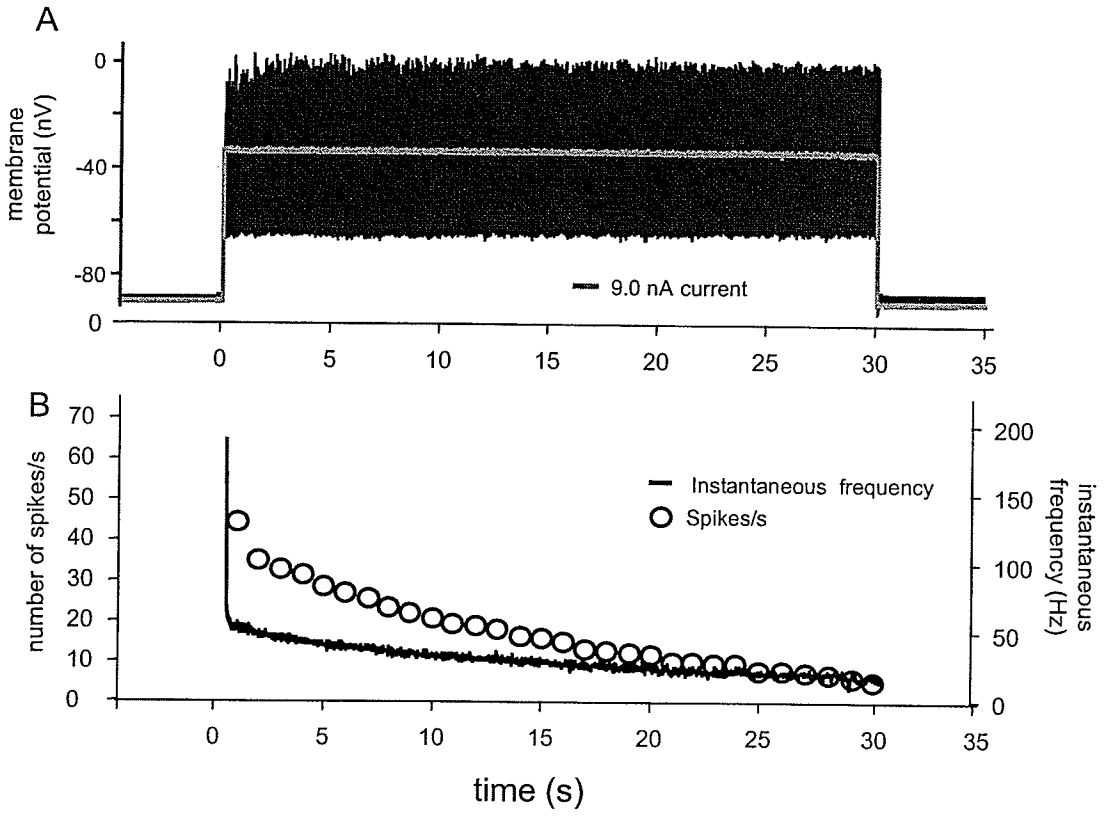

Figure 3. Control, ST and SI motoneurones were subjected to a 30-s sustained supra-threshold current injection to determine their SFA pattern. **A)** shows current injected and spikes (voltage measured in DCC mode). **B)** shows the instantaneous firing frequency rate (black line, right axis) and the normalized number of spikes discharged per second (left axis). The 1-s bins were normalized such that the final bin in the 30-s period of spike discharge always contained 5 spikes.

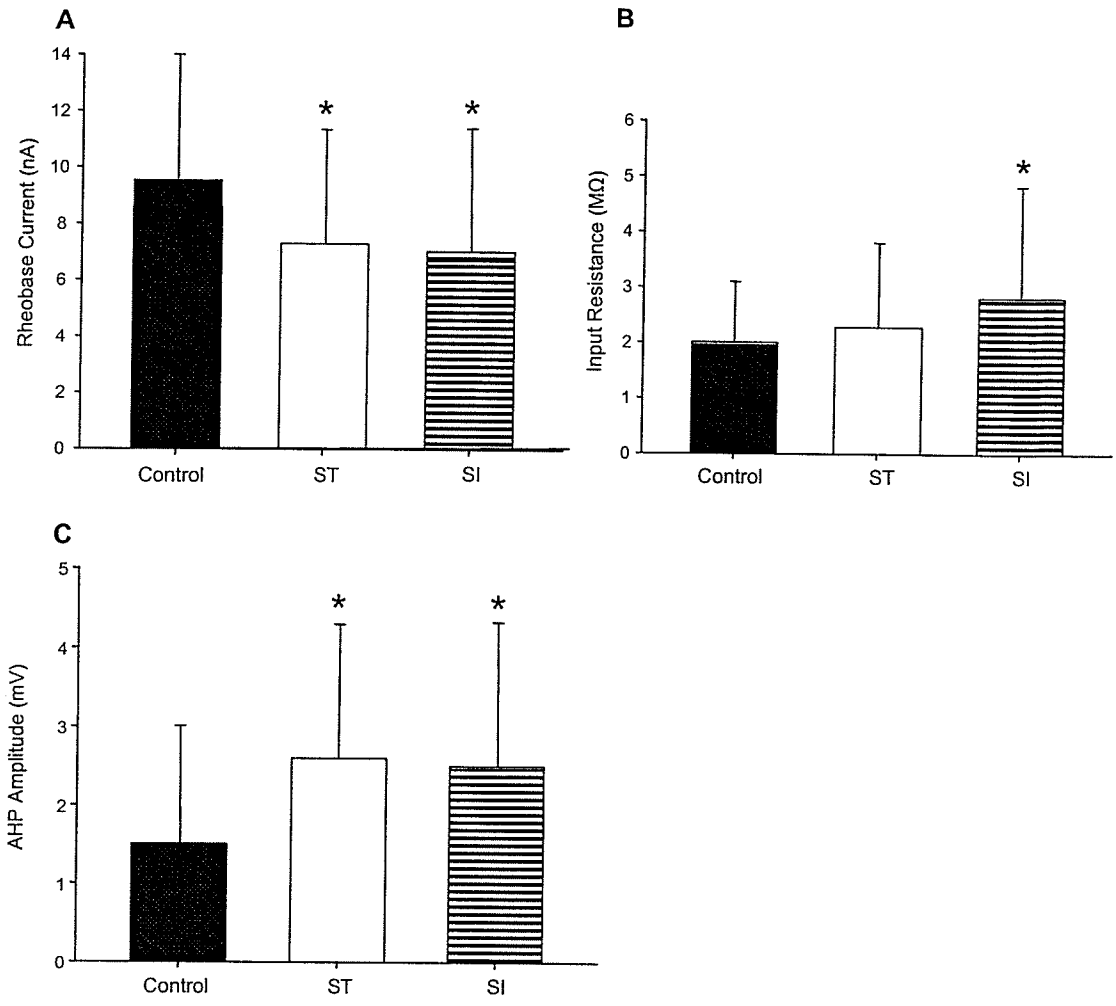

Figure 4. Following SI, motoneurone basic properties become like those typically seen in slow motoneurones. Motoneurone basic properties from Con, ST, and SI groups are displayed as means ± SD. Overall, SI motoneurones have significantly lower **A)** rheobase currents and significantly higher **B)** R_{in}s, and **C)** AHP amplitudes compared to Con. ST motoneurones have significantly lower rheobase currents, a trend to have higher mean R_{in}s than Con and have significantly higher motoneurone AHP amplitudes than Con. There were no significant differences between ST and SI for any of the three motoneurone properties. * denotes a significant difference from Con.

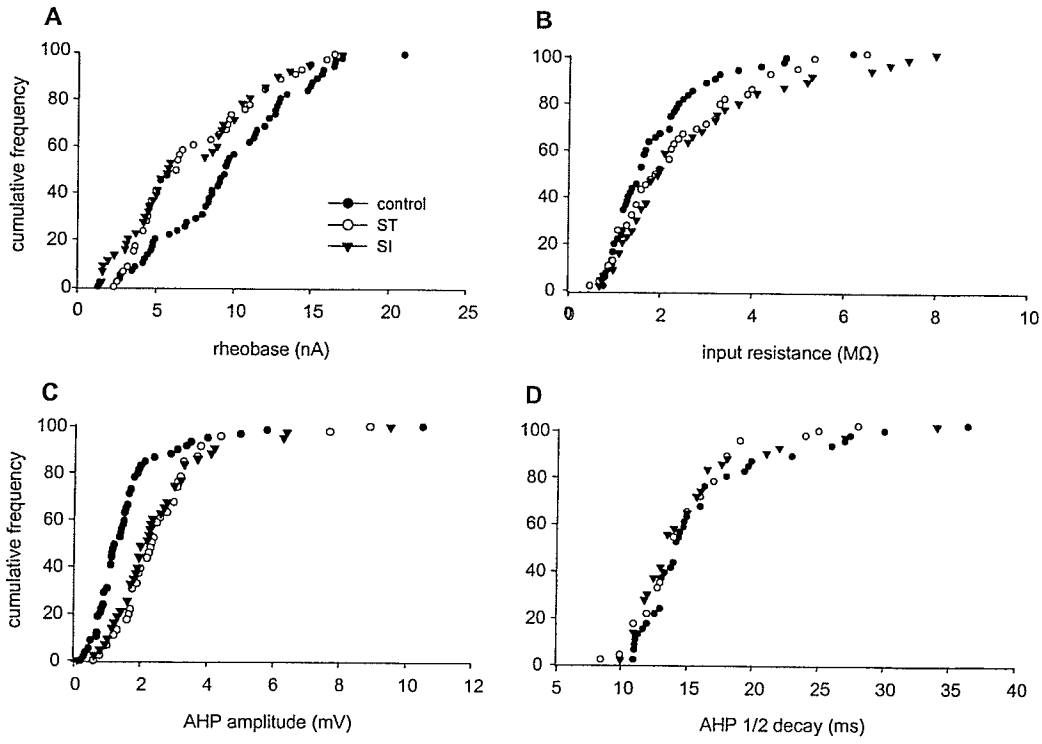

Figure 5. Although mean values for SI motoneurone basic properties become like those typically seen in slow motoneurones they still retain a range of values which indicate that heterogeneity is maintained (Fig. 1). Motoneurone basic properties from Con, ST, and SI groups are displayed as distributions and represent data of individual motoneurones from all experiments, whereas statistical comparisons in the Results were derived from means calculated for each group of motoneurones (Table 1). Shown is the range of values recorded from Con, ST, and SI motoneurones for **A)** rheobase current, **B)** R_{in}, **C)** AHP amplitude and **D)** AHP duration. Following ST and SI, motoneurone rheobase current, R_{in}, and AHP amplitude were similar to Con motoneurones at the low and high values but the values between these were shifted to the left for rheobase and shifted to the right for R_{in} and AHP amplitudes.

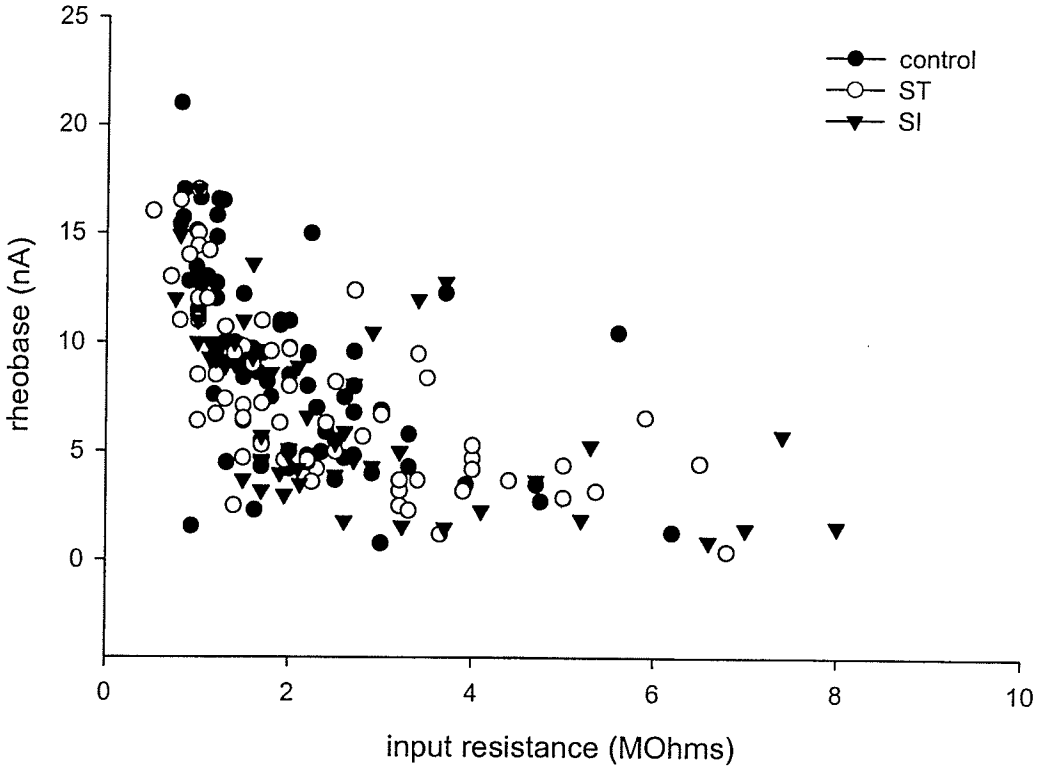

Figure 6. When motoneurone rheobase current is plotted against R_{in}, Con, ST and SI motoneurone group values overlap considerably. Motoneurone values are paired as rheobase current and R_{in} from individual motoneurones for Con, ST, and SI groups. Correlation coefficients for the Con, ST, and SI groups were all significant and very similar (see Results).

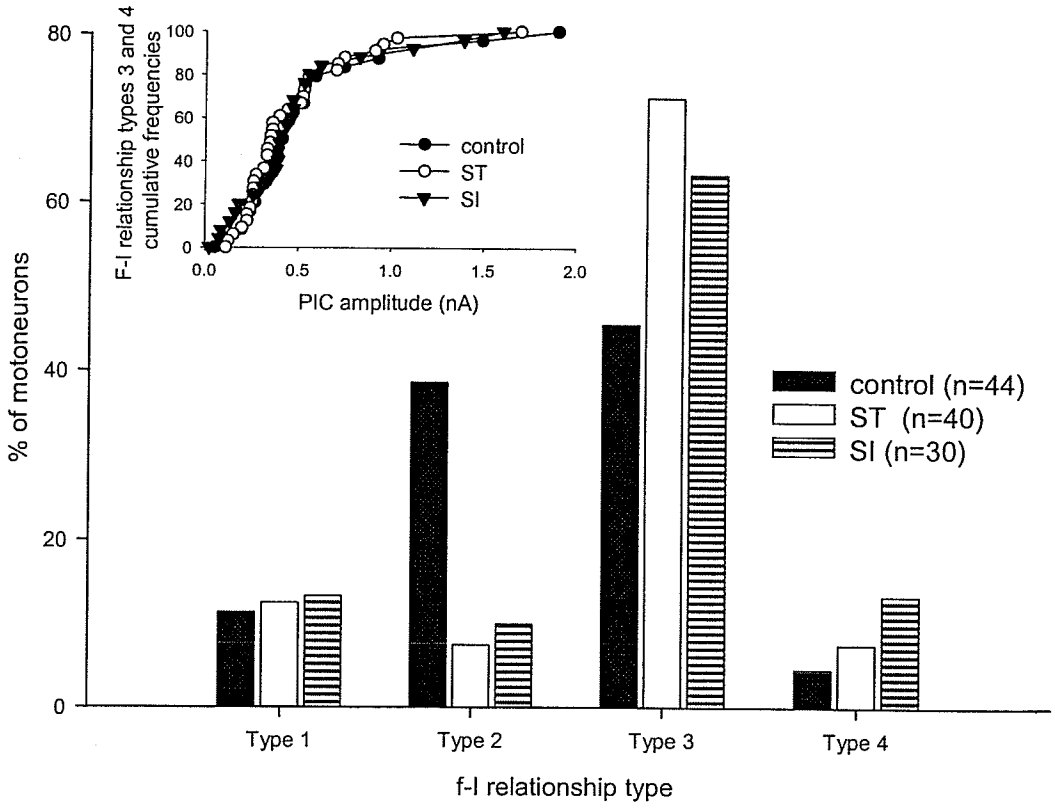

Figure 7. Con, ST and SI motoneurones have very similar PIC amplitudes, but their f-I relationship type distribution differ in that ST and SI groups have an increased number of motoneurones that demonstrate PIC. Four distinct types of f-I relationships are present in Con, ST and SI: 1) type 1 overlapping, 2) type 2 adapting, 3) type 3 linear plus sustained, and 4) type 4 acceleration (see Fig. 1). A greater percentage of motoneurones from ST and SI than Con rats are categorized as f-I relationship types 3 and 4 (activation of PIC) and a smaller percentage as type 2 (no activation of PIC). Chi-square analysis, $X^2 = 16.6$, revealed a significant difference ($p < 0.01$) in the distribution of the f-I relationships among the motoneurone groups. The inset shows the distributions of motoneurone PIC amplitudes for each group that

were calculated from only f-I relationship types 3 and 4. Note that the range of values and the mean (Table 1) was very similar for each group.

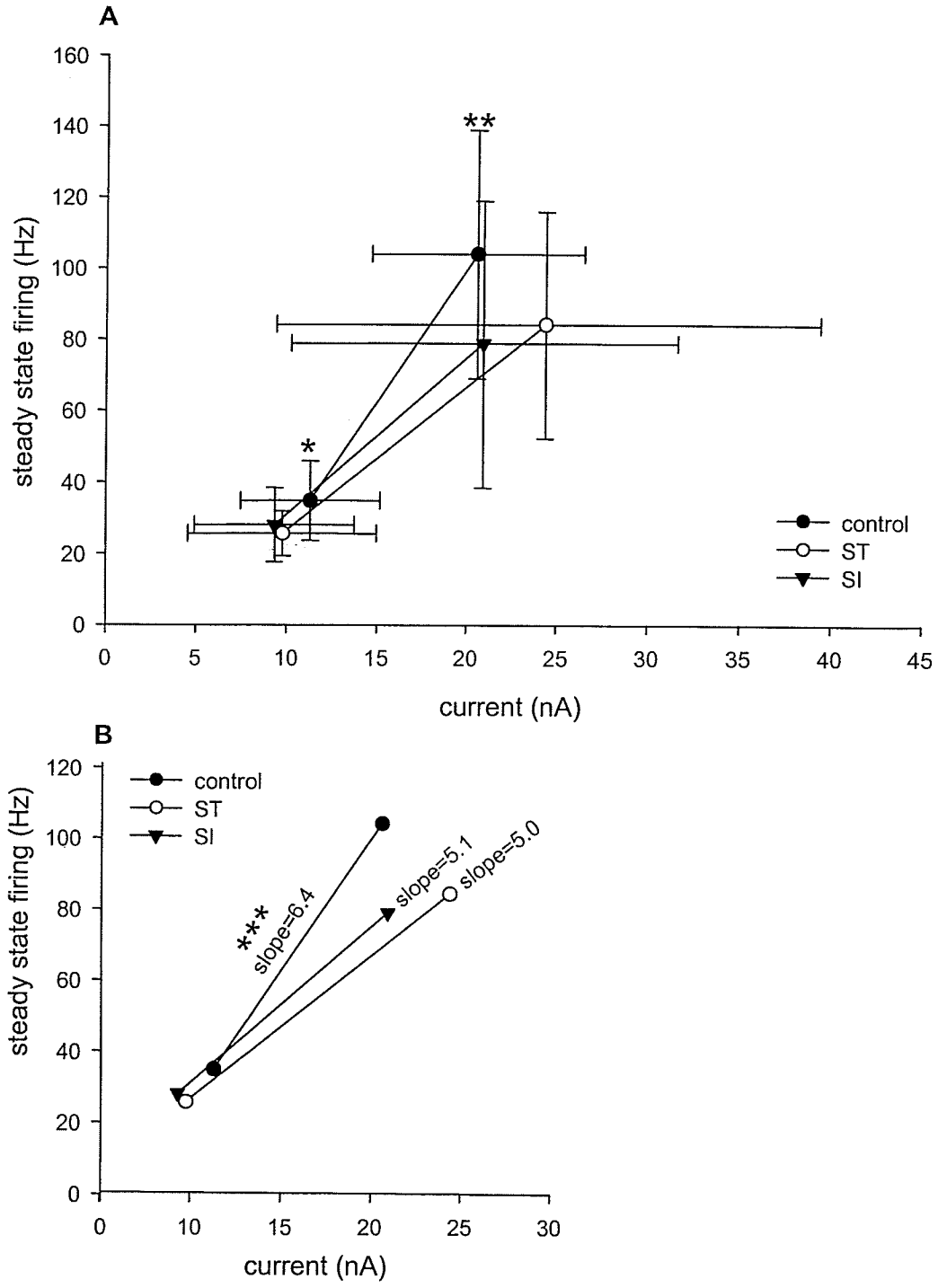

Figure 8. Motoneurone 500-ms steady state firing frequencies, currents, and f-I slopes are decreased after ST and SI, indicating decreased motoneurone input-output

gain. **A)** motoneurones from ST and SI rats require less current to induce lower SSFF Min and have lower firing frequencies at similar SSFF Max currents than motoneurones from Con rats. Data are presented as means ± SD (see Table 1). * denotes a significant difference for motoneurone SSFF Min between Con and ST and SI groups. ** denotes a significant difference for motoneurone SSFF Max between Con and SI groups. **B)** Compared to the Con group, there is a reduction or a shift to the right in the f-I slopes of motoneurones in the ST and SI groups. The slopes values in text are the mean of the slopes derived using linear regression from all points on the f-I curve as shown in Figure 2B (not just the minimum and maximum values plotted above). Slope values are presented as means (see Table 1). *** denotes a significant difference for motoneurone f-I slope between Con and SI and ST groups.

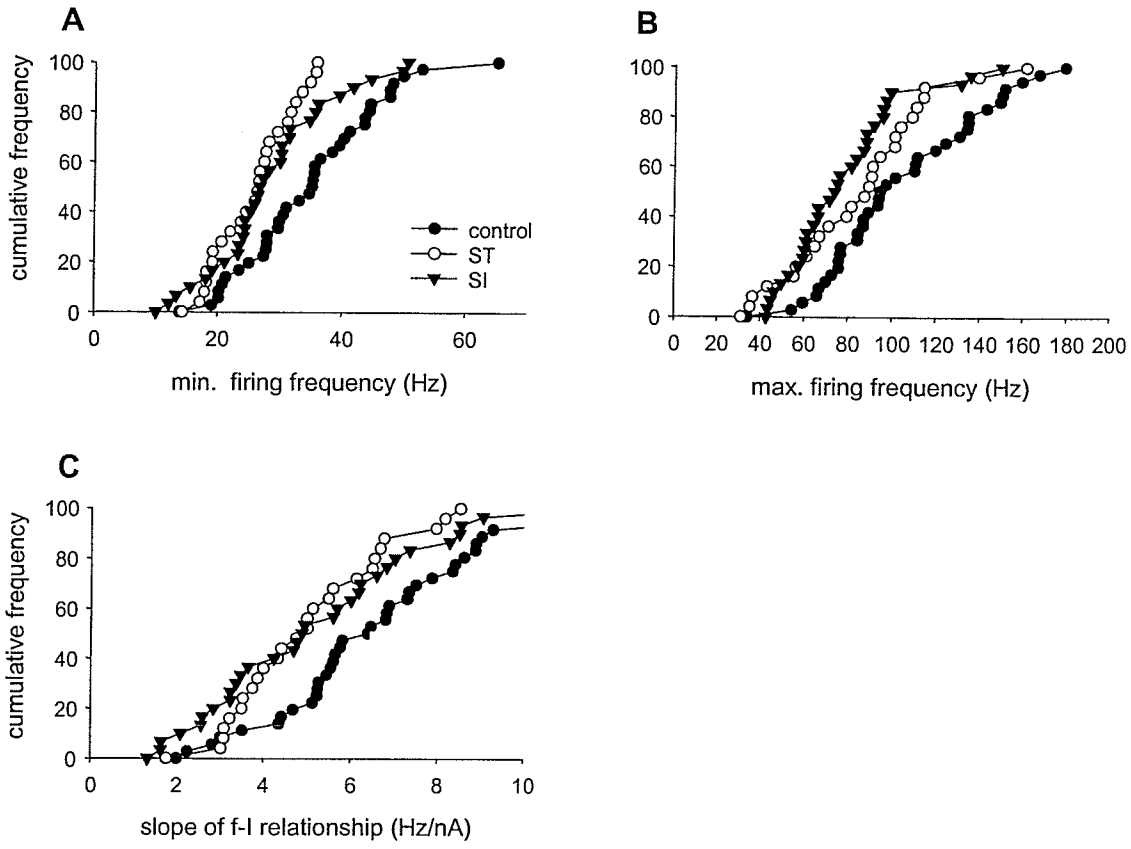

Figure 9. Following ST and SI, the range of values for motoneurone 500 ms f-I relationship properties are substantially decreased compared to Con. Motoneurone 500 ms f-I relationship properties from Con, ST, and SI groups are displayed as distributions and represent data of individual motoneurones from all experiments, whereas statistical comparisons in the Results were derived from means calculated for each group of motoneurones (Fig. 5, Table 1). Shown is the range of values recorded from Con, ST, and SI motoneurones for **A)** SSFF Min, **B)** SSFF Max and **C)** SSFF slopes. Following ST and SI, motoneurone SSFF Min, SSFF Max and SSFF slopes were similar to Con motoneurones at the low values but the values above these were

shifted to the left. However, ST and SI motoneurones still retain a range of values which indicate that heterogeneity is maintained.

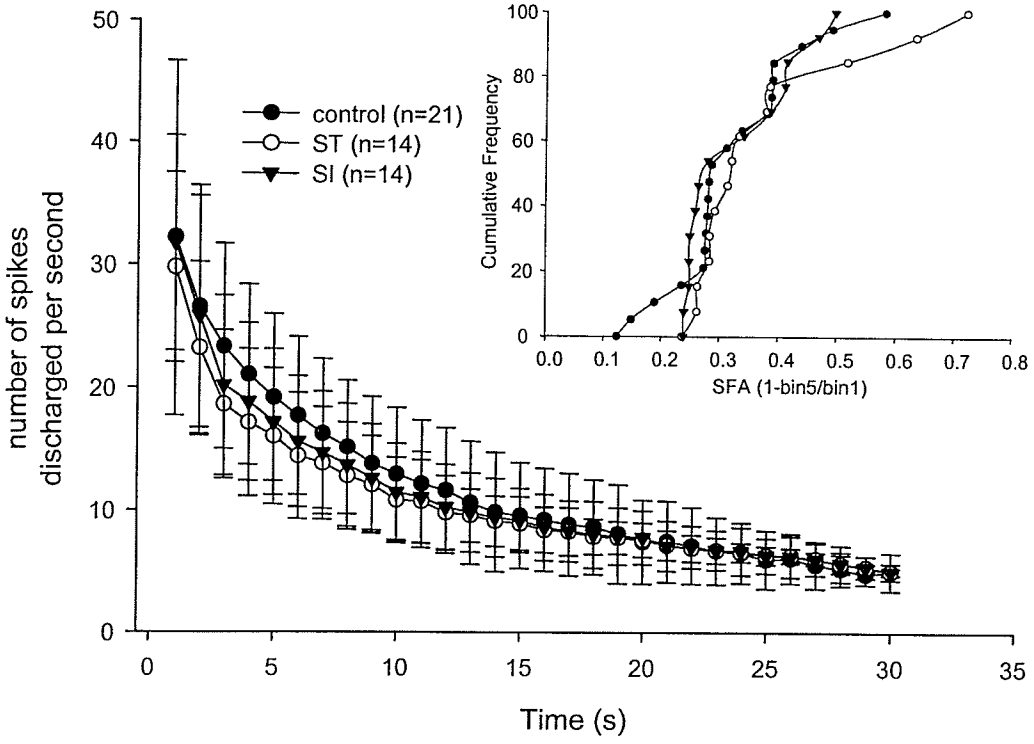

Figure 10. The pattern of motoneurone spike frequency adaptation is similar for Con, ST and SI motoneurones. Motoneurones from Con, ST and SI rats have a similar rate of decrease in the number of spikes (placed in one second bins) throughout 30-s of rhythmic discharge (see Fig. 3). Data are presented as means $\pm$ SD. The inset shows the distributions of the SFA index (1-bin5/bin1) that we developed and previously published as a simple and reliable way to measure motoneurone SFA (see Methods). The range of values was very similar for each group. Furthermore, the mean SFA indexes was similar among Con, ST, and SI motoneurones (see Table 1).

CHAPTER 5: GENERAL DISCUSSION

This thesis describes investigations on how adult rat MN biophysical properties change following ST and SI. The discussion will focus on; 1) the usefulness of the adult rat model for understanding MN electrophysiology, 2) the main findings of the three papers comprising this thesis and 3) limitations of the studies and future directions. For additional discussion the reader is referred to each relevant paper.

Section 1: The use of the *in vivo* rat model for understanding motoneurone biophysical properties. Until recently the in vivo cat preparation has been the dominant model for the purpose of recording hindlimb MN biophysical properties. Lately, laboratories are making use of the rat in vivo model for the same purposes. Each model has demonstrated that hindlimb MNs can be categorized based on innervated muscle fiber type and also be divided on the basis of different passive and action potential properties (Burke et al. 1982; Zengel et al. 1985; Gardiner 1993; Gustafsson & Pinter 1984b; Gustafsson & Pinter 1984a). However, the literature identifying differences among rat MNs is sparser, especially for rhythmic properties such as f-I relationships used to determine PIC and SFA, and is not as clear cut as in the cat. For example, relationships among MN properties indicative of cell size and excitability are much weaker in rat compared to cat and unlike rat, cat FF and FR MN properties can be distinguished (Zengel et al. 1985; Gardiner 1993).

In relation to activity-dependent (exercise, sedentary, injury) MN plasticity the rat model is very interesting. Generally, rats are highly exploratory even when they are caged. When rats are housed in voluntary wheel cages they run up to 16 km

in a 12 hour period (an observation in our laboratory). On the other hand cats spend much of their time resting and are more sedentary (Dards 1983). Rats are also more cost efficient than cats. Thus, the in vivo rat model is more practical to determine if and how MNs are altered by different types of increased or decreased neuromuscular activity. Rat MNs and muscles do indeed undergo significant changes following chronic-activity and –inactivity (Gardiner 2006; Gardiner et al. 2006; Gardiner et al. 2005; Gharakhanlou et al. 1999; Talmadge et al. 2002; Roy et al. 2002; Desaulniers et al. 2001). The rat model has also furthered our understanding of the mechanisms involved in the development of spasticity following ST (Li et al. 2004).

Our laboratory is very interested in the effects of activity on MNs. However, some aspects of rat hindlimb MN biophysical properties remained unknown. This thesis was developed to expand our knowledge on rat MN biophysical properties with the main focus being on rhythmicity and to determine whether or not these properties change following chronic spinal cord injury (ST vs. SI).

Section 2: Rat hindlimb motoneurone biophysical properties. There is very little literature reporting the repetitive firing properties of rat hindlimb MNs. Since MNs function in trains of action potentials as opposed to a single action potential we focused on recording f-I relationships to determine MN PIC amplitude, f-I gain, SFA, minimum and maximum firing frequencies, the current amplitudes used to induce the minimum and maximum firing frequencies, and whether or not any of these properties covary with MN single action potential properties and Rin. Furthermore we investigated the effects of anaesthetic, decerebration and chronic inactivity on these MN properties.

F-I relationships induced by ramp current injections. The main purpose of the first study (Button et al. 2006) was to describe f-I relationships evoked by ramps, of hindlimb MNs from rats in two separate physiological states; 1) anaesthetized (i.e "sleeping state") and 2) decerebrated (i.e. non-anaesthetized "awake state"). There were several key findings. First, ramp current injections into rat hindlimb MNs activated PICs and produced f-I relationships comparable to sacral-caudal MNs in vitro (Bennett et al. 2001) and cat hindlimb MNs in vivo (Hounsgaard et al. 1988). The corresponding f-I relationships of rat hindlimb MNs were categorized into 4 types as previously described (Bennett et al. 2001). What is strikingly different amongst rat sacro-caudal and hindlimb MNs is the f-I slope. Hindlimb MN f-I slopes measured during ramps are approximately double than that of rat sacro-caudal MNs (Button et al. 2006; Bennett et al. 2001). This may be due to sacro-caudal MNs being more excitable (higher Rin and lower rheobase), having greater AHP amplitudes and durations (Bennett et al. 2001; Button et al. 2006) and innervating a smaller muscle mass with different functions compared to hindlimb MNs. On the other hand rat and cat hindlimb MNs have similar ramp-induced f-I slopes (Lee & Heckman 1998b; Button et al. 2006). Although there is variability amongst the ramp-induced f-I relationship properties due to preparation type such as different animal species, anaesthetics, decerebration, in vitro or exposure to PIC enhancers like methoxamine (Lee & Heckman 1998b), and 5-HT (Hounsgaard et al. 1988) the PIC can be activated, subsequently altering firing frequency. Thus, PIC is an inherently important factor that contributes to MN firing frequencies. The persistent Na^{+} and L-type Ca^{++} channels responsible for this property are conveniently located on the soma

and proximal dendrites (Simon et al. 2003; Moritz et al. 2007; Crill 1996) for easy access for modulation. Functionally, these non-inactivating or slowly inactivating inward currents act to increase the gain of the f-I relationship and render the MN more excitable by generating depolarized states known as plateau potentials which reduce the need for steady on-going synaptic drive during muscular contraction.

Secondly, MN PIC amplitude did not differ between rats subjected to an anaesthetic mixture of ketamine/xylazine or a decerebration. This finding was novel since PICs and plateau potentials were not evident in previous experiments which animals were anaesthetized with barbiturates (Guertin & Hounsgaard 1999). Part of our experimental approach included the addition of barbiturate pentobaritoine to a rat anaesthetized with a ketamin/xylazine anaesthetic mixture. Following pentobarbitione application MN type 3 f-I relationship (i.e. PIC) was diminished to type 1 f-I relationship. Thus, we reconfirmed that barbiturates do indeed diminish or block PIC. The goal of using an anesthetized versus a decerebrate preparation was to investigate more functionally relevant motoneurone behaviours, although a decerebrated animal is not fully intact. The decerebrate preparation maintains tonic activity from brainstem projections, allowing the influence of neuromodulators such as serotonin and noradrenaline on MN properties. These intact projections permit the expression of PICs which facilitate MN bistability and subsequently alters MN rhythmic firing behaviour in response to injected currents. However, the MN PICs seen in both our preparations tended to be smaller than those seen in cats. Since the PICs were not smaller in decerebrate MNs, it is possible that our decerebrate preparation may have cut off some of the blood supply to the monoaminergic

brainstem regions which are important for activating PICs. Furthermore, ketamine may have decreased monoaminergic drive but not as much too completely inhibit MN PICs. During ramp current injections, decerebrated MN action potentials had depolarized voltage thresholds and greater AHP amplitudes and durations, but yet similar PIC amplitude and f-I slopes compared to anaesthetized MNs. Since AHP duration and amplitude help to determine f-I slope, one would expect that the f-I slope would be lower in decerebrated MNs compared to ketamine/xzlazine MNs. Nonetheless the use of a ketamine/xylazine anaesthetic mixture may partially disrupt the important brainstem projections, still allowing for PIC activation as compared to those seen in the decerebrate preparation.

Finally, PIC amplitude was not hindlimb MN type (slow, AHP > 20 ms vs. fast AHP < 20 ms) dependent. This was further confirmed by a lack of covariance between PIC amplitude and MN excitability properties rheobase current and Rin, which are both indicative of MN type. This finding was in agreement with Bennett et al. (2001) who also showed that based on rheobase current, sacral–caudal MN PIC amplitude was not MN type dependent. However, differences in this property are evident in comparing small, low input conductance (i.e. lower rheobase current) versus large, high input conductance MNs; the former tend to have plateau potentials below or at the threshold for action potential generation, while the latter have plateau thresholds above the action potential threshold (Lee & Heckman 1998a; Lee & Heckman 1998b). Activation of plateau potentials via PIC below or just at the onset of action potential initiation influence MN bistability (i.e. sudden increase or decrease in MN firing frequencies). Just like cat hindlimb MNs, lower rheobase rat MNs

tended to exhibit greater bistability. The lack of bistability in high rheobase current MNs may be attributed to a faster inactivation of the PIC channels. Motoneurones of all sizes illustrate the activation of PIC. At the two extremes, both low input conducatance and high input conducatance MNs have equivalent PIC amplitudes. Low input conductance MNs are more bistable allowing for on and off MN output which is probably important in postural adjustments and alleviate the need for continuous voluntary drive from the higher centres. The activation of PIC in high input conductance MNs may allow for the rapid development of high firing frequencies as to develop muscle force quickly, but perhaps inactivate quickly, with a concomitant decrease in firing frequency to match muscle force decline and fatigue.

The findings from the first study (Button et al. 2006) played a pivotal role in the ensuing two studies of this thesis. Since we found no PIC amplitude difference between decerebrated and anaesthetized rat hindlimb MNs we employed the ramp technique for our experiments on anaesthetized ST and SI rats and more recently aged rats. This was especially important because the addition of a decerebration to chronic ST and SI rats may have been detrimental. The development of ramp induced f-I relationships and ability to measure PIC amplitude in the rat hindlimb MN allowed for correlative analyses between PIC amplitude and other MN rhythmic properties measured from 500 ms and prolonged current injections.

Motoneurone spike frequency adaptation. The main purposes of the second study (Button et al. 2007) was to develop a method to quantify the amount of MN SFA and determine if the SFA pattern was current dependent. This was done by making a ratio of the number of spikes discharged over two separate time periods of

the same duration throughout 30 s of MN rhythmic discharge at 1.5, 3 and 5 nA above the threshold for rhythmic discharge. For example, one ratio included the total number of action potentials discharged from onset of discharge until 5 s over the number of spikes discharged from 20 to 25 s. Ratios were based on 1, 2 or 5 s action potential counts. In the end we had developed an index of different ratios that were sensitive to a variety of SFA patterns. Such an extensive description of quantified SFA had not been previously reported in the literature. Kernell & Monster (1982b) quantified the late phase of SFA as the decline in peak discharge frequency from the 2^{nd} s to the 26^{th} s. This method may not reflect the diverse patterns of spike frequency that occur between 2 and 26 s because it assumes that MN late adaptation patterns are similar across all MNs and that early SFA is negligible after 2 s of rhythmic discharge. Our indexes of MN SFA illustrated that SFA patterns are widely distributed among MNs, even after 3 s or more of rhythmic discharge. The 5 s SFA index [1 - (bin 5/bin 1)] (see Button et al. 2007 for more details) resulted in the greatest range of MN SFA values, which is probably due to capturing a greater time course of the different MN SFA phases.

We also found that MN SFA patterns were independent of current intensity that ranged from 1.5 – 3 nA above the threshold for rhythmic firing. At a current intensity higher than 3 nA the SFA MN pattern would differ but only during the first one or two seconds of discharge. This difference may be due to the MN firing in the secondary versus primary range of firing. Thus, it is apparent that MNs have a general SFA pattern that is similar throughout a range of current intensities. The quantification of SFA allowed for the determination of whether of not it covaried

with other biophysical properties of the MN including single action potential properties and excitability (rheobase current, Rin, PIC amplitude). Due to the lack of MN SFA quantification, there were no reports in the literature on whether or not SFA covaried with other MN properties indicative of excitability. Our findings showed that MN SFA did indeed covary with MN excitability. More excitable MNs had less SFA compared to less excitable MNs.

Since we developed the methods which estimated MN PIC amplitude and quantified MN SFA, we determined if the two covaried. Motoneurone SFA correlated inversely with PIC amplitude. Motoneurones with higher PIC amplitude had a lower rate of SFA. Blocking persistent Na^+ channels had no effect on the pattern of SFA in rat hypoglossal (Zeng et al. 2005) or mouse (Miles et al. 2005) MNs. Perhaps, ion channels other than persistent Na^+ channels work concomitantly in MNs to ensure maintenance of sustained firing. This may be the case since in hypoglossal MNs the Na^+ PIC only contributes towards 20% of the total PIC (Powers & Binder 2003). Perhaps the Ca^{++} channels play a more dominant role in hypoglossal MN SFA patterns. However, for spinal cord MNs, persistent Na^+ channels need to be active in order to sustain rhythmic firing (Lee & Heckman 2001; Harvey et al. 2006c). Different from hypoglossal MNs, the Na^+ PIC in sacral-caudal MNs contributes towards 50% of the initial PIC and 33% of total PIC (Li & Bennett 2003), thus perhaps playing a greater role in SFA patterns. The Na^+ PIC activates rapidly subthreshold to the action potential to initiate discharge but then partly inactivates and plays a more minimal role during sustained MN firing (Li & Bennett 2003). The inactivation of the Na^+ PIC may relate to the rate of SFA. Since, MN types (fast and

slow) have similar PIC amplitudes, greater rates of SFA seen in fast MN types may be due to faster inactivation of the Na^+ PIC. Interestingly, it has been hypothesized (Powers et al. 1999) and confirmed (Miles et al. 2005) that the transient Na^+ channels can regulate spinal cord MN SFA patterns. In other neurone types there is evidence that persistent and transient Na^+ channels are actually the same channel but have different activation mechanisms (Brown et al. 1994; Taddese & Bean 2002). Thus, the rate of inactivation of both the different or perhaps similar transient and PIC Na^+ channels may lead to differences in MN SFA patterns.

Functionally, SFA is a process of some physiological significance. To combat the process of MN SFA and maintain constant output, there would have to be an increase of supraspinal or afferent excitation to the MN. The process of MN SFA has been implicated as a possible contributor to neuromuscular fatigue (Kernell & Monster 1982a; Spielmann et al. 1993). During fatiguing contractions there may be cross talk between the metabolic demand on the muscle and the rate of MN firing frequency. Perhaps there is a minimum firing threshold that once crossed by the MN it is signaled via messages originating from the muscle to turn off and allow for muscle recovery while another MN turns on for muscle contraction to continue. Rotation of motor units has been shown to help maintain force output during prolonged isometric muscle contractions (Bawa et al. 2006). On the other hand, MN SFA is minimal in excitable MNs which is important in posture (Alaburda et al. 2002) and in MNs activated by the locomotor network (Brownstone et al. 1992). This may be due to postural MNs being more bistable and how the PIC is activated in MNs of the locomotor network.

Motoneurone biophysical properties following chronic spinal cord transection and spinal cord isolation. Following chronic ST there is minor changes in MN properties of the single action potential and passive properties (Beaumont et al. 2004; Hochman & McCrea 1994; Gustafsson et al. 1982; Cope et al. 1986; Munson et al. 1986). However, changes in MN rhythmicity appear to be more pronounced (Beaumont et al. 2004; Li & Bennett 2003). Although motor-unit properties are negatively impacted following short-term ST they regain most of their normal function when ST is prolonged (i.e. chronic) (Munson et al. 1986). The development of spasticity following ST (Li & Bennett 2003) may be one of the reasons why MNs maintain heterogeneity and why their biophysical properties and motor-units regain somewhat normal function. In the third study of this thesis we determined the role of hyperreflexia on MN properties by using both chronic ST (removal of descending input, afferents left intact, i.e. allows for the development of spasticity) and SI (bilateral dorsal rhizotomy between two transection sites, removal of descending, ascending and afferent input, i.e. no development of spasticity) rats. For a first time the SI procedure was used for the purposes to study MN biophysical properties. This study had several important findings. First, we hypothesized that ST would have less impact on MN properties than SI due to the development of spasticity. There were no differences between ST and SI MN properties. This finding was surprising since, following chronic ST and SI, rats develop different muscle type and function. Muscle fiber types change from slow isoforms to faster isoforms not long after the ST procedure but are reverted back as ST prolongs (Harris et al. 2007). In addition, muscle unit properties also partially recover following prolonged ST (Munson et al.

1986). Oppositely, following chronic SI, muscle fibers undergo significant changes that remain changed (Harris et al. 2007) and have greater losses in their functional properties compared to ST (Grossman et al. 1998; Roy et al. 2002). Thus, neither the development of spasticity nor afferent input is required for maintenance of MN properties and there is dissociation between MN properties and muscle following SI.

Second, part of the spasticity following ST has been attributed to the developement of enhanced PIC (Li & Bennett 2003). Upon the MN becoming reflexively activated, the PIC channels are activated and can not be inhibited by supraspinal centres which may lead to prolonged muscle contraction. Our findings showed that SI and ST MNs have similar PIC amplitudes compared to each other and Control. These findings lead to several observations. Following ST and SI, the PIC amplitudes of rat hindlimb MNs were smaller than those previously reported in rat sacral-caudal MNs (Li & Bennett 2003; Bennett et al. 2001). The PIC amplitudes may differ because of differences in the duration of ST, PIC amplitides in rat lumbar MNs are actually smaller than those of sacral-caudal MNs, and the function of the rat hindlimb versus tail is quite different which is accompanied by different MN PIC amplitudes. No direct comparison of PIC amplitude between Control and ST MNs has been illustrated in the literature, but rather between acute and chronic ST rat sacral-caudal MNs. Changes in 5-HT and NA receptor sensitivity to residual endogenous monoamines following chronic but not acute ST (Harvey et al. 2006b; Harvey et al. 2006a) may be enough to maintain MN PICs to match those seen where the monoaminergic system is left intact (i.e. Control MNs). Although no PIC amplitude difference existed between ST, SI and Control MNs, there was a

distribution shift of ramp-induced f-I relationship types towards type 3 and 4 (i.e. activation of PIC) following ST and SI compared to Control. Perhaps the intact MNs which do not show much presence of PIC become more sensitive to the monoaminergic mechanisms related to PIC or have a change in PIC channel profile following ST and SI. Finally, afferent input had little or no role in the modulation of PIC, whereas the loss of upstream innervation (including the important PIC facilatory brainstem projections) onto MNs did.

Third, MN f-I gain (the increase in firing frequency per unit of increased current injected) and maximum firing frequencies decreased following ST and SI. Part of this decrease may be related to the increase in AHP amplitude or decrease in neurotrophin levels which may alter ion channel profile or decrease in afferent activity. The MN f-I gain is decreased significantly following ST but alleviated by passive exercise to the hindlimbs or fetal tissue transplantation (i.e. source of growth factors like neurotrophins) into the spinal cord where the MNs of interest are located (Beaumont et al. 2004). Neurotrophins are decreased in the ventral horn of the spinal cord following injury (Gomez-Pinilla et al. 2004) and once an additional source is added back into the cord MN properties are reverted back towards normal (Beaumont et al. 2004). Passive exercise may also help MN properties to revert back to normal following ST due to an increase in neurotrophin levels or via increase in muscle activity or afferent input. Exercise does indeed increase neurotrophin levels in muscle and spinal cord (Gomez-Pinilla et al. 2001). Since afferent activity somewhat decreases following ST we can not exclude that fact

that it does play a small role in maintaining MN properties. However, this role is probably small since SI did not induce any further MN changes compared to ST.

Fourth, ST, SI and Control MNs had similar SFA patterns. This finding was interesting since following ST and SI muscle fatigue increases (Talmadge et al. 2002; Roy et al. 2002). Even after the development of spasticity and reverting of muscle fibers back to normal, increased levels of muscle fatigue persist (Harris et al. 2006). Furthermore, our results indicated that ST and SI MNs became more excitable as measured by rheobase, Rin and proportions of MNs demonstrating PIC. Typically, more excitable MNs have less pronounced SFA. Unlike normal MNs and muscle, following ST and SI there is a discordance between muscle and MN and how the two work together in relation to SFA and muscle fatigue. Since MN SFA appears not to be regulated by afferent or supraspinal inputs, the connection directly between muscle and MN which allows communication between the two may be the important controlling factor for MN SFA. However, the signal for MN SFA may be programmed in the original muscle fiber and remains unchanged even when the activity of the muscle is altered, like muscle fiber types changing to take on faster or slower phenotypes following acute versus prolonged ST, respectively or mainly a fast phenotype following SI.

In both ST and SI procedures the connection between muscle and MN are left intact. The importance of this connection between the two for maintaining MN properties have been demonstrated in cross-reinnervation studies of nerve onto muscle (Foehring et al. 1987a; Foehring et al. 1987b), the relatively few basic MN property changes following ST (Beaumont et al. 2004; Munson et al. 1986; Hochman

& McCrea 1994), the lack of changes following TTX cuffs placed around the nerve (Cormery et al. 2000), the uniformity of some MN properties following axotomy (Gustafsson 1979; Czeh et al. 1977), and now the maintenance of MN properties following SI. All of these studies report the importance of trophic substances and other messages retrogradely signaled from the muscle to the MN or anterogradely signaled from the MN to the muscle. A study just published (Bichler et al. 2007) once again revealed that the connection between muscle and MN, which allows retrograde signaling, is important for MN property maintenance. The novelty in this study is the finding that the mechanism of signaling for MN maintenance is not regulated by muscle fiber activity but rather by a retrograde signaling system coupled to activation of endplate acetylcholine receptors. Following ST and SI some muscle acetylcholine receptors become disorganized and disassemble with no difference between the amount in each model (Burns et al. 2007) and perhaps is one of the factors leading to changes in some MN properties following ST and SI. Nonetheless, many of the basic properties and even some of the rhythmic properties are relatively unchanged probably due to the connection between muscle and MN remaining intact and able to communicate in other ways than through the acetylcholine receptor.

Following SI, one of the most "severe" experimental models of spinal cord injury, the range of values for basic and active MN properties indicate that the heterogeneity among MNs is relatively maintained. The electrophysiological changes in mammalian MNs after spinal cord transection can be reverted back to normal by rehabilitation (i.e. exercise, step training and fetal tissue transplants). Perhaps this may be the case following SI. Nonetheless, maintenance of MN properties following

such devastating procedures allows the possibility to restore walking function following spinal cord injury.

In summary, our laboratory has utilized the rat model to demonstrate how MN properties change throughout a range of altered physiological conditions. This model has allowed us to study the effect of extreme ranges of chronic activity on MN properties. The Gardiner lab has subjected rats to voluntary wheel and treadmill running, hindlimb unweighting, TTX, ST and now SI. Strikingly, there are relatively minute changes in MN basic properties and MNs retain their profile type following these different chronic activity conditions. However, there are greater changes in MN repetitive firing properties suggesting that the mechanisms underlying MN basic and repetitive firing properties differ. Although MN rhythmic properties change following chronic inactivity they retain a high degree of heterogeneity and range of values that are seen in control MNs including SFA patterns, f-I slopes and firing frequencies.

Section 4: Limitations of the studies and future directions. One limitation for the collection of studies included the fact that we recorded from sciatic MNs. Conceivably, the significant results we reported may be do to differences in the population of MNs we recorded from (i.e. flexor MNs versus extensor MNs). Different populations of MNs have different property values. For example, flexor MNs tend to show less bistability than extensors (Conway et al. 1988), PIC amplitude varies with joint angle (Hyngstrom et al. 2007) and AHP half-decay times differ between extensors and flexors as well (Bakels & Kernell 1993). Thus, it would be very interesting to do an in depth study on biophysical properties of rat hindlimb MN

types (extensors versus flexors). An extensive study on this has not been reported in the literature.

Although in the first study we reported MN properties of rats subjected to a decerebration, the data set was small. To my knowledge this is the only electrophysiological data on MNs from a decerebrate rat preparation. Just based on these MNs there were striking differences between sleeping and awake MNs. Thus, it is important to develop a full complement of MN data from decerebrate rats to really determine how they respond to current impulses compared to anaesthetized rat MNs. Although, we reported no PIC amplitude difference between anaesthetized and decerebrate MNs, another type of experiment to ensure that PIC amplitude is not decreased by the ketamine/xylazine mixture is we decerebrate the rat first and record the MN f-I relationship and then add the ketamine/xylazine mixture to the decerebate rat and once again record the MN f-I relationship.

Another, method we could have employed and will in the near future to measure PIC amplitude is a voltage ramp or holding the MN membrane at steady linear voltages to measure current changes. Voltage ramps have been utilized (Bennett et al. 2001; Schwindt & Crill 1982; Schwindt & Crill 1977; Wu et al. 2005) to induce the activation of PIC channels and quantify the amount of PIC. In rat sacral-caudal MNs current and voltage ramps give similar PIC amplitudes (Li & Bennett 2003). Voltage ramps also determine the on and off-set voltage for PICs and whether or not they are similar amongst MNs and between animal models. In rat hindlimb MNs, I would expect that voltage ramps would give similar PIC amplitudes

as calculated from f-I relationships and the voltage at which the PIC is turned on will vary from ~ -60 mV to -45 mV.

Finally, we did not perform any experiments in this thesis where we used pharmacological agents to enhance the PIC. It would be interesting to maximize PIC amplitudes or the potential for PIC channel activation and analyze the f-I relationships and the proportions of MNs categorized into the four different f-I relationship types.

Another reason why it is important to further develop the decerebrate rat preparation is for the use of studying MN properties during fictive locomotion. To date the literature does not report how rat hindlimb MNs respond during fictive locomotion. We do know that MN properties seen in anaesthetized and decerebrate cat properties differ from those recorded from MNs active during fictive locomotion (Dai et al. 2002; Brownstone et al. 1992; Krawitz et al. 2001) and thus would expect similar findings from rat MNs. The study of MNs during locomotion is probably more functional than recording from them during an anaesthetized preparation. However, it is important to understand how the MN functions without other compensatory mechanisms that may take place during locomotion. Furthermore, not every movement in mammals involves locomotion.

Following the SI procedure, there is a lot of damage and inflammation in the spinal cord. In some cases the spinal cord scar tissue induces causes the cord to twist making electrophysiological recordings from MNs very hard. The twisted shape of the cord may have occurred because of the bilateral dorsal rhizotomy. Perhaps a technique could be developed to combat using separate animals for ST and SI and at

the same time eliminate the growth of the twisted spinal cord. One way to do this is performing a complete transection at ~ T8 and a hemi-section at S1 with a unilateral dorsal rhizotomy between the complete transection and the hemi-section. That way we could compare MN properties recorded from each side of the spinal cord. Another experiment that would be interesting would be to add an axotomy to the SI procedure. This would alleviate descending, ascending, afferent and the ever important connection between MN and muscle. That way the MN really is isolated. I would hypothesize that many of the MN properties would become homogeneous with very little output capabilities. Finally, following SI and ST, properties of MN excitability demonstrated that MNs become more like MNs that innervate slow muscles which are typically smaller in size. Unfortunately we did not make any electrical or morphological measurements to determine overall MN size. An extensive analysis of MN size following ST and SI is needed at the present time because the literature is very contradictory on this subject.

The published results in the studies composing this thesis have been deemed as significant contributions to the literature by the reviewers. However, I realize that other than the mechanistic approach we took by using chronically inactive versus control rats, the findings on MN properties reported in this thesis are highly descriptive as opposed to mechanistic. Our lab is attempting to develop molecular biology techniques to help determine some of the mechanisms underlying the electrophysiological properties of MNs and why they change with activity. Attempts to combine electrophysiological with molecular biological approaches to the issue of motoneuronal plasticity have been rare. The biophysical changes in motoneurones

with chronically decreased activity suggest possible chronic changes in: 1) ion channels (type, distribution, amount, and locations, 2) neurotransmitter receptors, 3) neurotrophin levels and 4) MN size. Another method to predict which ion channels underlie the MN properties we measured before and after chronic spinal cord injury is via computer simulations. This technique has been a useful resource to determine MN behaviours and the underlying ion channels involved.

REFERENCE LIST

Alaburda A, Perrier JF & Hounsgaard J (2002). Mechanisms causing plateau potentials in spinal motoneurones. Adv Exp Med Biol **508**, 219-26.

Bakels R & Kernell D (1993). Average but not continuous speed match between motoneurons and muscle units of rat tibialis anterior. J Neurophysiol **70**, 1300-6.

Bawa P, Pang MY, Olesen KA & Calancie B (2006). Rotation of motoneurons during prolonged isometric contractions in humans. J Neurophysiol **96**, 1135-40.

Beaumont E, Houle JD, Peterson CA & Gardiner PF (2004). Passive exercise and fetal spinal cord transplant both help to restore motoneuronal properties after spinal cord transection in rats. Muscle Nerve **29**, 234-42.

Bennett DJ, Li Y & Siu M (2001). Plateau potentials in sacrocaudal motoneurons of chronic spinal rats, recorded in vitro. J Neurophysiol **86**, 1955-71.

Bichler EK, Carrasco DI, Rich MM, Cope TC & Pinter MJ (2007). Rat motoneuron properties recover following reinnervation in the absence of muscle activity and evoked acetylcholine release. J Physiol .

Brown AM, Schwindt PC & Crill WE (1994). Different voltage dependence of transient and persistent Na+ currents is compatible with modal-gating hypothesis for sodium channels. J Neurophysiol **71**, 2562-5.

Brownstone RM, Jordan LM, Kriellaars DJ, Noga BR & Shefchyk SJ (1992). On the regulation of repetitive firing in lumbar motoneurones during fictive locomotion in the cat. Exp Brain Res **90**, 441-55.

Burke RE (1967). Motor unit types of cat triceps surae muscle. J Physiol **193**, 141-160.

Burke RE, Dum RP, Fleshman JW, Glenn LL, Lev-Tov A, O'Donovan MJ & Pinter MJ (1982). A HRP study of the relation between cell size and motor unit type in cat ankle extensor motoneurons. J Comp Neurol **209**, 17-28.

Burke RE, Levine DN, Tsairis P & Zajac FE 3rd (1973). Physiological types and histochemical profiles in motor units of the cat gastrocnemius. J Physiol **234**, 723-48.

Burns AS, Jawaid S, Zhong H, Yoshihara H, Bhagat S, Murray M, Roy RR, Tessler A & Son YJ (2007). Paralysis elicited by spinal cord injury evokes selective disassembly of neuromuscular synapses with and without terminal sprouting in ankle flexors of the adult rat. J Comp Neurol 500, 116-33.

Button DC, Gardiner K, Marqueste T & Gardiner PF (2006). Frequency-current relationships of rat hindlimb {alpha}-motoneurones. J Physiol **573**, 663-77.

Button DC, Kalmar JM, Gardiner K, Cahill F & Gardiner P (2007). Spike frequency adaptation of rat hindlimb motoneurones. J Appl Physiol **102**, 1041-50.

Conway BA, Hultborn H, Kiehn O & Mintz I (1988). Plateau potentials in alpha-motoneurones induced by intravenous injection of L-dopa and clonidine in the spinal cat. J Physiol **405**, 369-84.

Cope TC, Bodine SC, Fournier M & Edgerton VR (1986). Soleus motor units in chronic spinal transected cats: physiological and morphological alterations. J Neurophysiol **55**, 1202-20.

Cormery B, Marini JF & Gardiner PF (2000). Changes in electrophysiological properties of tibial motoneurones in the rat following 4 weeks of tetrodotoxin-induced paralysis. Neurosci Lett **287**, 21-4.

Crill WE (1996). Persistent sodium current in mammalian central neurons. Annu Rev Physiol **58**, 349-62.

Czeh G, Kudo N & Kuno M (1977). Membrane properties and conduction velocity in sensory neurones following central or peripheral axotomy. J Physiol **270**, 165-80.

Dai Y, Jones KE, Fedirchuk B, McCrea DA & Jordan LM (2002). A modelling study of locomotion-induced hyperpolarization of voltage threshold in cat lumbar motoneurones. J Physiol **544**, 521-36.

Dards JL (1983). The behaviour of dockyard cats: interactions of adult males. Applied Animal Ethology **10**, 133-53.

Desaulniers P, Lavoie PA & Gardiner PF (2001). Habitual exercise enhances neuromuscular transmission efficacy of rat soleus muscle in situ. J Appl Physiol **90**, 1041-8.

Foehring RC, Sypert GW & Munson JB (1987a). Motor-unit properties following cross-reinnervation of cat lateral gastrocnemius and soleus muscles with medial gastrocnemius nerve. II. Influence of muscle on motoneurons. J Neurophysiol **57**, 1227-45.

Foehring RC, Sypert GW & Munson JB (1987b). Motor-unit properties following cross-reinnervation of cat lateral gastrocnemius and soleus muscles with medial gastrocnemius nerve. I. Influence of motoneurons on muscle. J Neurophysiol **57**, 1210-26.

Gardiner P, Beaumont E & Cormery B (2005). Motoneurones "learn" and "forget" physical activity. Can J Appl Physiol **30**, 352-70.

Gardiner P, Dai Y & Heckman CJ (2006). Effects of exercise training on alpha-motoneurons. J Appl Physiol **101**, 1228-36.

Gardiner PF (1993). Physiological properties of motoneurons innervating different muscle unit types in rat gastrocnemius. J Neurophysiol **69**, 1160-70.

Gardiner PF (2006). Changes in alpha-motoneuron properties with altered physical activity levels. Exerc Sport Sci Rev **34**, 54-8.

Gharakhanlou R, Chadan S & Gardiner P (1999). Increased activity in the form of endurance training increases calcitonin gene-related peptide content in lumbar motoneuron cell bodies and in sciatic nerve in the rat. Neuroscience **89**, 1229-39.

Gomez-Pinilla F, Ying Z, Opazo P, Roy RR & Edgerton VR (2001). Differential regulation by exercise of BDNF and NT-3 in rat spinal cord and skeletal muscle. Eur J Neurosci **13**, 1078-84.

Gomez-Pinilla F, Ying Z, Roy RR, Hodgson J & Edgerton VR (2004). Afferent input modulates neurotrophins and synaptic plasticity in the spinal cord. J Neurophysiol **92**, 3423-32.

Grossman EJ, Roy RR, Talmadge RJ, Zhong H & Edgerton VR (1998). Effects of inactivity on myosin heavy chain composition and size of rat soleus fibers. Muscle Nerve **21**, 375-89.

Guertin PA & Hounsgaard J (1999). Non-volatile general anaesthetics reduce spinal activity by suppressing plateau potentials. Neuroscience **88**, 353-8.

Gustafsson B (1979). Changes in motoneurone electrical properties following axotomy. J Physiol **293**, 197-215.

Gustafsson B, Katz R & Malmsten J (1982). Effects of chronic partial deafferentiation on the electrical properties of lumbar alpha-motoneurones in the cat. Brain Res **246**, 23-33.

Gustafsson B & Pinter MJ (1984a). Relations among passive electrical properties of lumbar alpha-motoneurones of the cat. J Physiol **356**, 401-31.

Gustafsson B & Pinter MJ (1984b). An investigation of threshold properties among cat spinal alpha-motoneurones. J Physiol **357**, 453-83.

Harris RL, Bobet J, Sanelli L & Bennett DJ (2006). Tail muscles become slow but fatigable in chronic sacral spinal rats with spasticity. J Neurophysiol **95**, 1124-33.

Harris RL, Putman CT, Rank M, Sanelli L & Bennett DJ (2007). Spastic tail muscles recover from myofiber atrophy and myosin heavy chain transformations in chronic spinal rats. J Neurophysiol **97**, 1040-51.

Harvey PJ, Li X, Li Y & Bennett DJ (2006a). 5-ht2 receptor activation facilitates a persistent sodium current and repetitive firing in spinal motoneurons of rats with and without chronic spinal cord injury. J Neurophysiol **96**, 1158-70.

Harvey PJ, Li X, Li Y & Bennett DJ (2006b). Endogenous monoamine receptor activation is essential for enabling persistent sodium currents and repetitive firing in rat spinal motoneurons. J Neurophysiol **96**, 1171-86.

Harvey PJ, Li Y, Li X & Bennett DJ (2006c). Persistent sodium currents and repetitive firing in motoneurons of the sacrocaudal spinal cord of adult rats. J Neurophysiol **96**, 1141-57.

Hochman S & McCrea DA (1994). Effects of chronic spinalization on ankle extensor motoneurons. II. Motoneuron electrical properties. J Neurophysiol **71**, 1468-79.

Hounsgaard J, Hultborn H, Jespersen B & Kiehn O (1988). Bistability of alpha-motoneurones in the decerebrate cat and in the acute spinal cat after intravenous 5-hydroxytryptophan. J Physiol **405**, 345-67.

Hyngstrom AS, Johnson MD, Miller JF & Heckman CJ (2007). Intrinsic electrical properties of spinal motoneurons vary with joint angle. Nat Neurosci **10**, 363-9.

Kanda K & Hashizume K (1992). Factors causing difference in force output among motor units in the rat medial gastrocnemius muscle. J Physiol **448**, 677-95.

Kernell D & Monster AW (1982a). Motoneurone properties and motor fatigue. An intracellular study of gastrocnemius motoneurones of the cat. Exp Brain Res **46**, 197-204.

Kernell D & Monster AW (1982b). Time course and properties of late adaptation in spinal motoneurones of the cat. Exp Brain Res **46**, 191-6.

Krawitz S, Fedirchuk B, Dai Y, Jordan LM & McCrea DA (2001). State-dependent hyperpolarization of voltage threshold enhances motoneurone excitability during fictive locomotion in the cat. J Physiol **532**, 271-81.

Lee RH & Heckman CJ (1998a). Bistability in spinal motoneurons in vivo: systematic variations in persistent inward currents. J Neurophysiol **80**, 583-93.

Lee RH & Heckman CJ (1998b). Bistability in spinal motoneurons in vivo: systematic variations in rhythmic firing patterns. J Neurophysiol **80**, 572-82.

Lee RH & Heckman CJ (2001). Essential role of a fast persistent inward current in action potential initiation and control of rhythmic firing. J Neurophysiol **85**, 472-5 .

Li Y & Bennett DJ (2003). Persistent sodium and calcium currents cause plateau potentials in motoneurons of chronic spinal rats . J Neurophysiol **90**, 857-69.

Li Y, Gorassini MA & Bennett DJ (2004). Role of persistent sodium and calcium currents in motoneuron firing and spasticity in chronic spinal rats. J Neurophysiol **91**, 767-83.

Miles GB, Dai Y & Brownstone RM (2005). Mechanisms underlying the early phase of spike frequency adaptation in mouse spinal motoneurones. J Physiol **15**, 519-532 .

Moritz AT, Newkirk GS, Powers RK & Binder MD (2007). Facilitation of somatic calcium channels can evoke prolonged tail currents in rat hypoglossal motoneurons. J Neurophysiol .

Munson JB, Foehring RC, Lofton SA, Zengel JE & Sypert GW (1986). Plasticity of medial gastrocnemius motor units following cordotomy in the cat. J Neurophysiol **55**, 619-34.

Nemeth PM & Turk WR (1984). Biochemistry of rat single muscle fibres in newly assembled motor units following nerve crush. J Physiol **355**, 547-55.

Perrier JF & Tresch MC (2005). Recruitment of motor neuronal persistent inward currents shapes withdrawal reflexes in the frog. J Physiol **562**, 507-20.

Powers RK & Binder MD (2003). Persistent sodium and calcium currents in rat hypoglossal motoneurons. J Neurophysiol **89**, 615-24.

Powers RK, Sawczuk A, Musick JR & Binder MD (1999). Multiple mechanisms of spike-frequency adaptation in motoneurones. J Physiol Paris **93**, 101-14.

Roy RR, Zhong H, Monti RJ, Vallance KA & Edgerton VR (2002). Mechanical properties of the electrically silent adult rat soleus muscle. Muscle Nerve **26**, 404-12.

Schwindt P & Crill WE (1977). A persistent negative resistance in cat lumbar motoneurons. *Brain Res* **120**, 173-8.

Schwindt PC & Crill WE (1982). Factors influencing motoneuron rhythmic firing: results from a voltage-clamp study. *J Neurophysiol* **48**, 875-90.

Simon M, Perrier JF & Hounsgaard J (2003). Subcellular distribution of L-type Ca2+ channels responsible for plateau potentials in motoneurons from the lumbar spinal cord of the turtle. Eur J Neurosci **18**, 258-66.

Spielmann JM, Laouris Y, Nordstrom MA, Robinson GA, Reinking RM & Stuart DG (1993). Adaptation of cat motoneurons to sustained and intermittent extracellular activation. J Physiol **464**, 75-120.

Taddese A & Bean BP (2002). Subthreshold sodium current from rapidly inactivating sodium channels drives spontaneous firing of tuberomammillary neurons. Neuron **33**, 587-600.

Talmadge RJ, Roy RR, Caiozzo VJ & Edgerton VR (2002). Mechanical properties of rat soleus after long-term spinal cord transection. J Appl Physiol **93**, 1487-97.

Wu N, Enomoto A, Tanaka S, Hsiao CF, Nykamp DQ, Izhikevich E & Chandler SH (2005). Persistent sodium currents in mesencephalic v neurons participate in burst generation and control of membrane excitability. J Neurophysiol 93, 2710-22.

Zeng J, Powers RK, Newkirk G, Yonkers M & Binder MD (2005). Contribution of persistent sodium currents to spike-frequency adaptation in rat hypoglossal motoneurons. J Neurophysiol **93**, 1035-41.

Zengel JE, Reid SA, Sypert GW & Munson JB (1985). Membrane electrical properties and prediction of motor-unit type of medial gastrocnemius motoneurons in the cat. J Neurophysiol **53**, 1323-44.